

# Sensitivity of African Easterly Waves to Dust Forcing

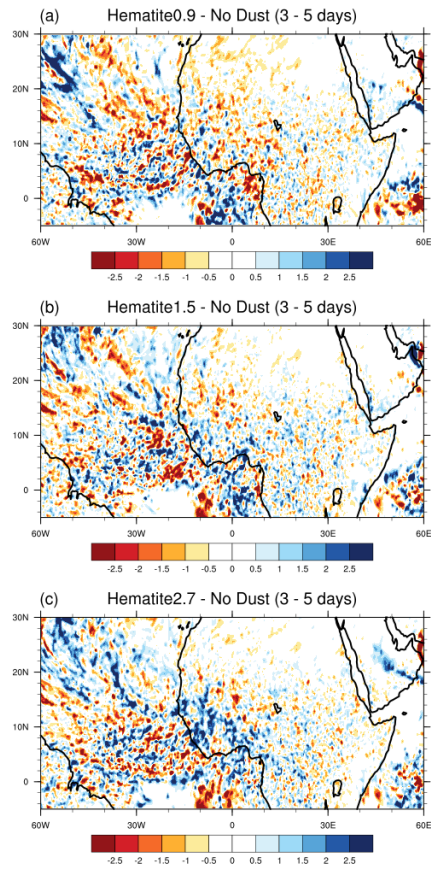
Hamza Kunhu Bangalath<sup>1</sup>, Jerry Raj<sup>1</sup>, and Georgiy Stenchikov<sup>1</sup>

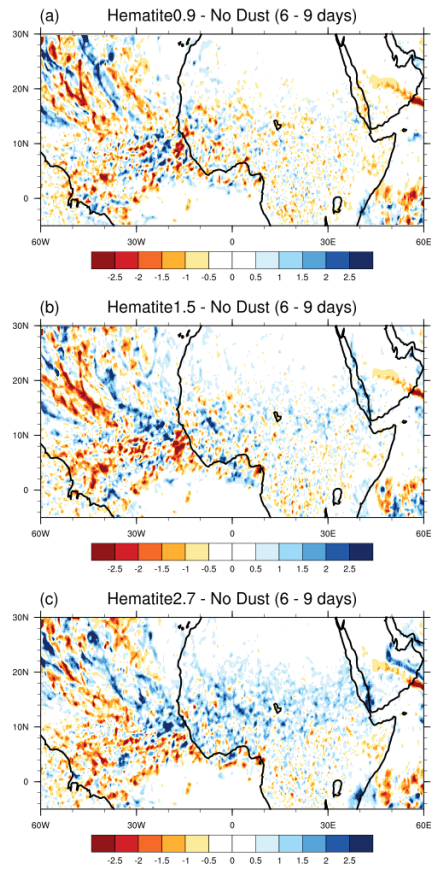
<sup>1</sup>King Abdullah University of Science and Technology

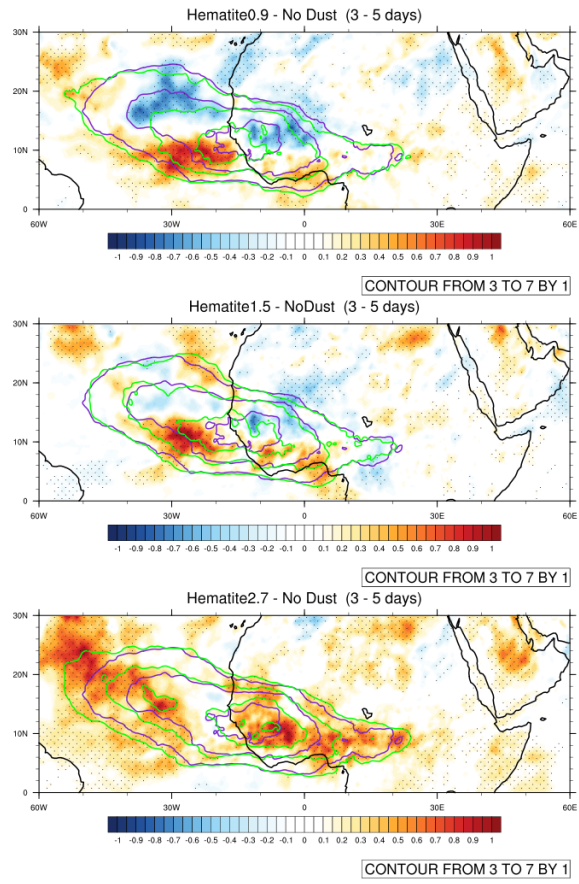
February 13, 2023

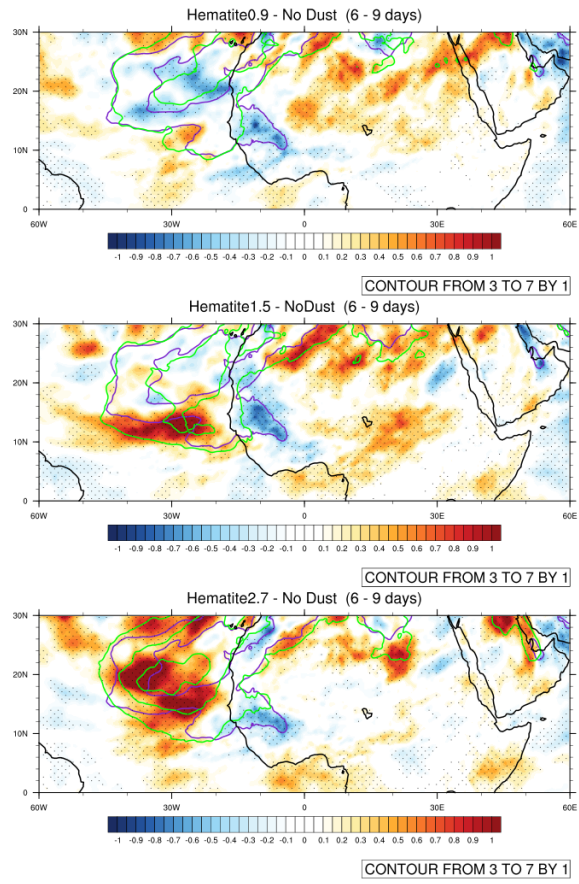
## Abstract

[There is a lack of agreement on the sign and magnitude of the effect of dust-radiative forcing on African easterly waves (AEWs) among past studies. The uncertainty in the dust-radiative forcing associated with the estimation of shortwave absorption is a leading cause of disagreement in the literature. The inability of models to represent various dust-AEW interaction pathways also leads to uncertainty among modeling studies. The present study investigates the sensitivity of AEWs to the observed variability in dust shortwave absorption using a high-resolution atmospheric general circulation model. Global simulations are conducted at a spatial resolution of about 25 km to simulate AEWs and associated circulation features adequately well. The results reveal that AEWs are highly sensitive to dust shortwave absorption. In addition, the AEW activity intensifies and broadens the wave track with a southward shift in response to dust shortwave absorption. There is approximately a 25 % change in eddy kinetic energy (EKE) associated with AEWs for the range of dust shortwave absorption used. The 6–9–day waves are more sensitive to dust shortwave absorption than the 3–5–day waves, where the response in the former has a stark land–sea contrast. The sensitivity of AEW to dust heating stems from a combination of the response from various energy conversions. Although baroclinic energy conversion is the leading term in the energy cycle, the responses to dust shortwave heating in barotropic and generation terms are comparable to those in baroclinic conversion.]









# Sensitivity of African Easterly Waves to Dust Forcing

Hamza Kunhu Bangalath<sup>1</sup>, Jerry Raj<sup>1</sup>, and Georgiy Stenchikov<sup>1</sup>

<sup>1</sup>Physical Science and Engineering Division, King Abdullah University of Science and Technology,  
Thuwal, Saudi Arabia

## Key Points:

- African easterly waves are highly sensitive to dust shortwave absorption.
- Wave track intensifies, broadens, and shifts southward in response to dust shortwave absorption
- AEW sensitivity to dust stems primarily from baroclinic and barotropic energy conversions and energy generation by adiabatic heating.

---

Corresponding author: Hamza Kunhu Bangalath, [hamzakunhu.bangalath@kaust.edu.sa](mailto:hamzakunhu.bangalath@kaust.edu.sa)

**Abstract**

[There is a lack of agreement on the sign and magnitude of the effect of dust-radiative forcing on African easterly waves (AEWs) among past studies. The uncertainty in the dust-radiative forcing associated with the estimation of shortwave absorption is a leading cause of disagreement in the literature. The inability of models to represent various dust–AEW interaction pathways also leads to uncertainty among modeling studies. The present study investigates the sensitivity of AEWs to the observed variability in dust shortwave absorption using a high-resolution atmospheric general circulation model. Global simulations are conducted at a spatial resolution of about 25 km to simulate AEWs and associated circulation features adequately well. The results reveal that AEWs are highly sensitive to dust shortwave absorption. In addition, the AEW activity intensifies and broadens the wave track with a southward shift in response to dust shortwave absorption. There is approximately a 25 % change in eddy kinetic energy (EKE) associated with AEWs for the range of dust shortwave absorption used. The 6–9-day waves are more sensitive to dust shortwave absorption than the 3–5-day waves, where the response in the former has a stark land–sea contrast. The sensitivity of AEW to dust heating stems from a combination of the response from various energy conversions. Although baroclinic energy conversion is the leading term in the energy cycle, the responses to dust shortwave heating in barotropic and generation terms are comparable to those in baroclinic conversion.]

**Plain Language Summary**

African easterly waves (AEWs) occur in the dust-laden atmosphere over tropical Africa and the Atlantic. Dust and AEWs interact with each other in multiple ways. However, there has yet to be a general agreement on the sign and magnitude of dust effect on the AEWs. A primary uncertainty comes from estimating dust’s ability to absorb shortwave radiation and heat the atmosphere. This study investigates the sensitivity of AEWs to the observed variability in dust shortwave absorption using a high-resolution atmospheric general circulation model. The results demonstrate that AEWs are highly sensitive to dust shortwave absorption. The AEW activity intensifies and broadens the wave track as the dust becomes more absorbing. Wave track widens primarily towards the equator, leading to a southward track shift. There is approximately a 25 % change in the eddy kinetic energy, a proxy for AEW activities, for the observed range of dust shortwave absorption. Hence, accurately representing dust optical properties is crucial to predict the AEWs and the overall African climate better, especially in the global warming context where both AEWs and dust loading change.

**1 Introduction**

Heavy loading of mineral dust aerosols and African easterly waves (AEWs) co-exist in the Sahara–Sahel–tropical Atlantic region. The interaction between AEWs and dust-radiative forcing has been the subject of active scientific inquiry since the 1970s (e.g., Carlson & Prospero, 1972). Although a vast body of modeling and observational studies have been conducted on dust–AEW interaction to date, no general agreement has been reached on the effect of dust on AEWs. Some studies have demonstrated the enhancement of AEW activities as a response to dust-radiative forcing (e.g., Karyampudi & Carlson, 1988; Reale et al., 2009; Jury & Santiago, 2010), whereas other studies have suggested the weakening of AEWs due to dust forcing (e.g., Jones et al., 2004; Ma et al., 2012; Grogan et al., 2016; Lavaysse et al., 2011). The disagreement among studies stems primarily from the uncertainties in estimating dust-radiative forcing and from the inability of models to incorporate all possible dust–AEW interaction pathways adequately.

One of the main uncertainties in estimating dust-radiative forcing lies in the estimation of dust shortwave absorption and its associated radiative heating (e.g., Solmon et al., 2008; Miller et al., 2004). Balkanski et al. (2007) found that the imaginary part

61 of the refractive index, which decides the dust shortwave absorption and radiative heat-  
62 ing rate, varies by an order of magnitude among various studies. Accordingly, single scat-  
63 tering albedo, the ratio of scattering and absorption in the total extinction, varies sig-  
64 nificantly (0.7 to 0.99) (e.g., J. M. Haywood et al., 2001; Slingo et al., 2006; Otto et al.,  
65 2009; Raut & Chazette, 2008). There is also a disparity between in situ and satellite mea-  
66 surements; in situ measurements generally lead to a higher shortwave absorption esti-  
67 mation than satellite-based estimates (e.g., Kaufman et al., 2001; J. Haywood et al., 2003).  
68 Hence, modeling studies struggle with the uncertainty of radiative forcing estimation.

69 Changes in dust shortwave absorption can affect the generation and maintenance  
70 of AEWs in many ways. Many previous studies have demonstrated that dust-induced  
71 radiative heating in the lower and mid-troposphere alters the static stability of the at-  
72 mosphere, influencing the AEWs (e.g., Jones et al., 2004). Another vital pathway of dust-  
73 AEW interaction is through the instabilities of the African easterly jet (AEJ). The dust-  
74 induced changes in the shear on the AEJ and the consequent barotropic-baroclinic in-  
75 stabilities are necessary to maintain the AEW (e.g., Thorncroft & Hoskins, 1994a, 1994b;  
76 Hall et al., 2006; Cornforth et al., 2009). However, more recent studies (Grogan et al.,  
77 2016, 2017; Nathan et al., 2017; Bercos-Hickey et al., 2017) have revealed that changes  
78 in the dust-induced zonal mean and eddy heating can also influence AEWs.

79 Bangalath and Stenchikov (2016) studied the sensitivity of the Middle East and  
80 North African (MENA) climate to the uncertainty in dust shortwave absorption. The  
81 study found that dust acts as an off-equatorial heating source collocated with the solar  
82 insolation maximum and enhances the meridional mean temperature gradient over the  
83 MENA region during summer. The tropical rain-belt, surface circulation (trade winds),  
84 and AEJ intensify and shift northward as dust shortwave absorption increases. The sen-  
85 sitivity of the tropical rain-belt and AEJ to dust shortwave absorption indeed translates  
86 into AEW sensitivity because the generation and maintenance of AEWs greatly depend  
87 on the moist convection and instabilities of AEJ. The tropical rainbelt shifts northward  
88 and intensifies as a response to dust heating. The latent heat release from the enhanced  
89 precipitation alters the meridional temperature gradient in the mid-upper troposphere.  
90 The circulation responses at the surface and at the level of the AEJ are particularly cru-  
91 cial for AEWs. The surface circulation south of the inter-tropical depression (monsoonal  
92 trade wind) enhances, and the circulation north of it (Harmattan wind) weakens due to  
93 dust shortwave heating. In contrast, circulation weakens on the southern flank of the AEJ  
94 and enhances on its northern flank. The contrasting response pattern in surface and mid-  
95 tropospheric circulation induces vertical shear in the zonal and meridional velocities. Per-  
96 turbations in wind shear and temperature gradients change all energy conversion terms  
97 in the regional energy cycle, ultimately changing the eddy kinetic energy (EKE) avail-  
98 able for AEWs (e.g., Grogan et al., 2016, 2017; Nathan et al., 2017; Bercos-Hickey et al.,  
99 2017).

100 The present study investigates the sensitivity of AEWs to the observed variabil-  
101 ity in dust shortwave absorption using a high-resolution atmospheric general circulation  
102 model-HiRAM-developed at the Geophysical Fluid Dynamics Laboratory (GFDL) (Zhao  
103 et al., 2009). In order to quantify the sensitivity, the study conducts climate simulations  
104 with seasonally varying dust assuming dust is an inefficient, standard, and efficient short-  
105 wave absorber, following Bangalath and Stenchikov (2016). Apart from quantifying the  
106 sensitivity of AEWs to dust shortwave absorption, this research specifically investigates  
107 the causality of sensitivity using energetics analysis. The study analyzes the response  
108 of 3-5-day and 6-9-day wave sensitivity separately over continental Africa and the At-  
109 lantic. The HiRAM simulations are conducted at a spatial resolution of 25 km. It is worth  
110 noting that most past AEW modeling studies have used coarse-resolution general cir-  
111 culation models (GCMs), which often fail to resolve the topography and mesoscale sys-  
112 tems well enough to produce realistic AEWs. The HiRAM simulations at 25 km have  
113 been proven to resolve AEWs adequately (Raj et al., 2022). This study specifically ap-

114 plies energetic analysis to understand the sensitivity of AEWs to dust shortwave absorp-  
 115 tion.

## 116 2 Model and Experiment

117 HiRAM was developed from the Atmospheric Model version 2 (AM2) of GFDL by  
 118 modifying certain aspects (Zhao et al., 2009), which has flexibility in the horizontal res-  
 119 olution of up to a few kilometers and improved vertical resolution (32 levels) compared  
 120 to AM2. The current study uses the C360 version (spatial resolution of about 25km) of  
 121 the HiRAM, which employs a hydrostatic finite-volume cubed-sphere dynamical core (Lin  
 122 2004; Putman and Lin 2007). A major modification from AM2 is that its customary deep  
 123 convective scheme is replaced by a nonintrusive shallow convective scheme (Bretherton  
 124 et al. 2004) by extending it to simulate deep convection (Zhao et al. 2009). Moreover,  
 125 HiRAM preserves most of the parameterizations from AM2, such as radiative transfer,  
 126 surface flux, boundary layer, orographic gravity wave drag parameterizations, and large-  
 127 scale cloud microphysics, with necessary modifications as the resolution increases. Fur-  
 128 ther, HiRAM is coupled to GFDL land model LM3, and sea surface temperature (SST)  
 129 is prescribed from the monthly Hadley Centre Sea Ice and Sea Surface Temperature (HadISST)  
 130 dataset (Rayner et al., 2003). It should be noted that the simulations do not account  
 131 for the SST feedback to dust loading, and the response to dust is solely from the atmo-  
 132 spheric response.

133 Originally HiRAM was designed to provide an improved representation of weather  
 134 events in a GCM and for applications ranging from weekly forecasts to climate projec-  
 135 tions. A resolution of 25km allows models to resolve important mesoscale weather events  
 136 (e.g., Zhao et al., 2009; Jung et al., 2012) and major orographically induced circulations  
 137 (e.g., Boyle & Klein, 2010; Lau & Ploshay, 2009). Therefore, the simulations enable the  
 138 examination of sub-seasonal (synoptic scale) variability such as AEWs. A detailed val-  
 139 idation of HiRAM’s ability to reasonably simulate AEW activities has been reported by  
 140 Raj et al. (2022). In general, HiRAM simulates EKE reasonably well for both 3-5-day  
 141 and 6-9-day waves compared to different reanalysis data. It has also been shown that  
 142 the model is capable of simulating all major circulation features and various energy con-  
 143 versions that make up available potential energy for eddies.

144 We conducted four experiments: one without dust loading (“NoDUST” experiment)  
 145 and three with seasonally varying dust loading but with different dust optical proper-  
 146 ties. The dust and other aerosol concentrations were prescribed from the Model for Ozone  
 147 and Related Chemical Tracers (MOZART) offline calculations (Horowitz et al. 2003).  
 148 Dust loading is discretized into eight bins from 0.1 to 10  $\mu\text{m}$ . Specific extinction coef-  
 149 ficients of dust are calculated using the Mie theory, assuming refractive indices for the  
 150 shortwave spectrum from the estimates by Balkanski et al. (2007) and indices for the  
 151 longwave spectrum by Volz (1973). Three cases of dust with a hematite content (by vol-  
 152 ume) of 0.9%, 1.5%, and 2.7% were selected. The cases of 0.9% of hematite (“DUST0.9”  
 153 experiment), 1.5% of hematite (“DUST1.5” experiment), and 2.7% of hematite (“DUST0.9”  
 154 experiment) represent dust as an inefficient, standard and efficient shortwave absorber,  
 155 respectively. A detailed explanation of the model and dust representation is presented  
 156 in Bangalath and Stenchikov (2016).

157 The sensitivity of AEWs to dust shortwave absorption and the associated heating  
 158 is estimated by comparing the three dust simulations with simulations without dust. All  
 159 four experiments were run for an 11-year period with three ensembles (perturbed ini-  
 160 tial condition runs), and the first year is omitted from the analysis considering the spin-  
 161 up period.

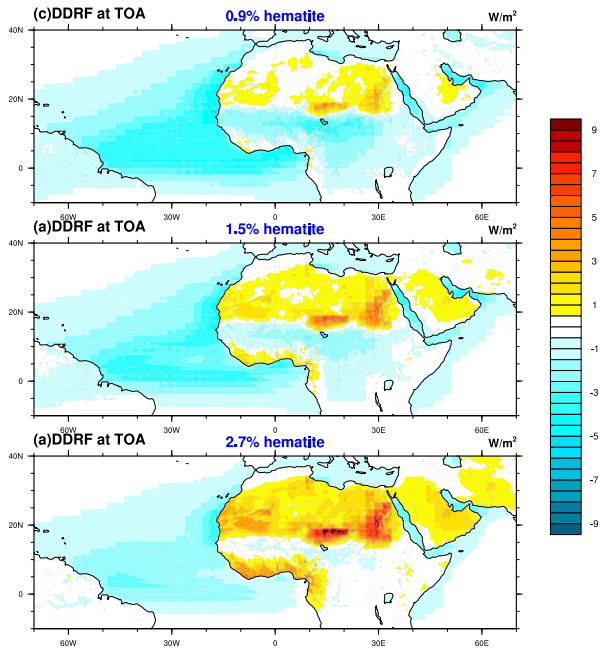


**Figure 1.** Summer (June–September) all-sky DDRF ( $Wm^2$ ) at the TOA in the DUST0.9, DUST1.5, and DUST2.7 experiments. Positive values represent the warming of the system, and negative values denote the cooling of the system, by definition

### 3 Results

#### 3.1 Dust-Radiative Forcing and Atmospheric Heating

Instantaneous radiative forcing and heating rate anomalies were calculated following (Bangalath & Stenchikov, 2015, 2016) in each simulation for analyzing the direct radiative effect of dust. Dust direct radiative forcing (DDRF) is defined as the net (long-wave plus shortwave) radiative flux difference between a state with dust loading and one without dust loading (downwelling minus upwelling), calculated under the same meteorological conditions. Hence, positive (negative) DDRF indicates the warming (cooling) of a system. The radiative fluxes of dust were estimated at each radiation time-step by calling the radiation routine twice, with and without the presence of dust. The DDRF and dust-induced atmospheric heating estimates in the present study are calculated under all-sky conditions. A detailed discussion of the dust-radiative forcing and heating rates is available in Bangalath and Stenchikov (2016).

The present study focuses on June–September, the AEW season. The analysis was separately performed over the African continent and the Atlantic. Figure 1 illustrates the top of the atmosphere (TOA) DDRF over MENA and the Atlantic region in all three cases of hematite content. There is a strong north–south gradient in forcing over MENA; the forcing is positive over Saharan-Arabian deserts and negative over sub-Saharan and Oceanic regions. The change in the sign of forcing between bright deserts and relatively dark surfaces, including vegetated canopy and oceans, is due to the albedo effect (e.g., Bangalath & Stenchikov, 2015; Osipov et al., 2015). The TOA aerosol forcing is a strong function of the effective albedo of the underlying surface. As dust becomes more absorbing, the positive forcing over the desert region intensifies, and the negative forcing over the ocean and sub-Saharan region diminishes. The variability of forcing over the Sahel is especially interesting. The forcing changes sign from negative to positive as the dust

187 becomes more absorbing. As a result, dust-radiative forcing becomes larger over land  
188 than over the ocean when the dust becomes more absorbing.

189 The presence of the north–south gradient in forcing over the African continent is  
190 particularly important for AEW activity. Such a north–south contrast in radiative forc-  
191 ing and its strengthening in response to dust shortwave absorption leads to the strength-  
192 ening and northward shift of the Hadley Cell, rainbelt, and AEJ (Bangalath & Stenchikov,  
193 2015, 2016). The generation and maintenance of AEW greatly depend on the barotropic-  
194 baroclinic instabilities; thus, the dust-induced changes in the latent heating and wind  
195 shears will affect AEW. To explicitly demonstrate these processes, we separately display  
196 the meridional cross sections of zonally averaged dust-induced heating rate anomalies  
197 over the continent and Atlantic (Fig. 2). Heating from dust shortwave absorption is con-  
198 fined to the northern hemispheric subtropics centered at  $20^{\circ}\text{N}$  in all three experiments.  
199 Dust-induced heating is concentrated north of the AEJ core ( $12^{\circ}\text{N}$ ), which has impli-  
200 cations for AEW growth (Grogan et al., 2016, 2017; Grogan & Thorncroft, 2019). As  
201 the hematite content increases, the heating increases and broadens meridionally and ver-  
202 tically. Over the Atlantic, the intensity and vertical extent of heating are almost half of  
203 those over the continent. Hence, dust forcing affects AEWs over the continent and ocean  
204 differently.

### 205 3.2 AEW Response

206 The EKE is a suitable metric to portray wave activity and is calculated as follows:

$$EKE = \frac{(u'^2 + v'^2)}{2} \quad (1)$$

207 where  $u$  and  $v$  are the zonal and meridional winds, respectively. The primes indicate But-  
208 terworth bandpass-filtered anomalies of the daily wind field. Figure 3 depicts the filtered  
209 EKE (for 3–5–day and 6–9–day bands) at 700 hPa (contours) as a measure of AEW ac-  
210 tivities and displays the difference in filtered EKE (shades) between simulations with and  
211 without dust. The differences are taken by subtracting the case with dust from that with-  
212 out dust such that the anomalies express the role of dust in the EKE. The areas where  
213 the effect of the dust is statistically significant at a 95% confidence level are marked by  
214 dots. The green contours represent the EKE in simulations with dust, and the violet con-  
215 tours represent the EKE in simulations without dust. The EKE is separately estimated  
216 for the 3–5–day and the 6–9–day waves. Raj et al. (2022) validated the HiRAM-produced  
217 EKE in detail.

218 In general, dust shortwave heating increases 3–5–day EKE, indicating increased AEW  
219 activities (Fig. 3, left column). In the DUST0.9 and DUST1.5 experiments, a north–south  
220 EKE dipole pattern occurs in response. Dust causes the weakening of the 3–5–day waves  
221 on the northern side of the wave track and enhances on the southern side. A compar-  
222 ison of filtered EKE contours of the DUST (green) and NoDUST (violet) experiments  
223 indicates a southward shift of the AEW track in both cases. The dipole response pat-  
224 tern and the southward track shift are more prominent in the DUST0.9 case. The dipole  
225 pattern of response disappears as the dust becomes an efficient shortwave absorber (DUST2.7).  
226 In this case, the 3–5–day wave activity intensifies everywhere, and the wave track broad-  
227 ens in all directions. Note that the AEW track extends about 450 km in the Atlantic.  
228 The broadening and intensification of the AEW track may have implications on the TC  
229 genesis in the basin as AEWs are often precursors to tropical cyclones (e.g., Landsea, 1993;  
230 Russell et al., 2017). However, care must be taken in drawing a direct correlation be-  
231 tween the AEWs and tropical cyclone activities, as a recent study by Patricola et al. (2018)  
232 has pointed out that the AEWs may not be a reliable predictor for the seasonal variabil-  
233 ity and changes in Atlantic tropical cyclone frequency.

234 In contrast with 3–5–day waves, a striking land–sea contrast occurs in the 6–9–day  
235 waves (Fig. 3, right column). Over the land, the wave activity reduces in all three dust

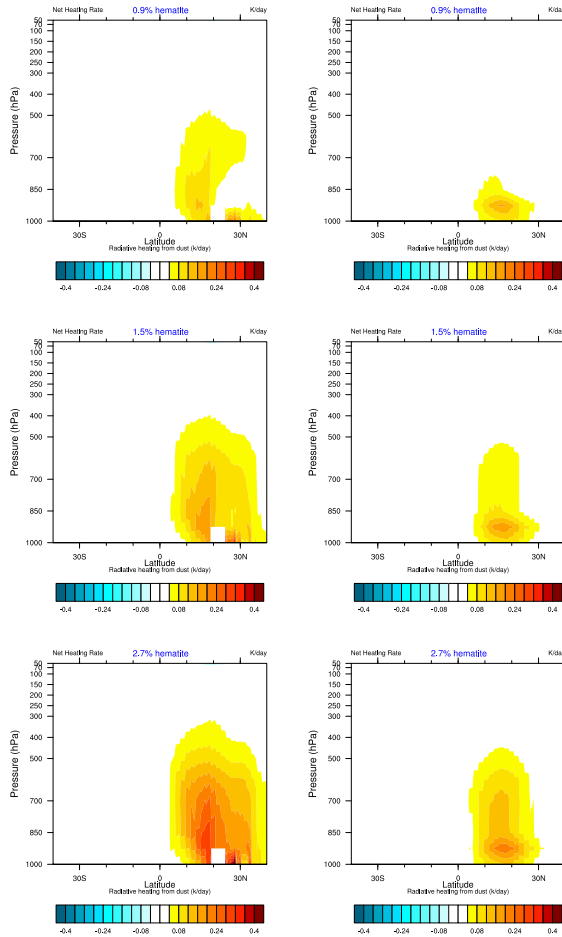


**Figure 2.** Meridional height cross-section of mean June–September radiative heating rate (shortwave plus longwave) anomaly induced by dust in all three with dust experiments. The left panel represents the vertical cross-section over the African continent (zoned between  $-15^{\circ}$  and  $20^{\circ}$ ), and the right panel is the cross-section for the Atlantic (zoned between  $-50^{\circ}$  and  $-15^{\circ}$ )

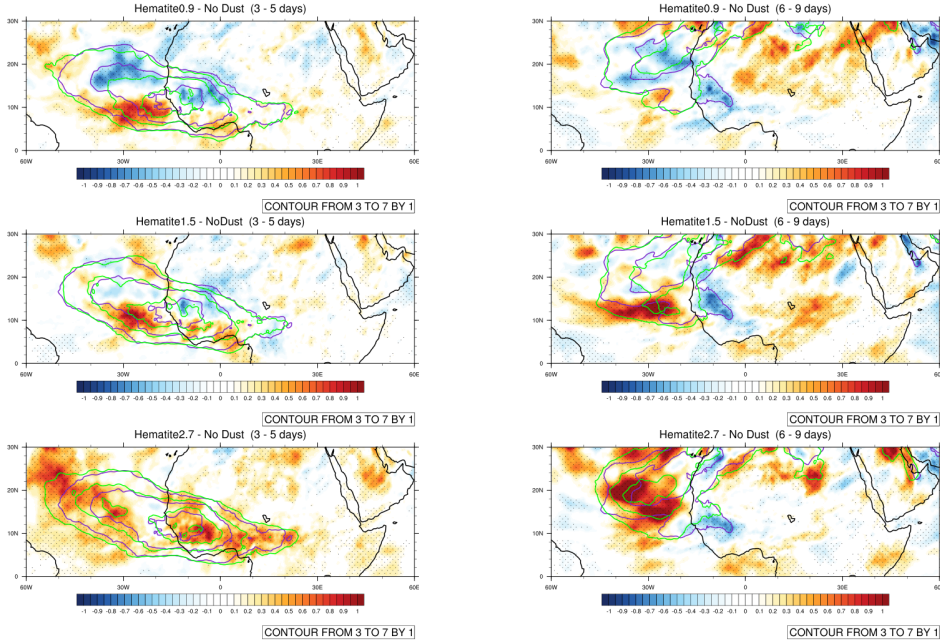


**Figure 3.** The EKE ( $m^2s^{-2}$ ) estimated from the 3–5-day band-pass-filtered zonal and meridional winds at 700 hPa. The contours represent the EKE from NoDUST (violet) and three different DUST (green) experiments. Red and blue shades mark the anomalies of EKE in each experiment (DUST–NoDUST). Dots mark areas where the EKE anomalies are statistically significant, at least at the 95% confidence level.

236 experiments. In addition, the wave track shrinks over land. However, the response over  
 237 the Atlantic is similar to that of the 3–5-day waves. In the DUST0.9 case, AEW activ-  
 238 ity decreases in most areas except a few patches to the southern edge of the track. How-  
 239 ever, a dipole pattern emerges in the DUST1.5 experiment. A southward shift of the  
 240 6–9-day wave track is also evident in the DUST1.5 case. Similar to the 3–5-day case, there  
 241 is an intense and widespread increase in the wave activity and the consequent broaden-  
 242 ing of wave track in all directions when the dust is highly absorbing (DUST2.7). Such  
 243 a strong response leads to a strong land–sea contrast in the response. If we assume all  
 244 individual waves originated over the continent, the strong land–sea contrast in the re-  
 245 sponse indicates an enhancement of AEWs once they enter the Atlantic. The magnitude  
 246 of response is higher in the 6–9-day waves than in the 3–5-day waves, although the mean  
 247 EKE of the 3–5-day waves is higher. Therefore, amplified EKE response occurs in the  
 248 6–9-day waves compared to the 3–5-day waves, especially in terms of the percentage of  
 249 change in EKE.

250 Standard deviations of band-pass-filtered outgoing longwave radiation (OLR) anom-  
 251 alies in 3–5-day and 6–9-day bands are depicted to elucidate the sensitivity of convective  
 252 activities associated with AEW (Fig. 4). The contours represent the band-pass-filtered  
 253 variability of OLR in the NoDUST case. The OLR variability is mostly concentrated over  
 254 tropical Africa and the Atlantic. Over the continent, the OLR variability is collocated  
 255 with the AEW track defined by the EKE. However, there is a southward shift of the At-  
 256 lantic AEW track defined by the OLR compared to that defined by the EKE. In other  
 257 words, the convective activity associated with AEWs is confined to the equator, whereas  
 258 the wind variability shifts further north in the Atlantic than over the continent. Such  
 259 a land–sea contrast might be due to the ITCZ’s relatively weaker seasonal (latitudinal)  
 260 oscillation over the Atlantic compared to that over continental Africa.

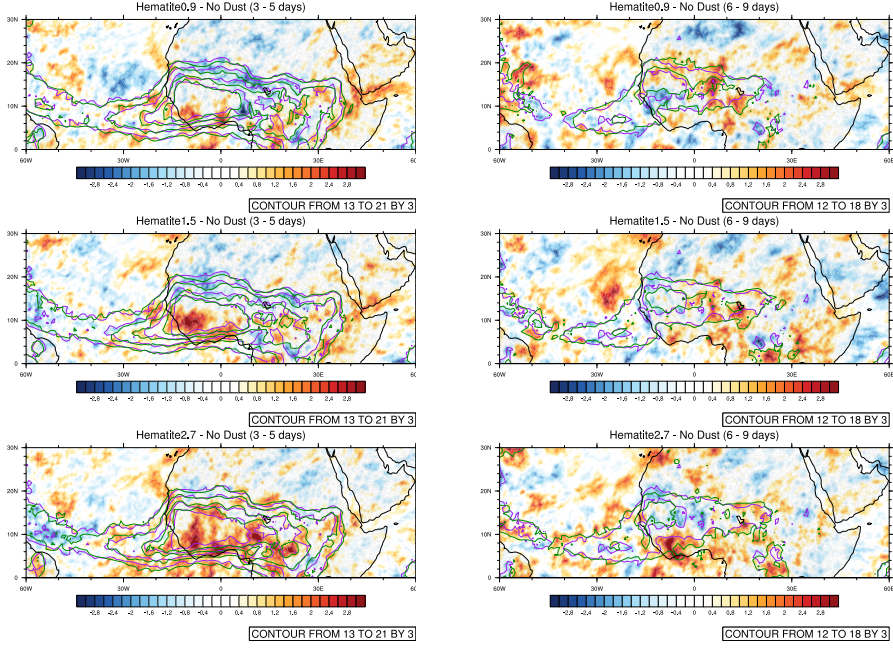


**Figure 4.** Difference in the 3–5–day band-pass-filtered OLR ( $wm^{-2}$ ) standard deviation (shading) between experiments with and without dust (DUST-NoDUST). The contours represent the standard deviation of the OLR in the experiment without dust (NoDUST).

261 Consistent with the response in the EKE field, a north–south dipole pattern occurs  
 262 in the OLR variability response in the DUST0.9 and DUST1.5 cases. The OLR vari-  
 263 ability decreases to the north and increases to the south of the AEW track. There is a  
 264 widespread increase in the OLR variability throughout the track in highly absorbing dust  
 265 cases (DUST2.7 case), similar to the EKE response. In the 6–9–day case, OLR variabil-  
 266 ity is reduced in most of the track over land. However, the OLR variability to the south  
 267 of the track intensifies as the dust becomes more absorbing. This is consistent with the  
 268 response in EKE, and it reaffirms the southward shift of the track response to dust short-  
 269 wave heating. Over the Atlantic, the OLR variability reduces in the core of the track.  
 270 However, the variability of OLR increases around the track in all directions indicating  
 271 the broadening of the track with a dust shortwave absorption increase.

### 272 3.3 Energetics Analysis

273 Energetic analysis is an excellent tool for understanding the generation and main-  
 274 tenance of AEWs (e.g., Norquist et al., 1977; Hsieh & Cook, 2007). This analysis has  
 275 also been used to assess the influence of dust-radiative forcing on AEWs (Bercos-Hickey  
 276 et al., 2022; Grogan et al., 2016; Grogan & Thorncroft, 2019). Here, we employed the  
 277 energetics analyses originally formulated by Lorenz (1955) for the general circulation of  
 278 the atmosphere and later modified for a limited area (Muench, 1965; Norquist et al., 1977;  
 279 Hsieh & Cook, 2007) by incorporating energy transport at the boundaries. In this for-  
 280 mulation, the governing equations for the EKE ( $K_E$ ) and available potential energy ( $A_E$ )  
 281 are as follows:

$$\frac{\partial K_E}{\partial t} = C_k + C_{pk} - D_E + K_{EB} + \phi_{EB} \quad (2)$$

282 and

$$\frac{\partial A_E}{\partial t} = C_A - C_{pk} + G_E + A_{EB} \quad (3)$$

283 In Equation 2,  $C_k$  is the barotropic energy conversion term estimating the conver-  
 284 sion of zonal kinetic energy to EKE associated with zonal ( $u$ ) and meridional ( $v$ ) wind  
 285 shears. The  $C_{pk}$  is the baroclinic energy conversion term which represents the conver-  
 286 sion of eddy available potential energy to EKE associated with the vertical overturning.  
 287 The  $C_{pk}$  appears in Equation 3 with a negative sign indicating that the  $A_E$  consumed  
 288 by baroclinic overturning is converted to  $K_E$ . The  $D_E$  is the frictional dissipation, and  
 289  $K_{EB}$  and  $\phi_{EB}$  are boundary EKE flux and pressure work done by the eddies at the bound-  
 290 aries, respectively. The conversion of zonal  $A_E$  to eddy  $A_E$  from the eddy heat flux along  
 291 mean zonal temperature gradient is represented by the  $C_A$  in Equation 3. The  $G_E$  es-  
 292 timates the  $A_E$  generation by diabatic heating, either by heating the warmer region and  
 293 cooling the colder region or by heating the colder region and cooling the warmer region  
 294 at the same latitude. Finally,  $A_E$  fluxes at the boundaries are indicated by  $A_{EB}$ . De-  
 295 tailed expressions of all individual terms are provided in Appendix A.

296 We analyzed the baroclinic ( $C_{pk}$ ), barotropic ( $C_k$ ), zonal to eddy potential tem-  
 297 perature conversion ( $C_A$ ), and generation term ( $G_E$ ) for both 3-5 and 6-9-day waves  
 298 separately. Dust-radiative forcing changes its sign from land to the ocean (Fig. 1); there-  
 299 fore, we also computed each term separately over the continent (averaged over 15°W to  
 300 20°E) and Atlantic (averaged over 50°W to 15°W).

301 Figure 5 presents  $C_{pk}$ , which is the most prominent term, over the continent for  
 302 the 3-5-day and 6-9-day waves. There are two centers with a positive value (generation  
 303 center) of  $C_{pk}$ : one in the subtropical (12°N - 30°N) lower troposphere (from surface to  
 304 700 hPa), and the second in the tropical (0° - 15°N) upper troposphere (from 500 hPa  
 305 to 200 hPa). The former is associated with either the warm air ascent (dry convection)  
 306 or cold air subsidence, mostly coincident with the Saharan heat-low region. The latter,  
 307 which is in the upper troposphere, is associated with the latent heat released from the  
 308 precipitation induced by AEWs. A region of energy destruction also occurs below 500  
 309 hPa in the tropics, although the values are at least one order less than the generation  
 310 center in the upper troposphere. This region of negative  $C_{pk}$  is associated with ascend-  
 311 ing cold air, possibly due to the dynamical forcing within the waves (Yanai, 1961; Died-  
 312 hiou et al., 2002; Hsieh & Cook, 2007). As baroclinic energy conversion is associated with  
 313 the overturning circulation, the centers can be understood as part of the tropical deep  
 314 and moist overturning circulation and the subtropical dry convection.

315 In the 3-5-day wave (left column),  $C_{pk}$  increases in the tropical upper tropospheric  
 316 generation center as dust shortwave absorption increases. There is approximately 20%  
 317 increase in the DUST2.7 case compared to NoDUST. The increase in  $C_{pk}$  in response  
 318 to the increase in shortwave heating is due to the enhanced latent heat release from the  
 319 wave-induced precipitation enhancement. In the subtropical lower tropospheric positive  
 320 maxima,  $C_{pk}$  is destroyed in the DUST0.9 and DUST1.5 cases compared to the NoDUST  
 321 case. However, intense  $C_{pk}$  generation occurs when the dust is an efficient shortwave ab-  
 322 sorber (DUST2.7). In the remaining area, the  $C_{pk}$  response is minimal.

323 In the 6-9-day wave (right panel Figure 5),  $C_{pk}$  is weaker compared to the 3-5-day  
 324 case due to the lesser convective precipitation associated with 6-9-day waves compared  
 325 to 3-5-day waves. The 6-9-day  $C_{pk}$  values are about half of those in the 3-5-day cases.  
 326 The  $C_{pk}$  patterns are similar in both cases. However, the response to dust shortwave ab-  
 327 sorption is more significant in the 6-9-day waves than in the 3-5-day waves with a strong  
 328 north-south dipole pattern, especially in the tropical upper tropospheric center. In ad-  
 329 dition,  $C_{pk}$  is generated towards the equator and destroyed towards the subtropics. The  
 330 dipole pattern of response enhances when dust-induced shortwave heating increases. Such  
 331 a dipole pattern of response may be related to the southward shift of 6-9-day AEWs (Fig.

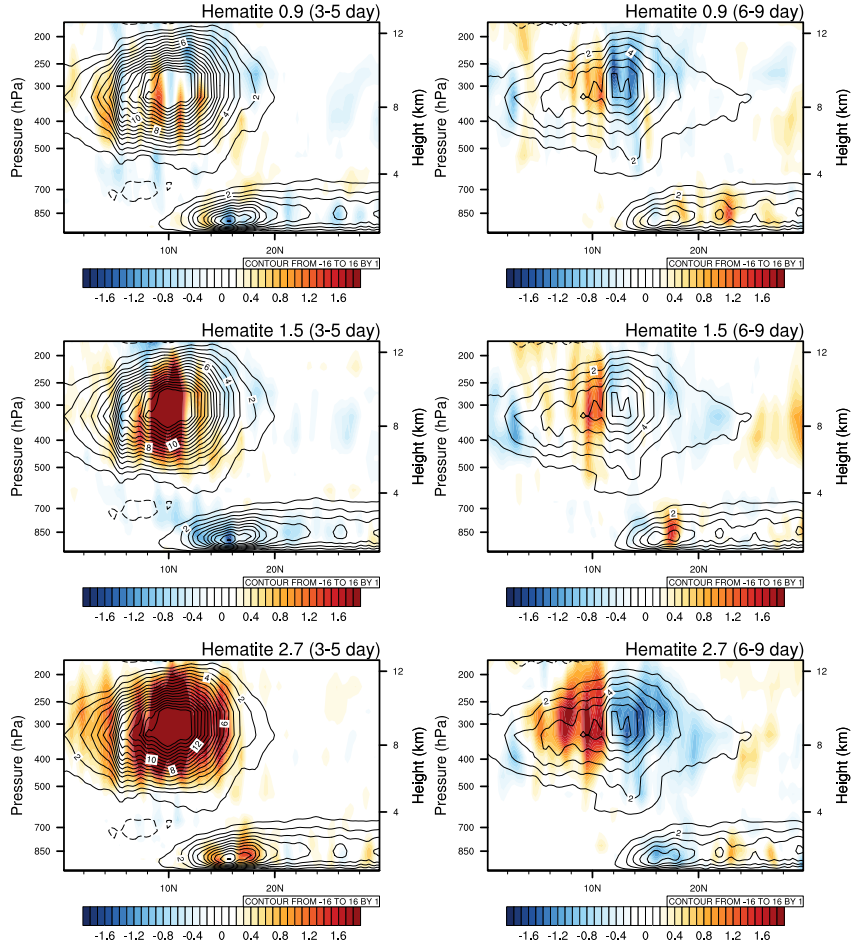


**Figure 5.** Meridional height cross-sections of the baroclinic energy conversion term ( $C_{pk}$ ) averaged ( $15^{\circ}$  W to  $20^{\circ}$  E) over the continental region. Contours represent the values of  $C_{pk}$  in the "NoDUST" simulation, and the shaded contours represent anomalies (DUST-NoDUST) in all three dust experiments.

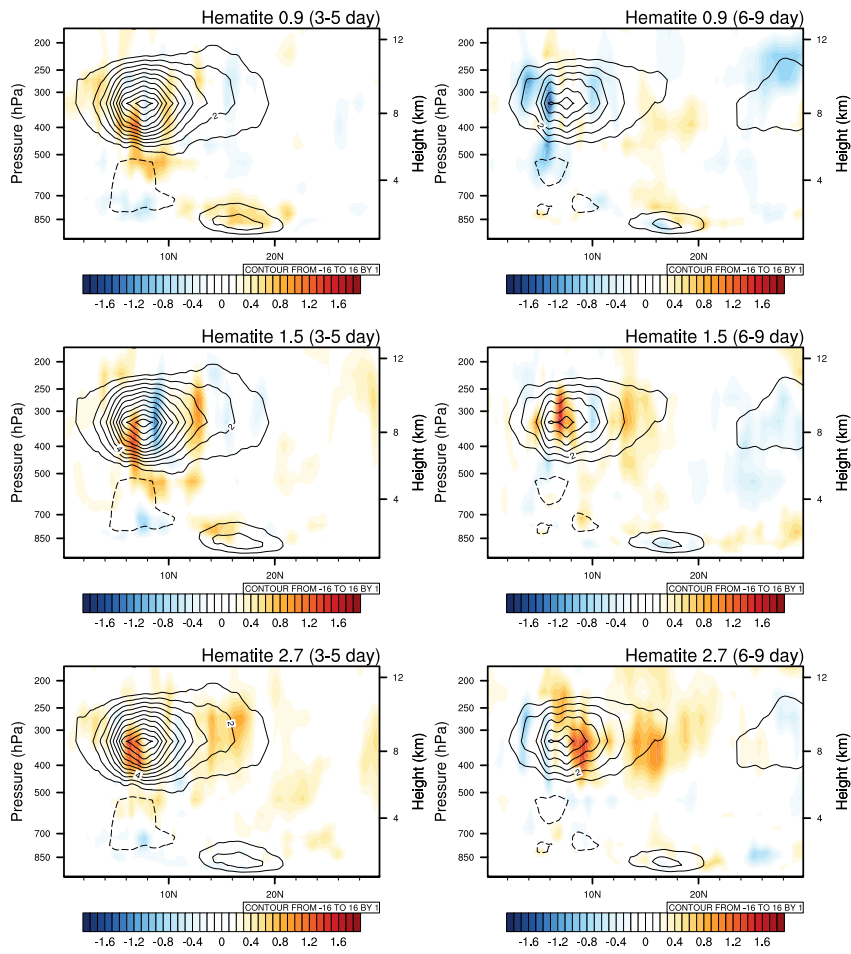


**Figure 6.** Same as Fig. 5, but averaged ( $50^{\circ}$  W to  $15^{\circ}$  W) over the Atlantic.

332 3) as a response to shortwave heating. On either side of the tropical upper tropospheric  
 333 center, the relative change (with respect to the NoDUST case) in  $C_{pk}$  is about 70% in  
 334 the DUST2.7 case. Therefore, the relative change in  $C_{pk}$  is much higher in the 6–9–day  
 335 waves than in the 3–5–day waves. The response in the subtropical lower tropospheric gen-  
 336 eration center also shifts, i.e., it exhibits a dipole response pattern, although the anom-  
 337 alies are weaker. Additionally,  $C_{pk}$  decreases on the southern extent of the subtropics, whereas  
 338  $C_{pk}$  is generated to the north. The dipole pattern enhances and shifts as dust heating  
 339 increases.

340 In the Atlantic (Fig. 6), the baroclinic generation of the EKE associated with both  
 341 3–5–day and 6–9–day waves is weak compared to the continental area because the waves  
 342 start to weaken as they pass through the Atlantic. As in the continental case,  $C_{pk}$  is weaker  
 343 in the 6–9–day waves compared to the 3–5–day waves. The Atlantic 3–5–day case response  
 344 is weaker than its continental counterpart, though there is a stronger increase (more than  
 345 50% increase in the DUST2.7 case) in  $C_{pk}$  to the northern edge of its upper tropospheric  
 346 maxima. Unlike the continental case, the subtropical lower tropospheric maxima reveal  
 347 an increase in the DUST0.9 case, and the response weakens as shortwave absorption in-  
 348 creases. The dipole response pattern in the 6–9–day case is relatively less defined over  
 349 the Atlantic than over land. Instead, widespread energy dissipation occurs in the upper  
 350 troposphere in the DUST0.9 case, whereas the DUST1.5 and DUST2.7 cases primarily  
 351 exhibit energy generation, especially on the northern side. The relative change in  $C_{pk}$   
 352 to the north of the upper tropospheric maxima is about 70% in the high-absorbing dust  
 353 case (DUST2.7).

354 Figure 7 presents  $C_k$ , which is the next most significant EKE-producing term af-  
 355 ter  $C_{pk}$ , over the continent for the 3–5 and 6–9–day waves. There are three energy pro-  
 356 duction (positive centers) regions. The first is in the deep tropics tropopause (around  
 357 200 hPa) associated with the wind shear in the TEJ. The second is in the tropical (cen-  
 358 tered at 10°N) mid-troposphere (850 hPa - 300 hPa) associated with the wind shear in  
 359 the AEJ. The third is in the subtropical (15°N - 25°N) lower troposphere (below 850 hPa)  
 360 associated with Saharan heat low where trade wind meets the dry Harmattan winds (see  
 361 figure 11 Bangalath and Stenchikov (2016)). It has to be noted that the positive barotropic  
 362 energy conversion occurs on the equator side of the AEJ (the jet core is at 12° lat). The  
 363  $C_k$  is close to zero or negative on the poleward flank of the AEJ. In other words, barotropic  
 364 energy conversion that maintains AEWs primarily occurs to the south of the AEJ, where  
 365 mostly 3–5–day waves happen. On the northern side of the jet,  $C_k$  is either small or con-  
 366 sumed. However, a strong production of  $C_k$  occurs below AEJ to the north of the jet core  
 367 associated with the Saharan heat low, where trade winds converge in summer. A large  
 368 region of EKE sink (negative  $C_k$ ) towards the north extends from 850 hPa to the tropopause,  
 369 with the center near the tropopause. This sink is associated with the shear in the sub-  
 370 tropical jet.

371 In the 3–5–day waves (Fig. 7 left column), the generation of the EKE from the  $C_k$   
 372 associated with the wind shear in the equatorward flank of AEJ has an intense response  
 373 to dust shortwave absorption. In the DUST0.9 case, the EKE dissipates in this region,  
 374 whereas the EKE is generated in favor of the AEW as the dust shortwave absorption in-  
 375 creases (DUST0.9 and DUST2.7 cases). In addition,  $C_k$  changes more than 50% between  
 376 DUST0.9 and DUST2.7 cases on the southern side of the AEJ. In the subtropical gen-  
 377 eration center in the lower troposphere,  $C_k$  is generated and increases with dust-induced  
 378 heating. However, the maximum response is observed near the tropopause collocated with  
 379 the TEJ and STJ. As the dust shortwave absorption increases,  $C_k$  reduces in this region.  
 380 The changes in the STJ and TEJ might be caused by AEW modulations or be forced  
 381 by the dust-radiative forcing. However, disentangling these two possible effects and their  
 382 interactions with AEW is beyond the scope of the present paper.

383 In the 6–9–day waves (Fig. 7 left column),  $C_k$  over the AEJ location is relatively  
 384 weaker compared to the 3–5–day waves. The magnitude of response to the dust short-

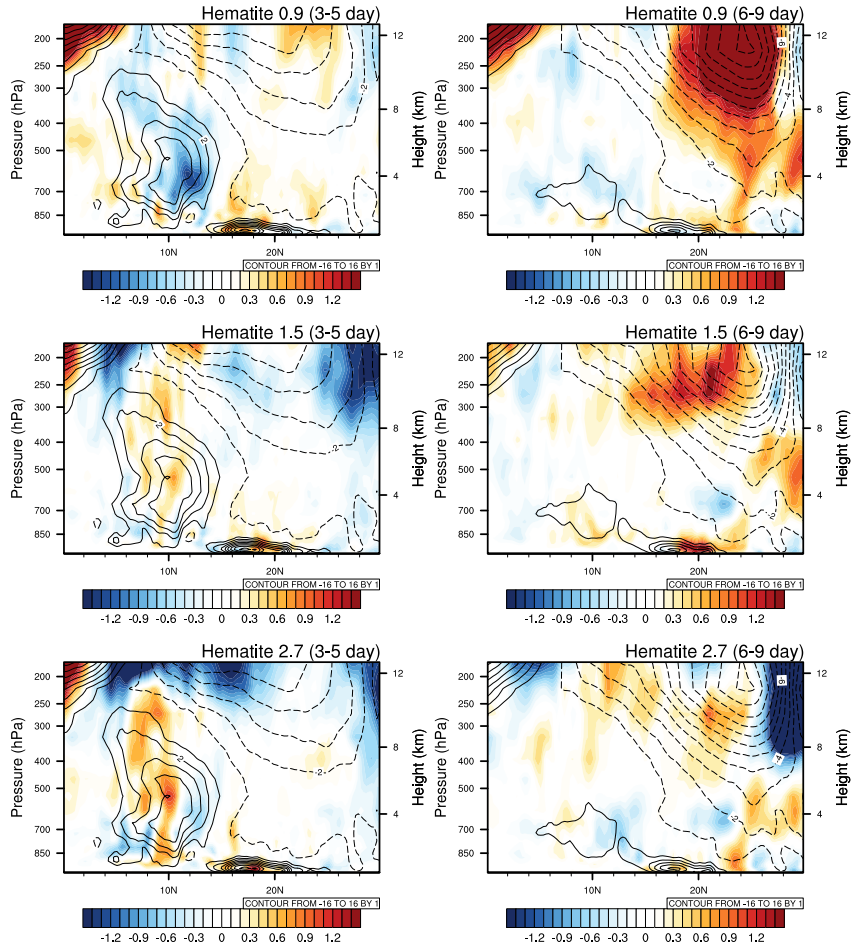


**Figure 7.** Meridional height cross-sections of the barotropic energy conversion term ( $C_k$ ) averaged ( $15^{\circ}$  W to  $20^{\circ}$  E) over the continental region. Contours represent the values of  $C_k$  in the "NoDUST" simulation, and the shaded contours represent anomalies (DUST-NoDUST) in all three dust experiments.

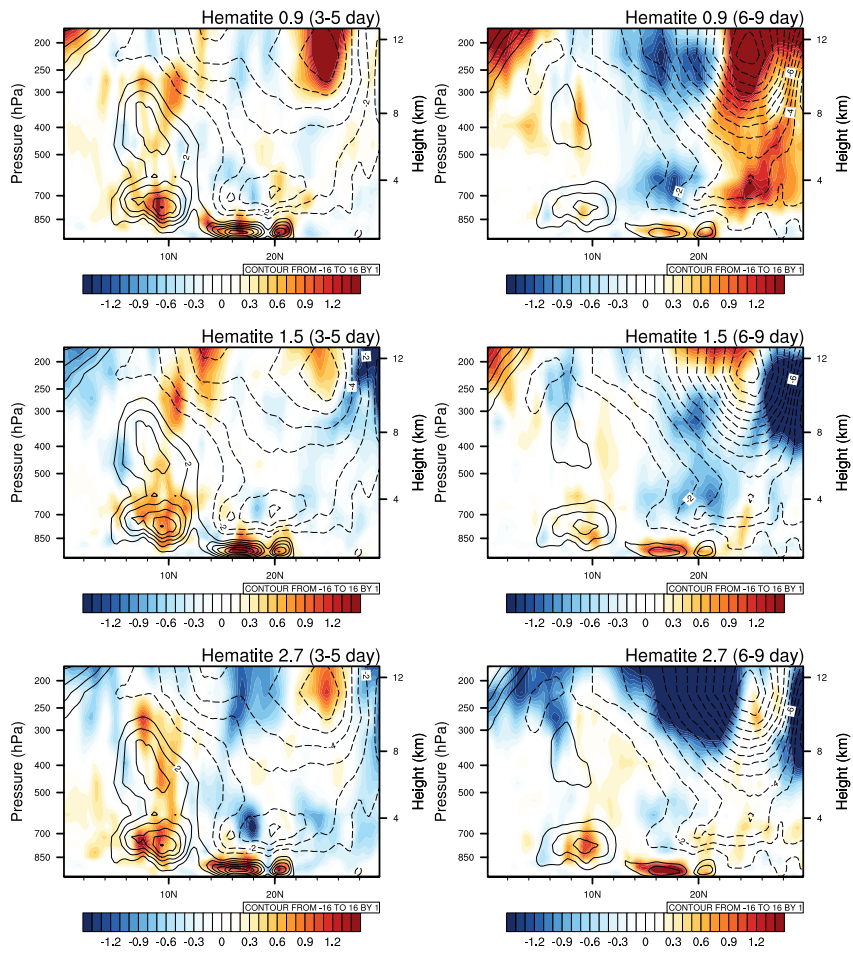


**Figure 8.** Same as Fig. 7, but averaged ( $50^{\circ}$  W to  $15^{\circ}$  W) over the Atlantic.

385 wave absorption is also small, although the relative change is about 40%. Therefore, the  
 386 contribution of the barotropic term in the 6-9-day waves is small compared to the 3-5-  
 387 day waves. In the subtropical lower tropospheric generation center,  $C_k$  increases slightly  
 388 due to dust-induced shortwave heating. In contrast to the 3-5-day case, the response near  
 389 the tropopause associated with STJ is intense in the 6-9-day case.

390 Figure 8 depicts  $C_k$  over the Atlantic. In the 3-5-day waves,  $C_k$  associated with  
 391 the shear of AEJ is intense but more confined to the jet core over the Atlantic compared  
 392 to its continental counterpart. Unlike the continental case, dust causes an increase of  $C_k$   
 393 to the south of the AEJ core in all three cases, strengthening AEWs. The response is  
 394 stronger than that over the continent. The response in the subtropical lower tropospheric  
 395 positive  $C_k$  center is similar to its continental southern part but is more intense (75%).  
 396 In the 6-9-day case also,  $C_k$  associated with the AEJ and its response to dust forcing  
 397 is stronger over the Atlantic than the continent (Fig. 8 right column). As the dust short-  
 398 wave absorption increases, more energy is converted to EKE. The energy generation in  
 399 the 6-9-day AEWs associated with the  $C_k$  term is more sensitive to dust heating over  
 400 the Atlantic than over continental Africa. The response in barotropic terms to the dust  
 401 shortwave absorption is not as linear as in the baroclinic case, which might be because  
 402  $C_k$  involves four individual energy conversion terms, each of which interacts with dust  
 403 forcing differently.

404 The next term in the energy cycle is the generation of EKE through diabatic heating,  $G_E$   
 405 (Fig. 9 and 10). The  $G_E$  has a very similar pattern to that of  $C_{pk}$  with two major gen-  
 406 eration centers at the subtropical lower and tropical upper troposphere. The similarity  
 407 in the pattern of  $G_E$  and  $C_{pk}$  is because the  $G_E$  largely compensates for the  $A_E$  con-  
 408 sumed by the  $C_{pk}$ . A positive  $G_E$  over the tropical upper troposphere is generated by  
 409 the latent heat release from the precipitation, whereas the generation center over the sub-  
 410 subtropical lower troposphere (Sahara) is from dry convection and dust-induced diabatic  
 411 heating. The magnitude of  $G_E$  is almost half that of  $C_{pk}$ .

412 The response of  $G_E$  to shortwave absorption is also very similar to that of  $C_{pk}$ , but  
 413 its magnitude is smaller. However, the relative change in  $G_E$  is generally higher than  
 414 that of  $C_{pk}$ . In the 3-5-day case,  $G_E$  enhances in both the tropical upper and subtrop-  
 415 ical lower tropospheric centers as the dust shortwave absorption increases. The former  
 416 arises from the enhanced precipitation response to dust-radiative heating, and the lat-  
 417 ter is due to increased dust heating and possibly by the enhancement in the dry convec-  
 418 tion over this region. In the DUST2.7 case, approximately 50% increase occurs in the  
 419 3-5-day  $G_E$  compared to the NoDUST case.

420 In the 6-9-day case, the dipole response pattern in  $C_{pk}$  is replicated in  $G_E$ . The  
 421  $G_E$  is generated on the equator side and dissipated over the subtropics. The response  
 422 intensifies as shortwave absorption increases. The response is consistent with the south-  
 423 ward shift of 6-9-day AEWs as a response to dust shortwave heating. Approximately  
 424 75% change occurs in  $G_E$  on either side of the dipole. The subtropical lower tropospheric  
 425 generation center also displays a strong response consistent with the  $C_{pk}$  response. That  
 426 is, generation of  $G_E$  occurs in the less absorbing dust case, and destruction occurs in the  
 427 high absorbing case.

428 Over the Atlantic, the generation of diabatic heating and its response to dust heat-  
 429 ing is smaller than the continental part (almost half). However, there is a significant de-  
 430 crease of  $G_E$  in the tropical lower troposphere under the upper tropospheric positive max-  
 431 ima region. The decrease in  $G_E$  at this location intensifies as the shortwave absorption  
 432 increases.

433 Figures. 11 and 12 depicts the response in the conversion of zonal  $A_E$  to eddy  $A_E$   
 434 due to the eddy heat flux along the zonal mean temperature gradient,  $C_A$ . Unlike other  
 435 terms, only one major location of zonal to eddy  $A_E$  conversion exists, starting from  $12^{\circ}$

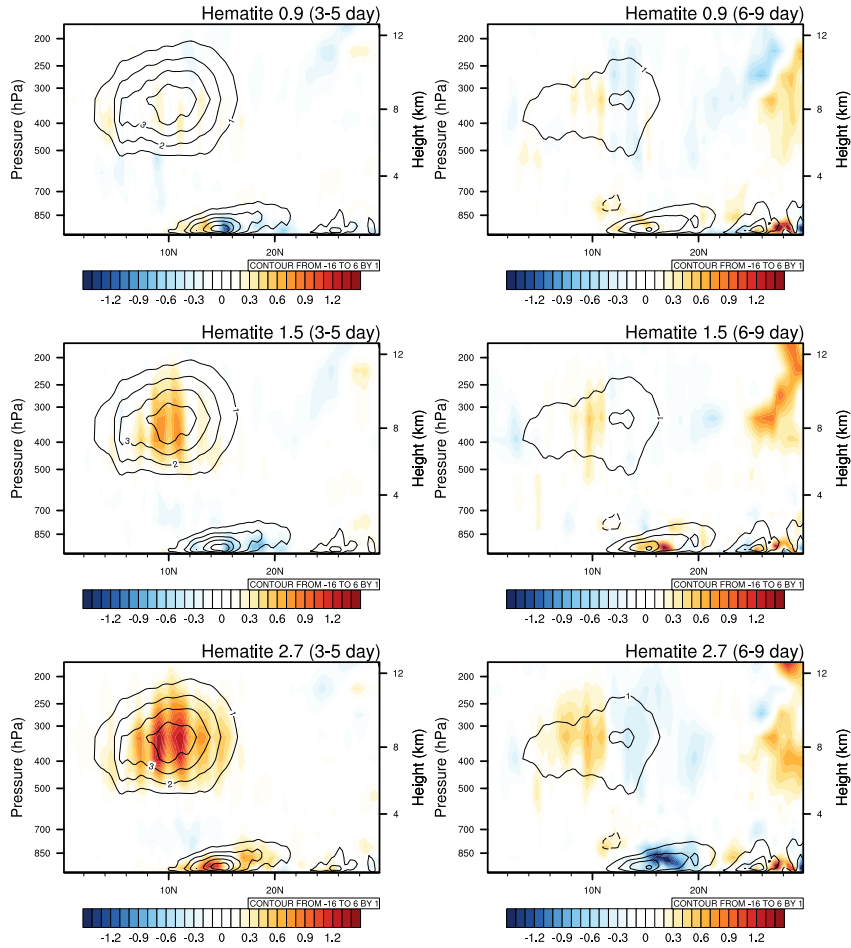


**Figure 9.** Meridional height cross-sections of the barotropic energy conversion term ( $G_E$ ) averaged ( $15^0$  W to  $20^0$  E) over the continental region. Contours represent the values of  $G_E$  in the "NoDUST" simulation, and the shaded contours represent anomalies (DUST-NoDUST) in all three dust experiments.

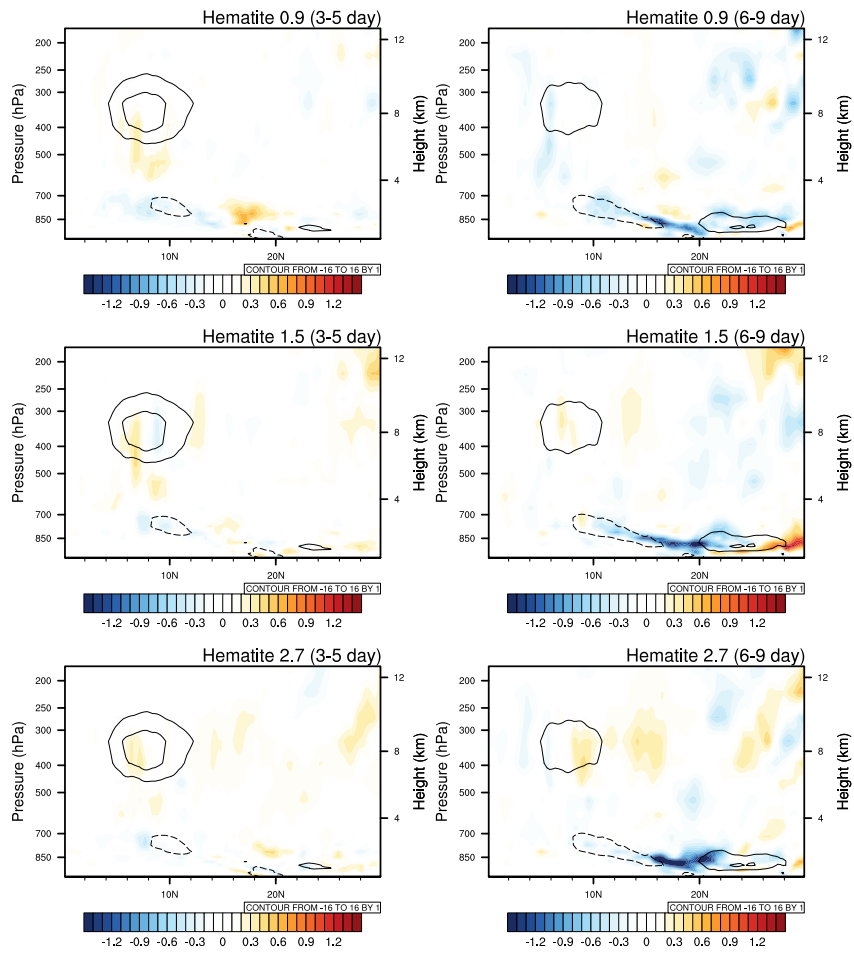


**Figure 10.** Same as Fig. 9, but averaged ( $50^{\circ}$  W to  $15^{\circ}$  W) over the Atlantic.

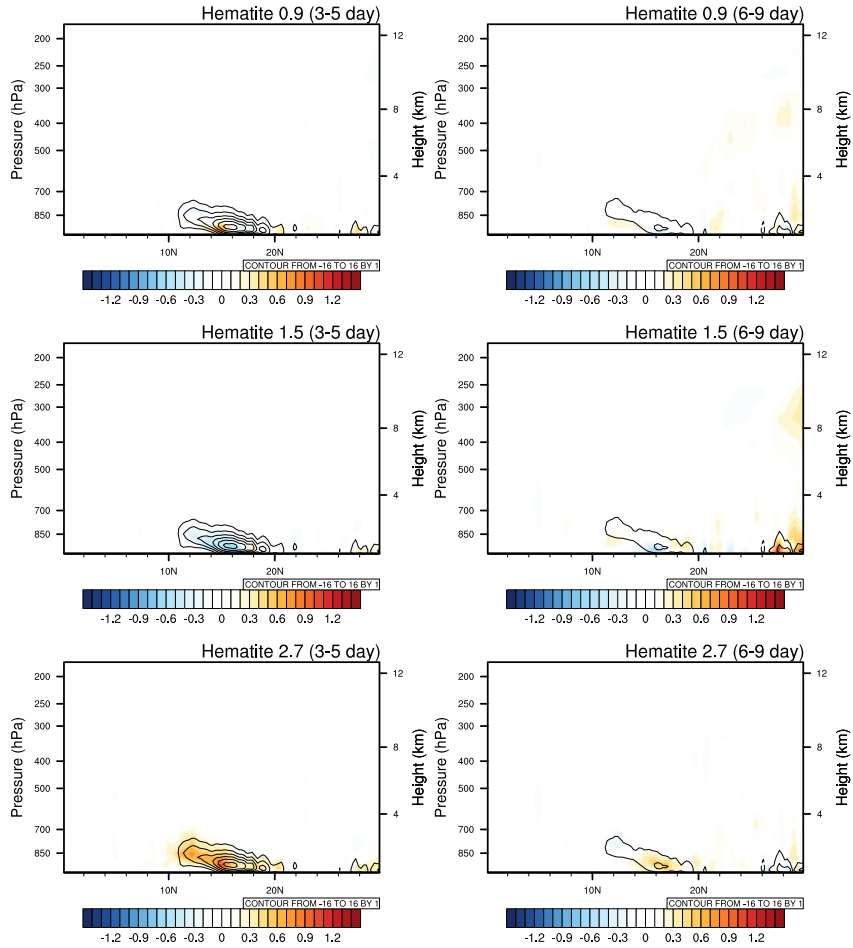


**Figure 11.** Meridional height cross-sections of the barotropic energy conversion term ( $C_A$ ) averaged ( $15^{\circ}$  W to  $20^{\circ}$  E) over the continental region. Contours represent the values of  $C_A$  in the "NoDUST" simulation, and the shaded contours represent anomalies (DUST-NoDUST) in all three dust experiments.

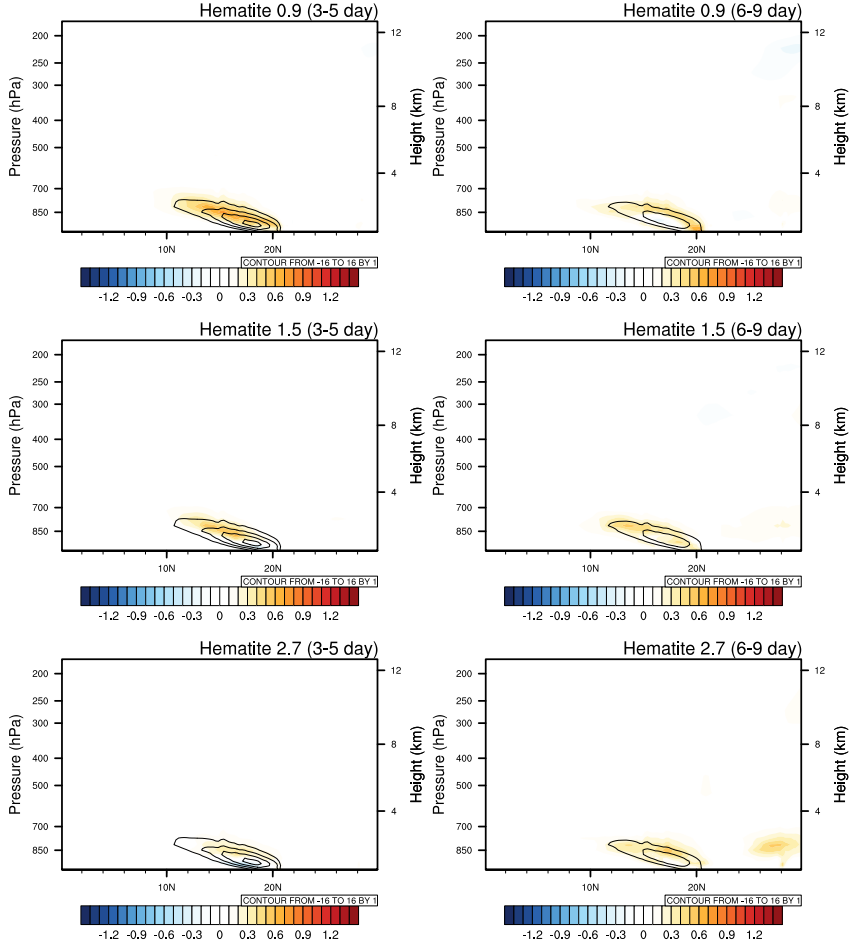


**Figure 12.** Same as Fig. 11, but averaged ( $50^{\circ}$  W to  $15^{\circ}$  W) over the Atlantic.

436 N to  $20^{\circ}$  N in the lower troposphere (below 700 hPa). The magnitude of  $C_A$  over this  
 437 region is comparable to  $G_E$ , indicating a comparable contribution to the baroclinic con-  
 438 version over this region. The leading contribution in  $C_A$  results from the thermal advec-  
 439 tion by the large-scale meridional temperature gradient. The dust shortwave absorption  
 440 heats the subtropical lower-mid troposphere, strengthening the meridional temperature  
 441 gradient and  $C_A$ . In general,  $C_A$  increases with the dust shortwave absorption over the  
 442 African continent (Fig. 11) and vice versa over the Atlantic (Fig. 12). The absolute mag-  
 443 nitude of  $C_A$  and its response to dust heating is small for the 6–9-day case compared with  
 444 the 3–5-day case.

445 **4 Discussion and Summary**

446 The radiative impact of mineral dust aerosols on AEWs over tropical Africa and  
 447 the Atlantic has drawn scientific attention concerning their interactions since the 1970s.  
 448 Although several studies have investigated the role of DDRF in AEW genesis and main-  
 449 tenance, less attention has been focused on the sensitivity of AEWs to the uncertainty  
 450 in dust shortwave absorption. The present study conducted global high-resolution at-  
 451 mospheric simulations with the dust having various shortwave absorption properties to  
 452 assess the sensitivity of the AEWs to dust-induced atmospheric heating rate. The anal-

453 yses were conducted separately for the 3–5–day and 6–9–day waves. We also analyzed the  
454 AEW’s response over the African continent and the tropical Atlantic separately.

455 Generally, AEW activity intensifies and broadens the wave track in response to in-  
456 creased dust shortwave absorption and the consequent increase in atmospheric heating.  
457 The broadening of the track is primarily towards the equator, causing a southward shift  
458 of the track. The 6–9–day waves are more sensitive to dust shortwave absorption, com-  
459 pared to the 3–5–day wave, especially in terms of the percentage change. The 6–9–day  
460 waves weaken over the continent and the Atlantic in the inefficient absorbing case (DUST0.9),  
461 whereas they intensify and broaden over the Atlantic when the dust becomes an efficient  
462 absorber. The response over the continent is minimal, which is weakening of the 6–9–  
463 day waves in all three dust cases, leaving a stark land–sea contrast in the sensitivity of  
464 AEWs to dust heating. In the 3–5–day wave case, no evident land–sea contrast occurs  
465 in response to dust heating. When dust is an inefficient absorber, the 3–5–day waves weaken,  
466 except over the southern flank of the wave track. However, if dust efficiently absorbs short-  
467 wave radiation, the 3–5–day wave track intensifies and broadens in all directions.

468 We analyzed the response in various energetic terms to understand how dust-radiative  
469 heating interacts with AEW dynamics. Baroclinic energy conversion is the leading or-  
470 der term for the maintenance of AEWs. The next two vital terms are the barotropic en-  
471 ergy conversion term and  $A_E$  generation via diabatic heating. Their magnitudes are al-  
472 most half the magnitude of the Baroclinic conversion. For waves on the southern flank  
473 of the AEJ, which are mostly 3–5–day waves, the most crucial energy source is the baro-  
474 clinic energy conversion associated with the tropical vertical overturning, followed by the  
475 zonal to eddy kinetic energy conversion associated with shear in AEJ. However, to the  
476 northern side of the AEJ core, where most of the 6–9–day waves occur, the source of en-  
477 ergy perturbation is primarily from the baroclinic conversion associated with the sub-  
478 tropical dry convection and the northern edge of the tropical overturning. The contri-  
479 bution from the barotropic term is negligible or negative in the mid-troposphere to the  
480 north of the AEJ. However, intense production of barotropic energy conversion is con-  
481 fined to the layer of the atmosphere below 850 hPa. Note that the contribution of the  
482 generation of diabatic heating and conversion of zonal to eddy  $A_E$  reaches up to 700 hPa.

483 The sensitivity of AEWs to dust heating stems from a combination of the response  
484 from various energetic terms. Although baroclinic energy conversion is the leading or-  
485 der term, the response to dust shortwave heating in barotropic and generation terms is  
486 comparable to that in baroclinic conversion. In other words, the relative change (per-  
487 centage change) is higher in barotropic and generation terms than in baroclinic terms  
488 in response to dust. As the dust shortwave absorption increases, baroclinic energy con-  
489 version increases in favor of the AEWs. However, baroclinic energy conversion reduces  
490 in response to dust heating and opposes AEW growth on the poleward side of the AEJ  
491 in 6–9–day waves over the continent. The response of barotropic energy conversion is not  
492 unidirectional. Over the land, barotropic energy conversion associated with the shear on  
493 the AEJ reduces and opposes AEW growth in low-absorbing dust cases and increases  
494 in favor of 3–5–day AEW growth in high-absorbing dust cases. However, the  $C_k$  asso-  
495 ciated with the shear in the trade wind over the Sahara increases in response to dust short-  
496 wave heating rate. In the 6–9–day case over land, significant reduction occurs in  $C_k$  around  
497 the jet core in both low and high-absorbing dust cases. Over the ocean, the  $C_k$  related  
498 to the shear on the AEJ and intertropical depression increases in all dust cases propor-  
499 tionally, in both 3–5–day and 6–9–day waves. The response in the generation term mim-  
500 ics the response in the baroclinic term. In addition,  $G_E$  increases in favor of AEWs in  
501 all cases, except for 6–9–day AEWs over the continent. In the 6–9–day case,  $G_E$  also pro-  
502 duces a dipole pattern of response with the destruction of energy to the north and gen-  
503 eration to the south in response to dust heating. Additionally, there is an intense reduc-  
504 tion in the  $G_E$  in the lower troposphere centered around 20°N over the Atlantic, in a 6-  
505 9–day case. Moreover,  $C_A$  increases in the subtropical lower troposphere below the jet

506 core as a response to dust heating. However, unlike other energetic terms, the  $C_A$  in-  
 507 crease is maximum in the DUST0.9 case for 3–5–day waves over the Atlantic.

508 The land–sea contrast in the response of 6–9–day waves (weakening of EKE over  
 509 the land and strengthening over the ocean) was mostly caused by the dipole pattern of  
 510 response in  $C_{pk}$  and  $G_E$ , which could be understood as a response to enhanced precip-  
 511 itation and weakening of the overturning circulation. The enhanced precipitation and  
 512 associated increase in the latent heat release ( $T'$ ) dominate the response in  $C_{pk}$  in the  
 513 tropics (south of the AEJ), and the reduced overturning circulation ( $\omega'$ ) dominates the  
 514 response north of AEJ.

515 In summary, AEWs are highly sensitive to dust shortwave absorption and conse-  
 516 quent atmosphere heating. The EKE, the proxy for AEW activities, increases (decreases)  
 517 by about 25% compared to NoDUST simulations over the AEW track when the dust is  
 518 assumed to be an efficient absorber (inefficient absorber). It is noteworthy that the AEWs  
 519 exhibit strong seasonal and interannual variabilities, which are expected to change with  
 520 global warming. Moreover, the dust loading and their optical characteristics are also chang-  
 521 ing. Therefore, accurately representing dust optical properties is crucial for better pre-  
 522 dicting AEWs and the overall African climate.

## 523 Appendix A Energy Cycle Terms

524 The energy conversion terms are calculated as follows:

$$C_k = -\overline{\vec{V}'_H \cdot (\vec{V}' \cdot \nabla) \vec{V}'_H} \quad (\text{A1})$$

$$C_{pk} = -\frac{R}{p} \overline{\omega' T'} \quad (\text{A2})$$

$$C_A = -\frac{c_p \gamma}{T} \overline{\vec{V}'_H T' \cdot \nabla_H \bar{T}} \quad (\text{A3})$$

$$G_E = \frac{\gamma}{T} \overline{Q'_1 T'} \quad (\text{A4})$$

525 where  $u$  and  $v$  are zonal and meridional velocities,  $\omega$  represents the vertical pres-  
 526 sure velocity,  $p$  denotes the pressure, and  $T$  denotes the temperature. In addition,  $\gamma =$   
 527  $\frac{\Gamma_d}{\Gamma_d - \Gamma}$ , where  $\Gamma_d$  and  $\Gamma$  are the dry adiabatic and observed lapse rates, respectively. The  
 528  $c_p$  denotes the heat capacity at constant pressure, and  $R$  represents the dry air gas con-  
 529 stant. Finally,  $\sigma$  is the dry static stability.  $Q_1$  is the apparent heat source. The  $Q_1$  is  
 530 calculated as follows:

$$Q_1 = \frac{c_p T}{\theta} \left( \frac{\partial \theta}{\partial t} + u \frac{\partial \theta}{\partial \phi} + v \frac{\partial \theta}{\partial \lambda} + \omega \frac{\partial \theta}{\partial p} \right) \quad (\text{A5})$$

531 where  $\theta$  is the potential temperature.

532 Primes in these equations are calculated using the 3–5–day and 6–9–day Butterworth  
 533 bandpass filter. The higher-order terms in (A1) and (A2) are omitted from the analy-  
 534 sis. The positive and negative values in these figures represent the gain and loss of the  
 535 EKE or eddy available potential energy, respectively.

## 536 Open Research

537 The source code of HiRAM is publicly available online (at <https://www.gfdl.noaa.gov/hiram-quickstart/>). The simulation results, figures, and code are available from the authors upon  
 538 request.  
 539

## Acknowledgments

The research reported in this publication was supported by funding from the King Abdullah University of Science and Technology (KAUST) through the Grant (BAS/1/1309-01-01) and Belmont Forum Grant (REP/1/3963-01-01/RFBR #20-55-75002), "Coastal Ocean Sustainability in Changing Climate (COAST)." For computer time, this research used the resources of the Supercomputing Laboratory at KAUST.

## References

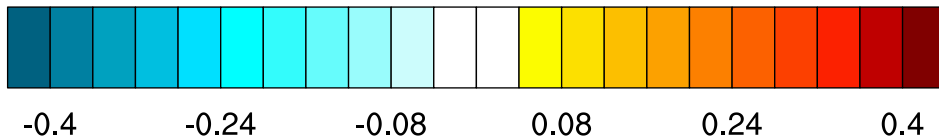
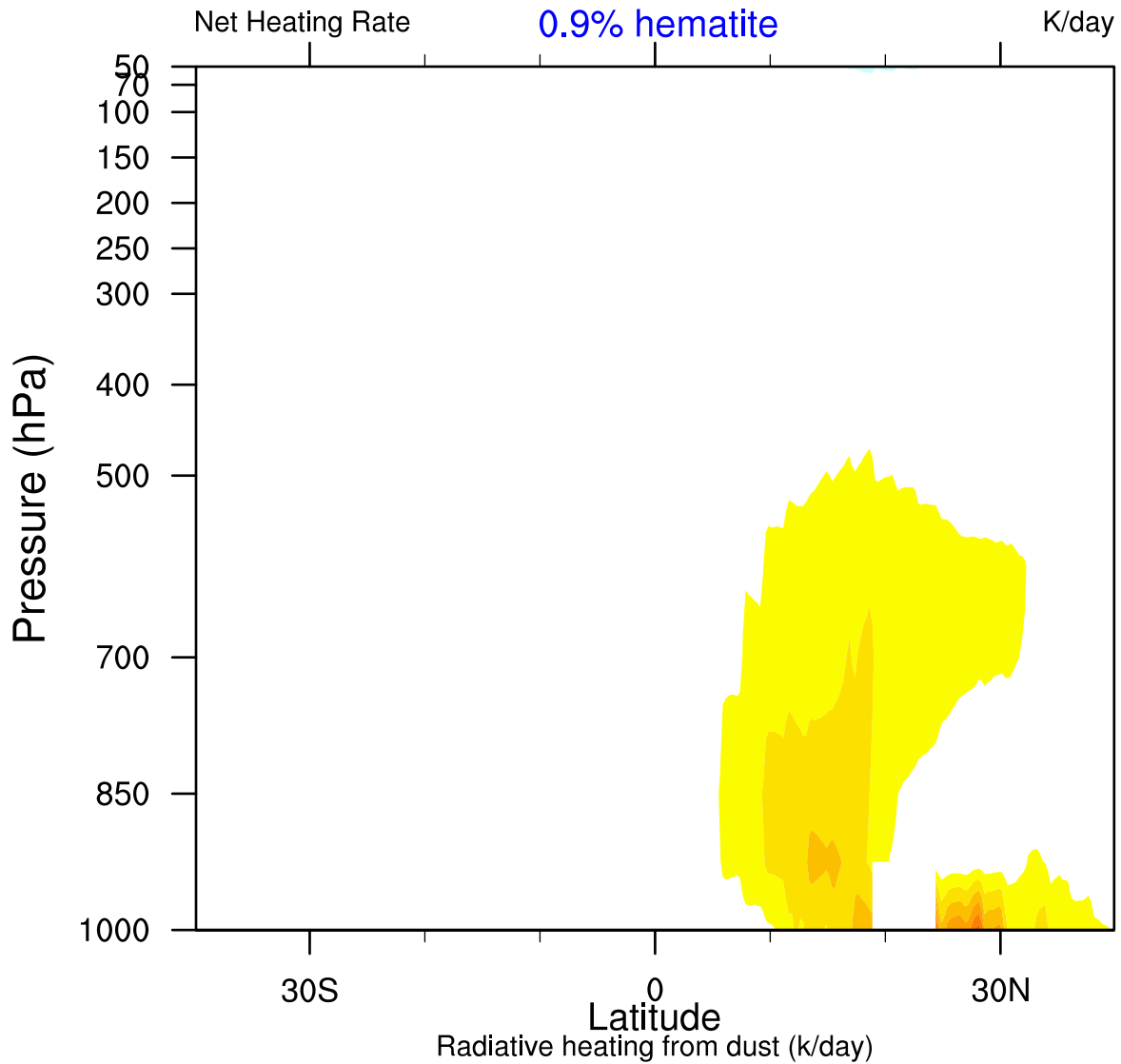
- Balkanski, Y., Schulz, M., Claquin, T., & Guibert, S. (2007). Reevaluation of mineral aerosol radiative forcings suggests a better agreement with satellite and aeronet data. *Atmospheric Chemistry and Physics*, *7*(1), 81–95.
- Bangalath, H. K., & Stenchikov, G. (2015). Role of dust direct radiative effect on the tropical rainbelt over middle east and north africa: A high resolution agcm study. *Journal of Geophysical Research: Atmospheres*, *120*, 4564–4584. doi: 10.1002/2015JD023122
- Bangalath, H. K., & Stenchikov, G. (2016). Sensitivity of the middle east–north african tropical rainbelt to dust shortwave absorption: A high-resolution agcm experiment. *Journal of Climate*, *29*(19), 7103–7126.
- Bercos-Hickey, E., Nathan, T. R., & Chen, S.-H. (2017). Saharan dust and the african easterly jet–african easterly wave system: Structure, location and energetics. *Quarterly Journal of the Royal Meteorological Society*, *143*(708), 2797–2808. Retrieved from <https://rmets.onlinelibrary.wiley.com/doi/abs/10.1002/qj.3128> doi: <https://doi.org/10.1002/qj.3128>
- Bercos-Hickey, E., Nathan, T. R., & Chen, S.-H. (2022). Effects of saharan dust aerosols and west african precipitation on the energetics of african easterly waves. *Journal of the Atmospheric Sciences*, *79*(7), 1911–1926.
- Boyle, J., & Klein, S. A. (2010). Impact of horizontal resolution on climate model forecasts of tropical precipitation and diabatic heating for the twp-ice period. *Journal of Geophysical Research: Atmospheres*, *115*(D23).
- Carlson, T. N., & Prospero, J. M. (1972). The large-scale movement of saharan air outbreaks over the northern equatorial atlantic. *Journal of Applied Meteorology and Climatology*, *11*(2), 283–297.
- Cornforth, R. J., Hoskins, B. J., & Thorncroft, C. D. (2009). The impact of moist processes on the african easterly jet–african easterly wave system. *Quarterly Journal of the Royal Meteorological Society: A journal of the atmospheric sciences, applied meteorology and physical oceanography*, *135*(641), 894–913.
- Diedhiou, A., Janicot, S., Viltard, A., & De Félice, P. (2002). Energetics of easterly wave disturbances over west africa and the tropical atlantic: A climatology from the 1979–95 ncep/ncar reanalyses. *Climate dynamics*, *18*, 487–500.
- Grogan, D. F., Nathan, T. R., & Chen, S.-H. (2016). Effects of saharan dust on the linear dynamics of african easterly waves. *Journal of the Atmospheric Sciences*, *73*(2), 891–911.
- Grogan, D. F., Nathan, T. R., & Chen, S.-H. (2017). Saharan dust and the nonlinear evolution of the african easterly jet–african easterly wave system. *Journal of the Atmospheric Sciences*, *74*(1), 27–47.
- Grogan, D. F., & Thorncroft, C. D. (2019). The characteristics of african easterly waves coupled to saharan mineral dust aerosols. *Quarterly Journal of the Royal Meteorological Society*, *145*(720), 1130–1146.
- Hall, N. M., Kiladis, G. N., & Thorncroft, C. D. (2006). Three-dimensional structure and dynamics of african easterly waves. part ii: Dynamical modes. *Journal of the atmospheric sciences*, *63*(9), 2231–2245.
- Haywood, J., Francis, P., Osborne, S., Glew, M., Loeb, N., Highwood, E., . . . Hirst, E. (2003). Radiative properties and direct radiative effect of saharan dust measured by the c-130 aircraft during shade: 1. solar spectrum. *Journal of*

- 593 *Geophysical Research: Atmospheres*, 108(D18). Retrieved from [https://](https://agupubs.onlinelibrary.wiley.com/doi/abs/10.1029/2002JD002687)  
 594 [agupubs.onlinelibrary.wiley.com/doi/abs/10.1029/2002JD002687](https://agupubs.onlinelibrary.wiley.com/doi/abs/10.1029/2002JD002687) doi:  
 595 <https://doi.org/10.1029/2002JD002687>
- 596 Haywood, J. M., Francis, P. N., Glew, M. D., & Taylor, J. P. (2001). Optical  
 597 properties and direct radiative effect of saharan dust: A case study of two  
 598 saharan dust outbreaks using aircraft data. *Journal of Geophysical Re-*  
 599 *search: Atmospheres*, 106(D16), 18417-18430. Retrieved from [https://](https://agupubs.onlinelibrary.wiley.com/doi/abs/10.1029/2000JD900319)  
 600 [agupubs.onlinelibrary.wiley.com/doi/abs/10.1029/2000JD900319](https://agupubs.onlinelibrary.wiley.com/doi/abs/10.1029/2000JD900319) doi:  
 601 <https://doi.org/10.1029/2000JD900319>
- 602 Hsieh, J.-S., & Cook, K. H. (2007). A study of the energetics of african easterly  
 603 waves using a regional climate model. *Journal of the Atmospheric Sciences*,  
 604 64(2), 421-440. Retrieved from <https://doi.org/10.1175/JAS3851.1> doi:  
 605 10.1175/JAS3851.1
- 606 Jones, C., Mahowald, N., & Luo, C. (2004). Observational evidence of african desert  
 607 dust intensification of easterly waves. *Geophysical research letters*, 31(17).
- 608 Jung, T., Miller, M., Palmer, T., Towers, P., Wedi, N., Achuthavarier, D., ... oth-  
 609 ers (2012). High-resolution global climate simulations with the ecmwf model  
 610 in project athena: Experimental design, model climate, and seasonal forecast  
 611 skill. *Journal of Climate*, 25(9), 3155-3172.
- 612 Jury, M. R., & Santiago, M. J. (2010). Composite analysis of dust impacts on  
 613 african easterly waves in the moderate resolution imaging spectrometer era.  
 614 *Journal of Geophysical Research: Atmospheres*, 115(D16).
- 615 Karyampudi, V. M., & Carlson, T. N. (1988). Analysis and numerical simulations  
 616 of the saharan air layer and its effect on easterly wave disturbances. *Journal of*  
 617 *the Atmospheric Sciences*, 45(21), 3102-3136.
- 618 Kaufman, Y. J., Tanré, D., Dubovik, O., Karnieli, A., & Remer, L. A. (2001).  
 619 Absorption of sunlight by dust as inferred from satellite and ground-based  
 620 remote sensing. *Geophysical Research Letters*, 28(8), 1479-1482. Retrieved  
 621 from [https://agupubs.onlinelibrary.wiley.com/doi/abs/10.1029/](https://agupubs.onlinelibrary.wiley.com/doi/abs/10.1029/2000GL012647)  
 622 [2000GL012647](https://agupubs.onlinelibrary.wiley.com/doi/abs/10.1029/2000GL012647) doi: <https://doi.org/10.1029/2000GL012647>
- 623 Landsea, C. W. (1993). A climatology of intense (or major) atlantic hurri-  
 624 canes. *Monthly Weather Review*, 121(6), 1703 - 1713. Retrieved from  
 625 [https://journals.ametsoc.org/view/journals/mwre/121/6/1520-0493](https://journals.ametsoc.org/view/journals/mwre/121/6/1520-0493_1993_121_1703_acoima_2_0_co_2.xml)  
 626 [\\_1993\\_121\\_1703\\_acoima\\_2\\_0\\_co\\_2.xml](https://journals.ametsoc.org/view/journals/mwre/121/6/1520-0493_1993_121_1703_acoima_2_0_co_2.xml) doi: 10.1175/1520-0493(1993)121<1703:  
 627 ACOIMA>2.0.CO;2
- 628 Lau, N.-C., & Ploshay, J. J. (2009). Simulation of synoptic-and subsynoptic-scale  
 629 phenomena associated with the east asian summer monsoon using a high-  
 630 resolution gcm. *Monthly Weather Review*, 137(1), 137-160.
- 631 Lavaysse, C., Chaboureaud, J.-P., & Flamant, C. (2011). Dust impact on the west  
 632 african heat low in summertime. *Quarterly Journal of the Royal Meteorological*  
 633 *Society*, 137(658), 1227-1240. Retrieved from [https://rmets.onlinelibrary](https://rmets.onlinelibrary.wiley.com/doi/abs/10.1002/qj.844)  
 634 [.wiley.com/doi/abs/10.1002/qj.844](https://rmets.onlinelibrary.wiley.com/doi/abs/10.1002/qj.844) doi: <https://doi.org/10.1002/qj.844>
- 635 Lorenz, E. N. (1955). Available potential energy and the maintenance of the general  
 636 circulation. *Tellus*, 7(2), 157-167.
- 637 Ma, P.-L., Zhang, K., Shi, J. J., Matsui, T., & Arking, A. (2012). Direct radi-  
 638 ative effect of mineral dust on the development of african easterly waves in late  
 639 summer, 2003-07. *Journal of applied meteorology and climatology*, 51(12),  
 640 2090-2104.
- 641 Miller, R., Perlwitz, J., & Tegen, I. (2004). Feedback upon dust emission by dust  
 642 radiative forcing through the planetary boundary layer. *Journal of Geophysical*  
 643 *Research: Atmospheres*, 109(D24).
- 644 Muench, H. S. (1965). On the dynamics of the wintertime stratosphere circula-  
 645 tion. *Journal of Atmospheric Sciences*, 22(4), 349 - 360. Retrieved from  
 646 [https://journals.ametsoc.org/view/journals/atsc/22/4/1520-0469](https://journals.ametsoc.org/view/journals/atsc/22/4/1520-0469_1965_022_0349_otdotw_2_0_co_2.xml)  
 647 [\\_1965\\_022\\_0349\\_otdotw\\_2\\_0\\_co\\_2.xml](https://journals.ametsoc.org/view/journals/atsc/22/4/1520-0469_1965_022_0349_otdotw_2_0_co_2.xml) doi: 10.1175/1520-0469(1965)022<0349:

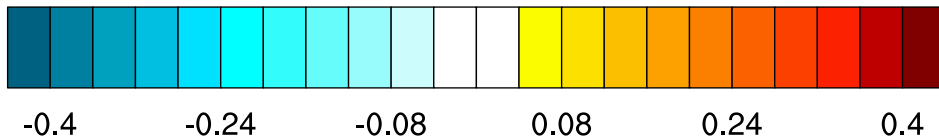
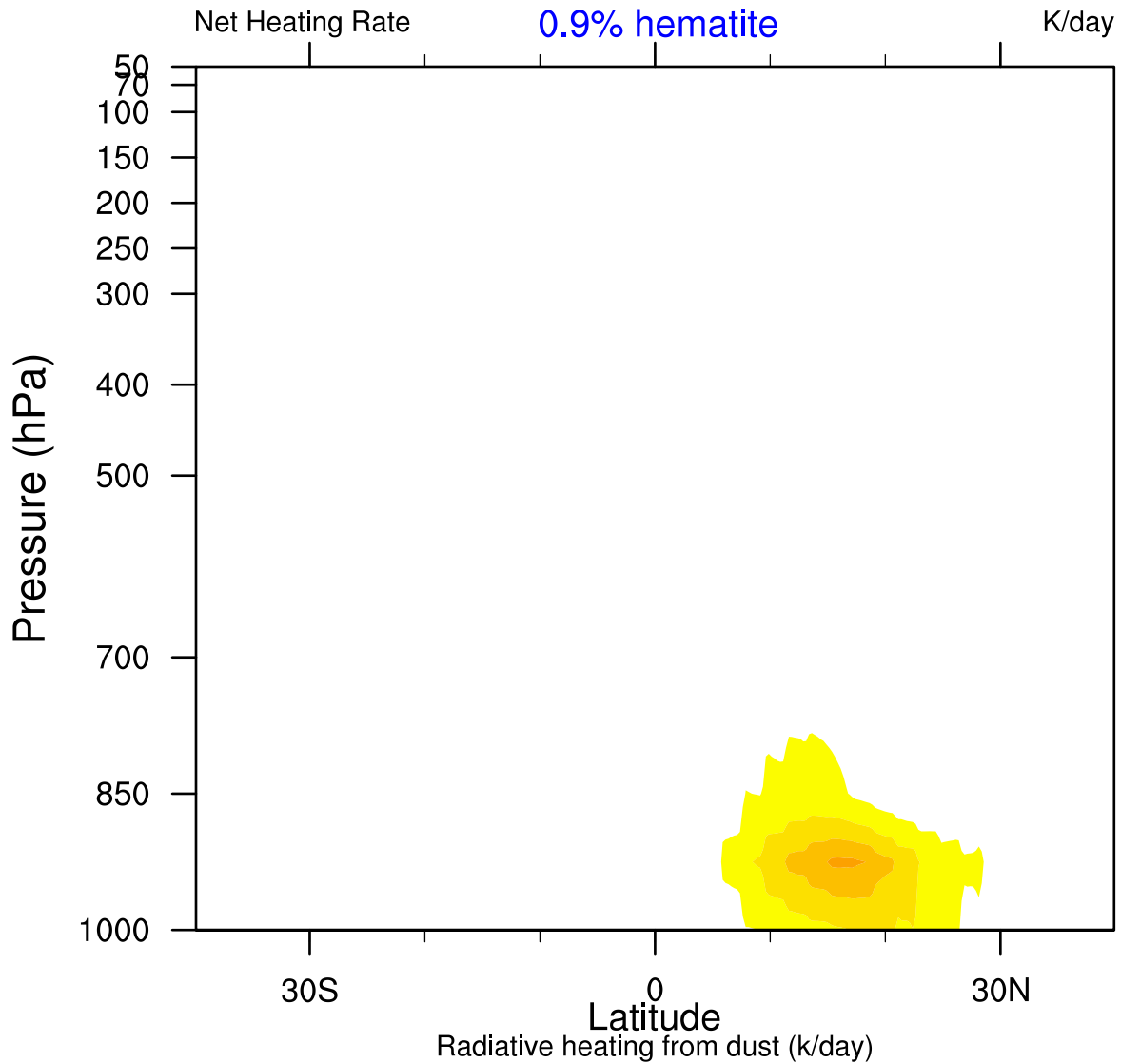
- OTDOTW)2.0.CO;2
- 648 Nathan, T. R., Grogan, D. F., & Chen, S.-H. (2017). Subcritical destabilization  
649 of african easterly waves by saharan mineral dust. *Journal of the Atmospheric*  
650 *Sciences*, *74*(4), 1039–1055.
- 651 Norquist, D. C., Recker, E. E., & Reed, R. J. (1977). The energetics of african  
652 wave disturbances as observed during phase iii of gate. *Monthly Weather Re-*  
653 *view*, *105*(3), 334–342.
- 654 Osipov, S., Stenchikov, G., Brindley, H., & Banks, J. (2015). Diurnal cycle of the  
655 dust instantaneous direct radiative forcing over the arabian peninsula. *Atmo-*  
656 *spheric Chemistry and Physics*, *15*(16), 9537–9553.
- 657 Otto, S., Bierwirth, E., Weinzierl, B., Kandler, K., Esselborn, M., Tesche, M., ...  
658 Trautmann, T. (2009). Solar radiative effects of a saharan dust plume ob-  
659 served during samum assuming spheroidal model particles. *Tellus B: Chemical*  
660 *and Physical Meteorology*, *61*(1), 270–296.
- 661 Patricola, C. M., Saravanan, R., & Chang, P. (2018). The response of at-  
662 lantic tropical cyclones to suppression of african easterly waves. *Geo-*  
663 *physical Research Letters*, *45*(1), 471–479. Retrieved from [https://](https://agupubs.onlinelibrary.wiley.com/doi/abs/10.1002/2017GL076081)  
664 [agupubs.onlinelibrary.wiley.com/doi/abs/10.1002/2017GL076081](https://agupubs.onlinelibrary.wiley.com/doi/abs/10.1002/2017GL076081) doi:  
665 <https://doi.org/10.1002/2017GL076081>
- 666 Raj, J., Bangalath, H. K., & Stenchikov, G. L. (2022). Future projection of the  
667 african easterly waves in a high-resolution atmospheric general circulation  
668 model.  
669 doi: <https://doi.org/10.21203/rs.3.rs-1501278/v1>
- 670 Raut, J.-C., & Chazette, P. (2008). Radiative budget in the presence of multi-  
671 layered aerosol structures in the framework of amma sop-0. *Atmospheric*  
672 *Chemistry and Physics*, *8*(22), 6839–6864.
- 673 Rayner, N., Parker, D. E., Horton, E., Folland, C. K., Alexander, L. V., Rowell, D.,  
674 ... Kaplan, A. (2003). Global analyses of sea surface temperature, sea ice,  
675 and night marine air temperature since the late nineteenth century. *Journal of*  
676 *Geophysical Research: Atmospheres*, *108*(D14).
- 677 Reale, O., Lau, W. K., Kim, K.-M., & Brin, E. (2009). Atlantic tropical cycloge-  
678 netic processes during sop-3 namma in the geos-5 global data assimilation and  
679 forecast system. *Journal of the atmospheric sciences*, *66*(12), 3563–3578.
- 680 Russell, J. O., Ayyer, A., White, J. D., & Hannah, W. (2017). Revisiting the con-  
681 nection between african easterly waves and atlantic tropical cyclogenesis. *Geo-*  
682 *physical Research Letters*, *44*(1), 587–595. Retrieved from [https://agupubs](https://agupubs.onlinelibrary.wiley.com/doi/abs/10.1002/2016GL071236)  
683 [.onlinelibrary.wiley.com/doi/abs/10.1002/2016GL071236](https://agupubs.onlinelibrary.wiley.com/doi/abs/10.1002/2016GL071236) doi: [https://](https://doi.org/10.1002/2016GL071236)  
684 [doi.org/10.1002/2016GL071236](https://doi.org/10.1002/2016GL071236)
- 685 Slingo, A., Ackerman, T. P., Allan, R. P., Kassianov, E. I., McFarlane, S. A.,  
686 Robinson, G. J., ... Dewitte, S. (2006). Observations of the impact of  
687 a major saharan dust storm on the atmospheric radiation balance. *Geo-*  
688 *physical Research Letters*, *33*(24). Retrieved from [https://agupubs](https://agupubs.onlinelibrary.wiley.com/doi/abs/10.1029/2006GL027869)  
689 [.onlinelibrary.wiley.com/doi/abs/10.1029/2006GL027869](https://agupubs.onlinelibrary.wiley.com/doi/abs/10.1029/2006GL027869) doi:  
690 <https://doi.org/10.1029/2006GL027869>
- 691 Solmon, F., Mallet, M., Elguindi, N., Giorgi, F., Zakey, A., & Konaré, A. (2008).  
692 Dust aerosol impact on regional precipitation over western africa, mechanisms  
693 and sensitivity to absorption properties. *Geophysical Research Letters*, *35*(24).
- 694 Thorncroft, C. D., & Hoskins, B. J. (1994a). An idealized study of african  
695 easterly waves. i: A linear view. *Quarterly Journal of the Royal Mete-*  
696 *orological Society*, *120*(518), 953–982. Retrieved from [https://rmets](https://rmets.onlinelibrary.wiley.com/doi/abs/10.1002/qj.49712051809)  
697 [.onlinelibrary.wiley.com/doi/abs/10.1002/qj.49712051809](https://rmets.onlinelibrary.wiley.com/doi/abs/10.1002/qj.49712051809) doi:  
698 <https://doi.org/10.1002/qj.49712051809>
- 699 Thorncroft, C. D., & Hoskins, B. J. (1994b). An idealized study of african  
700 easterly waves. i: A linear view. *Quarterly Journal of the Royal Mete-*  
701 *orological Society*, *120*(518), 953–982. Retrieved from [https://rmets](https://rmets.onlinelibrary.wiley.com/doi/abs/10.1002/qj.49712051809)  
702 [.onlinelibrary.wiley.com/doi/abs/10.1002/qj.49712051809](https://rmets.onlinelibrary.wiley.com/doi/abs/10.1002/qj.49712051809)

- 703            [.onlinelibrary.wiley.com/doi/abs/10.1002/qj.49712051809](https://onlinelibrary.wiley.com/doi/abs/10.1002/qj.49712051809)            doi:  
704            <https://doi.org/10.1002/qj.49712051809>  
705    Yanai, M. (1961). Dynamical aspects of typhoon formation. *Journal of the Meteorological Society of Japan. Ser. II*, 39(5), 282–309.  
706              
707    Zhao, M., Held, I. M., Lin, S.-J., & Vecchi, G. A. (2009). Simulations of global  
708    hurricane climatology, interannual variability, and response to global warming  
709    using a 50-km resolution gcm. *Journal of Climate*, 22(24), 6653–6678. doi:  
710    10.1175/2009JCLI3049.1

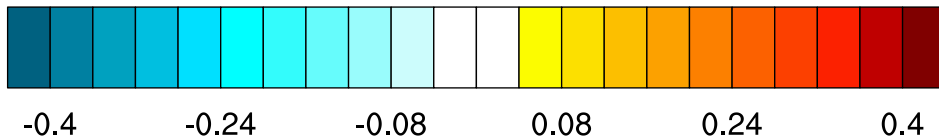
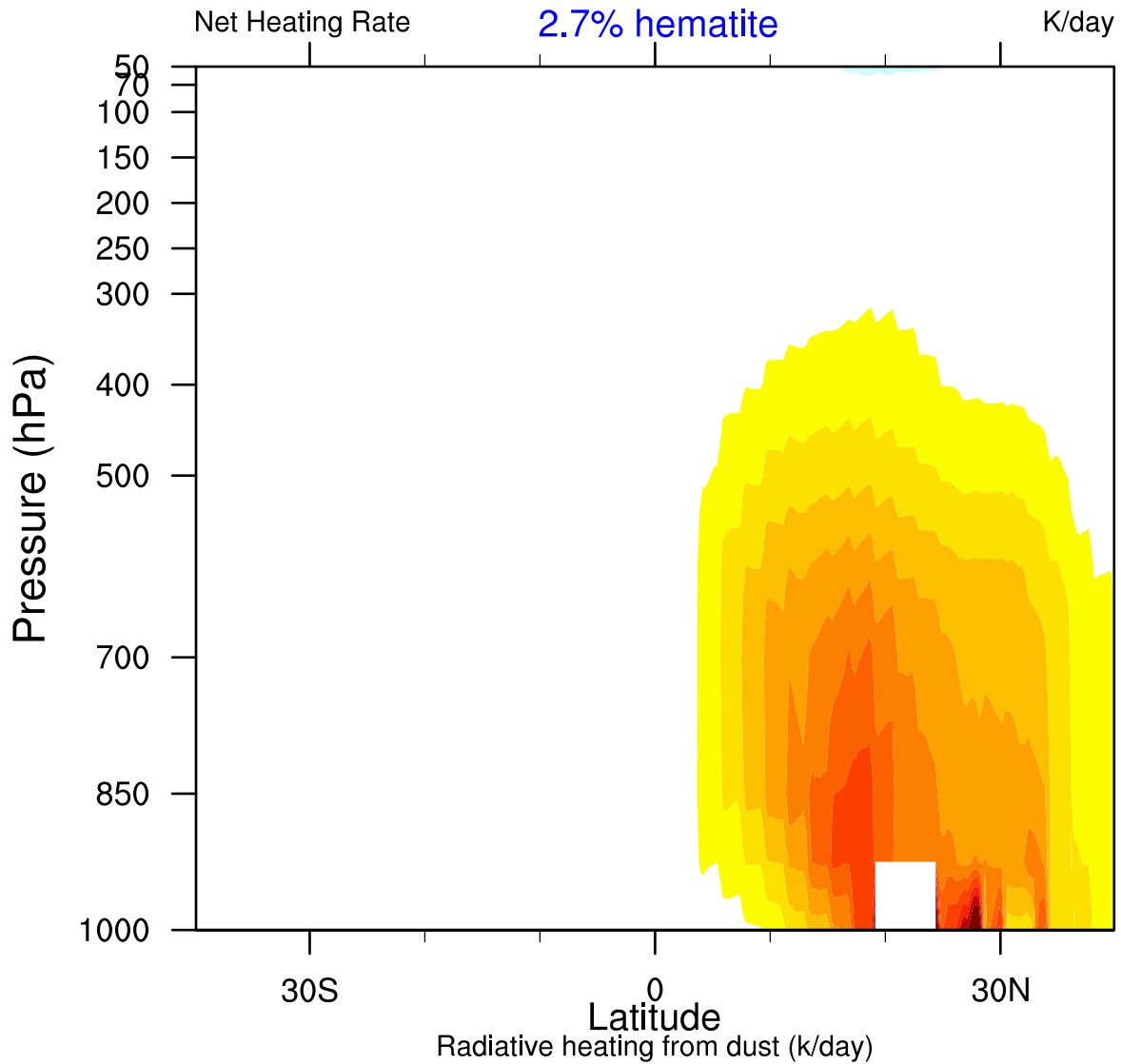




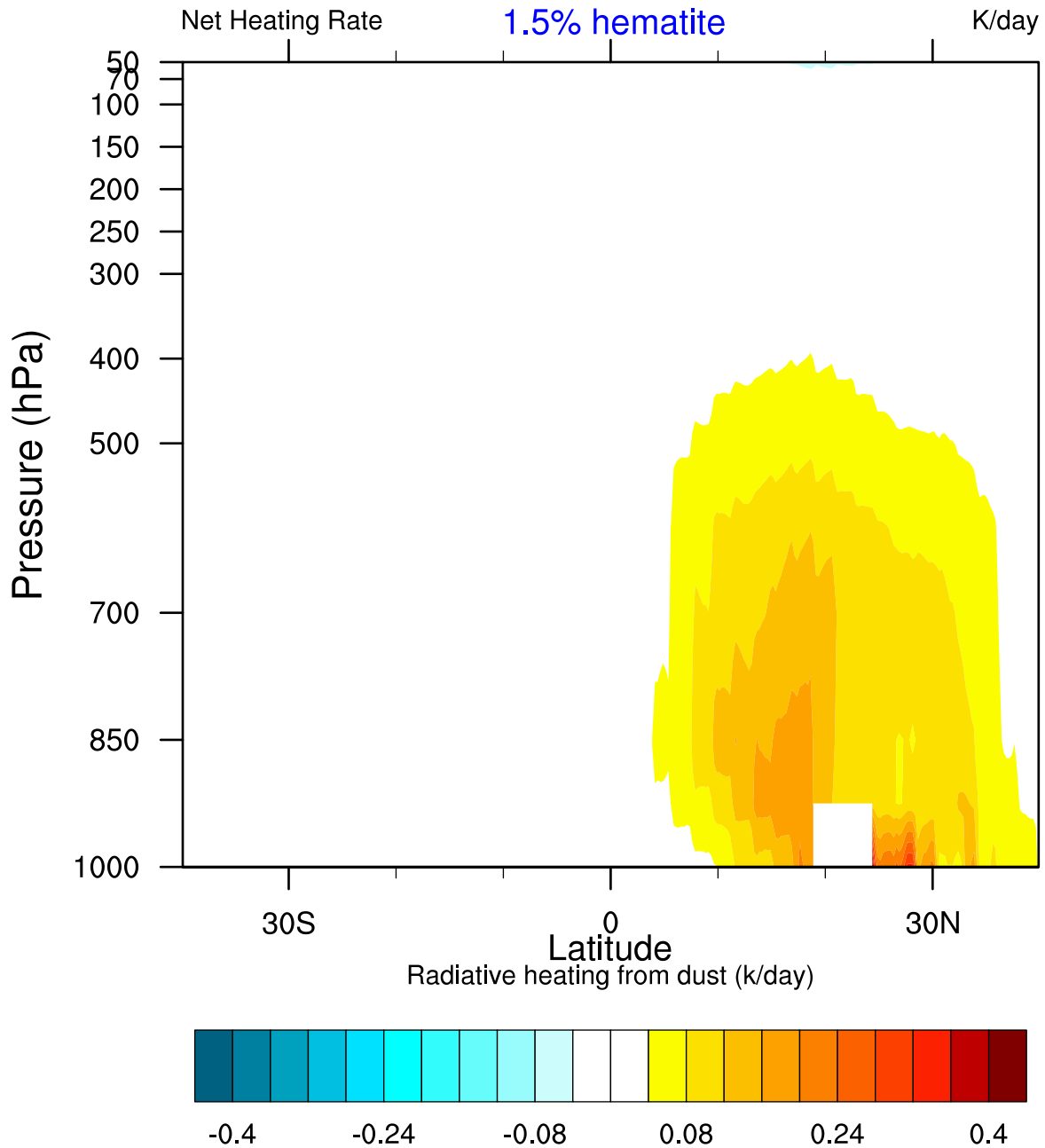
Net\_HeatingMeridionaMENA\_ocean\_JJA09.eps.



Net\_HeatingMeridionaMENA\_land\_JJA27.eps.



Net\_HeatingMeridionaMENA\_land\_JJA15.eps.

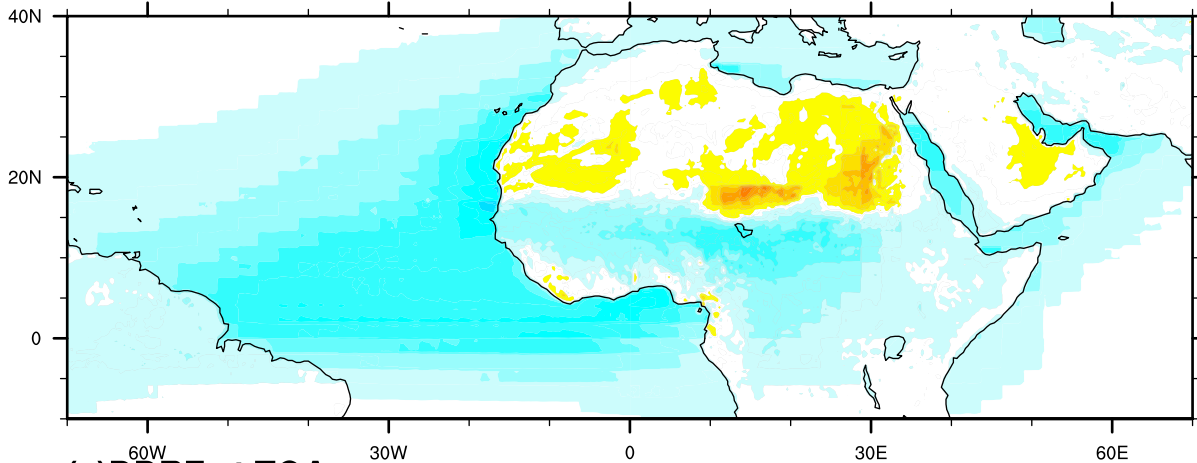


DDRF\_TOA\_ALL\_MENA\_JJAS.eps.

**(c) DDRF at TOA**

**0.9% hematite**

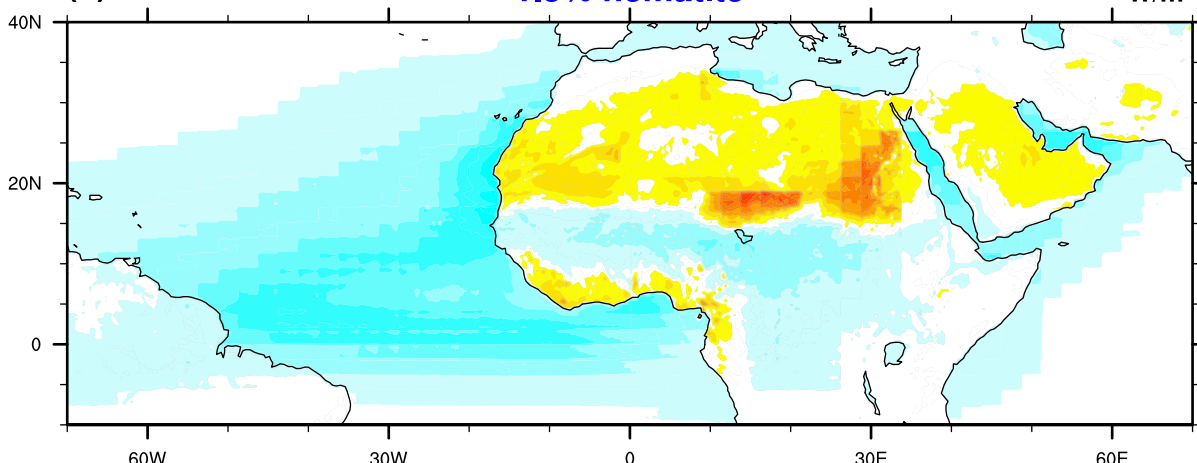
**W/m<sup>2</sup>**



**(a) DDRF at TOA**

**1.5% hematite**

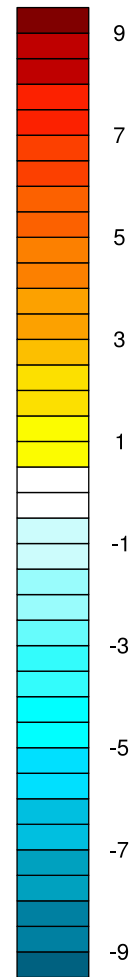
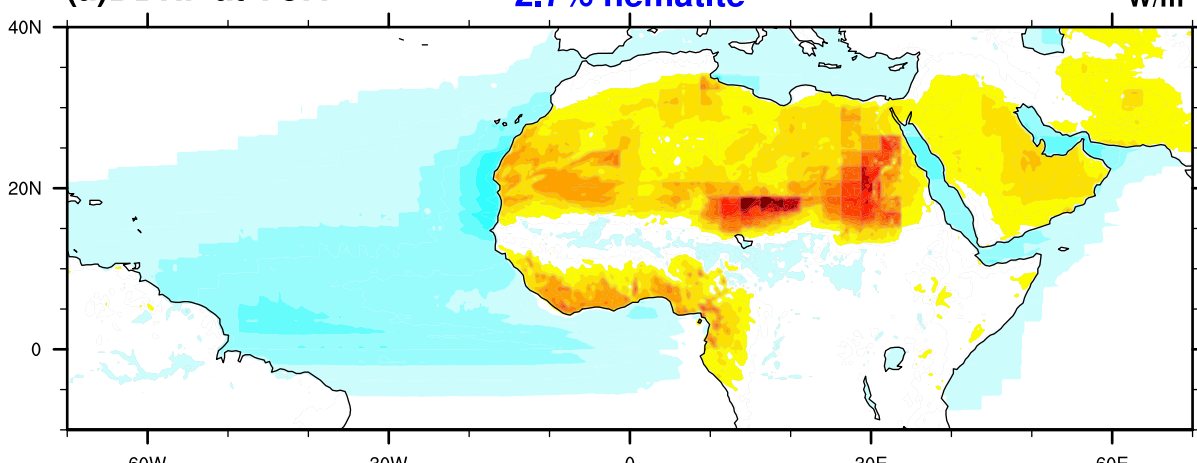
**W/m<sup>2</sup>**



**(a) DDRF at TOA**

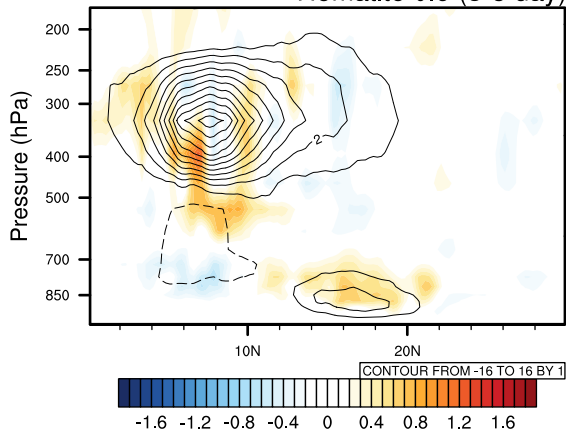
**2.7% hematite**

**W/m<sup>2</sup>**

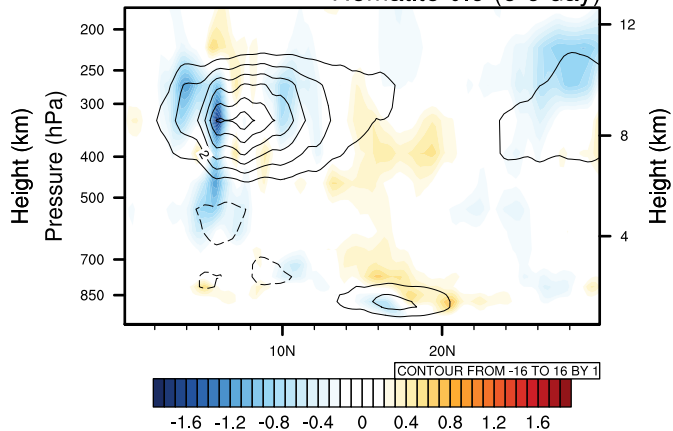


bc\_ocean.eps.

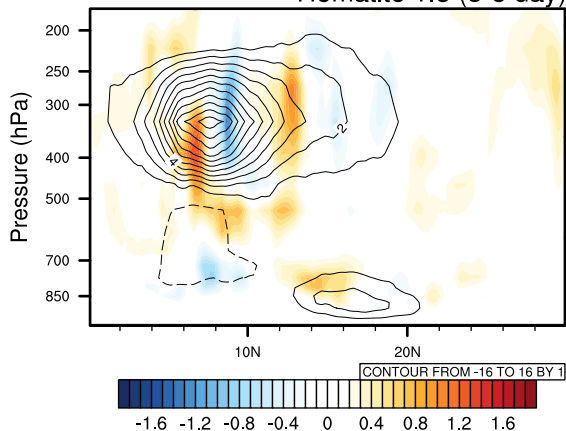
Hematite 0.9 (3-5 day)



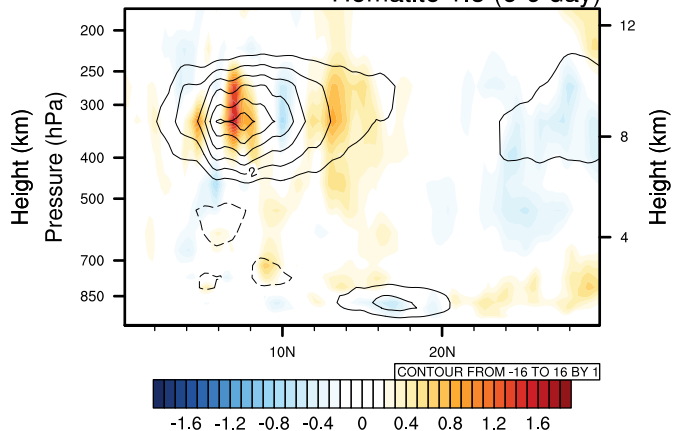
Hematite 0.9 (6-9 day)



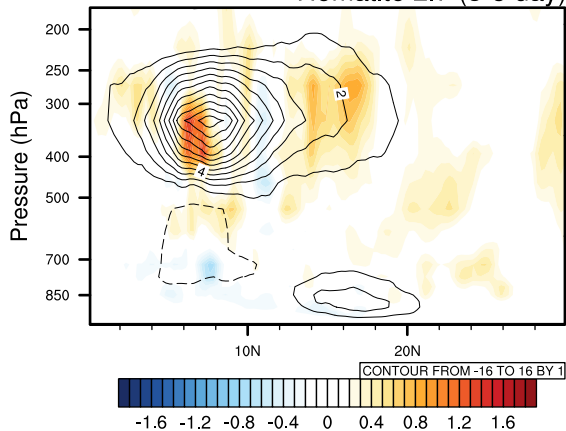
Hematite 1.5 (3-5 day)



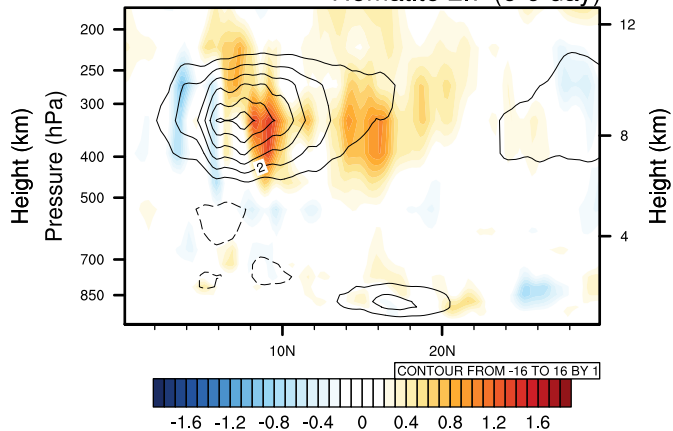
Hematite 1.5 (6-9 day)



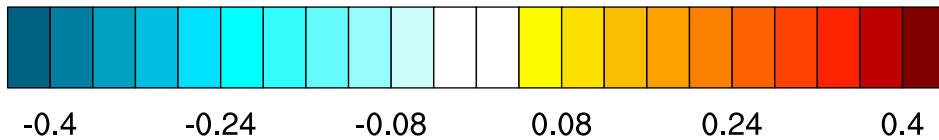
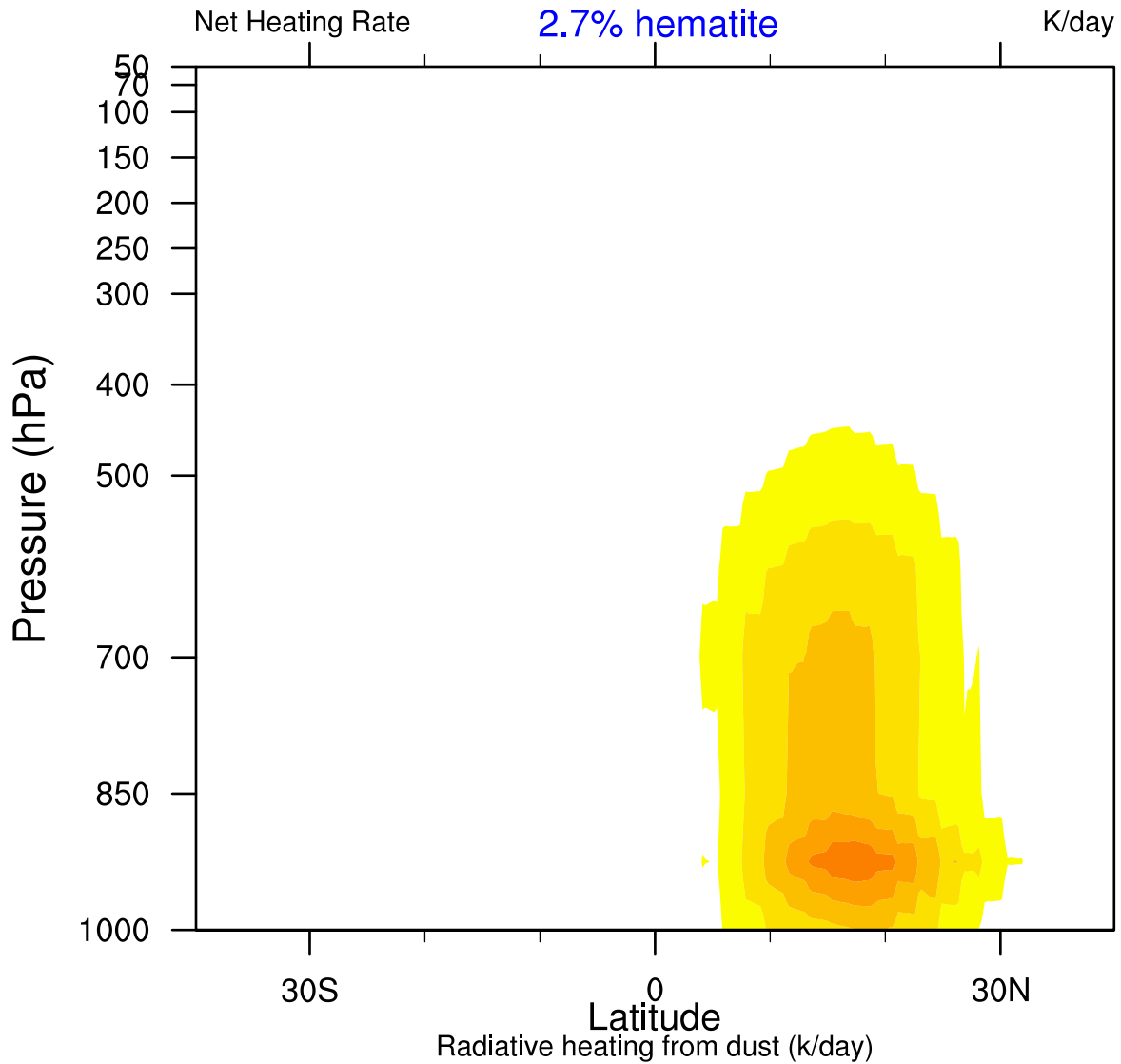
Hematite 2.7 (3-5 day)



Hematite 2.7 (6-9 day)

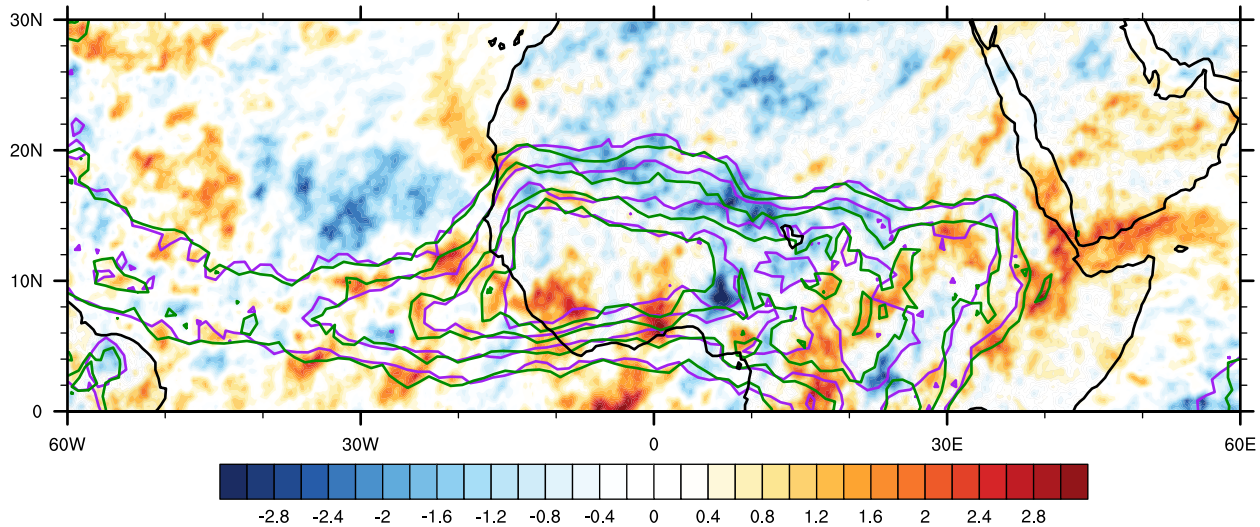


Net\_HeatingMeridionaMENA\_ocean\_JJA27.eps.



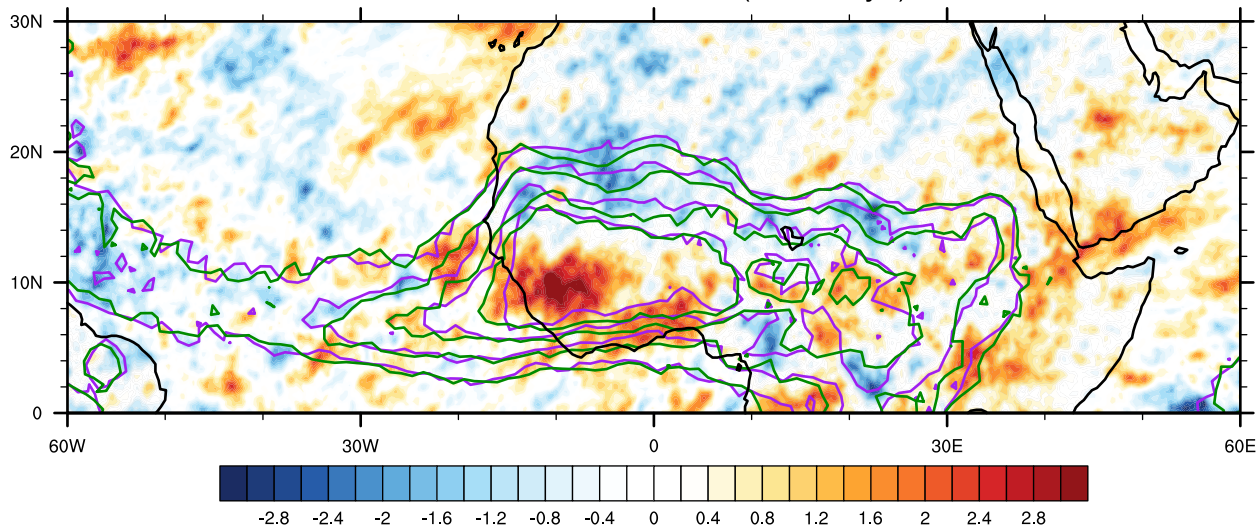
bpf\_35\_olr\_bias.eps.

Hematite0.9 - No Dust (3 - 5 days)



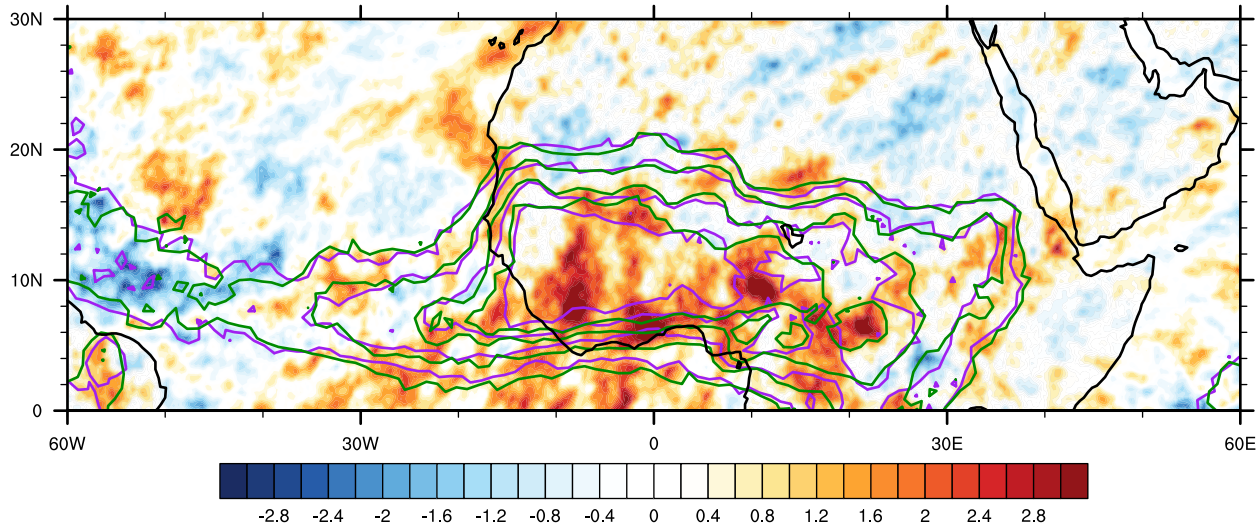
CONTOUR FROM 13 TO 21 BY 3

Hematite1.5 - No Dust (3 - 5 days)



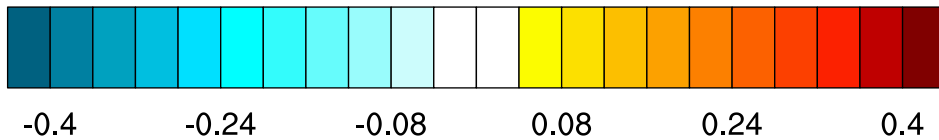
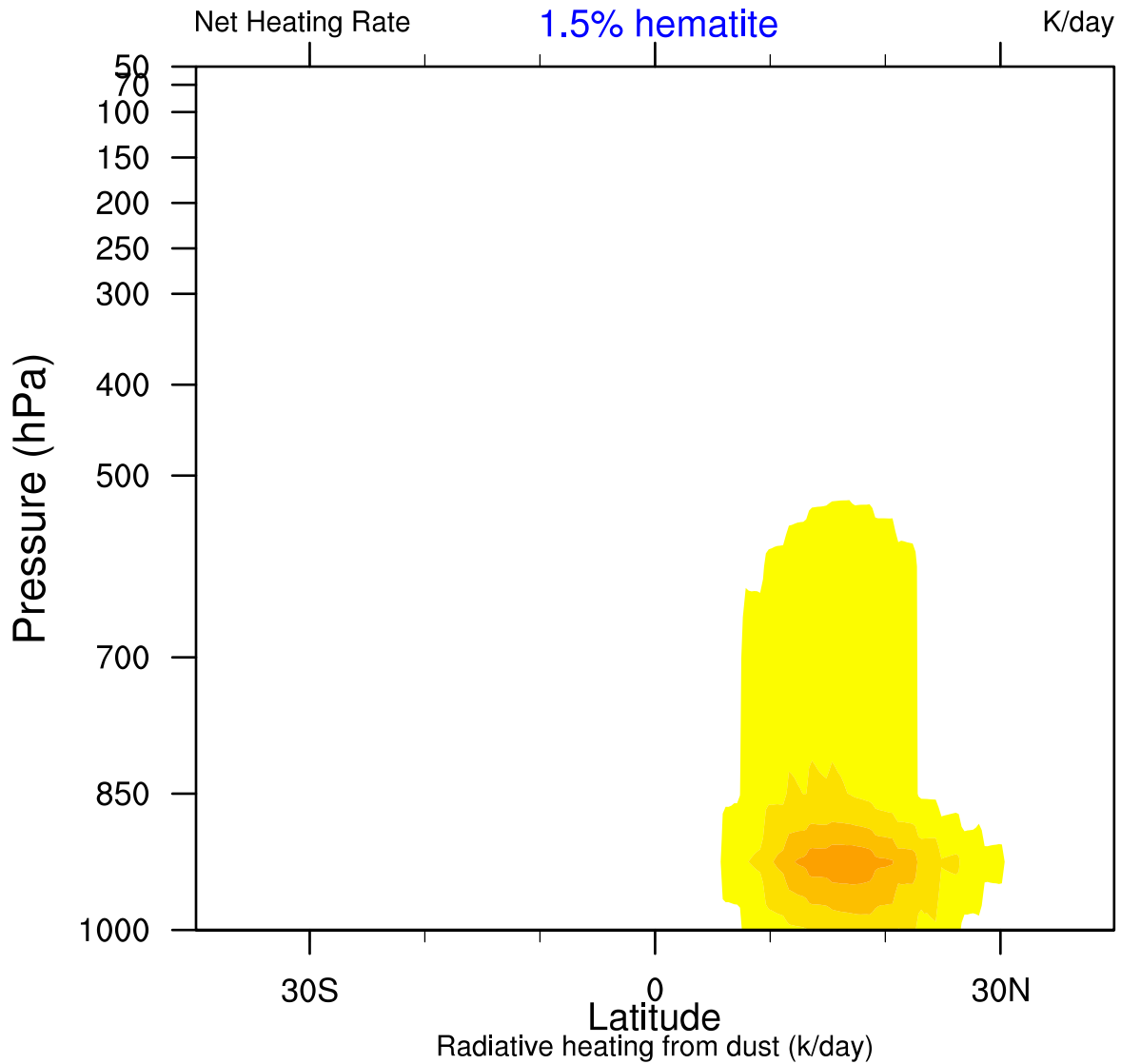
CONTOUR FROM 13 TO 21 BY 3

Hematite2.7 - No Dust (3 - 5 days)

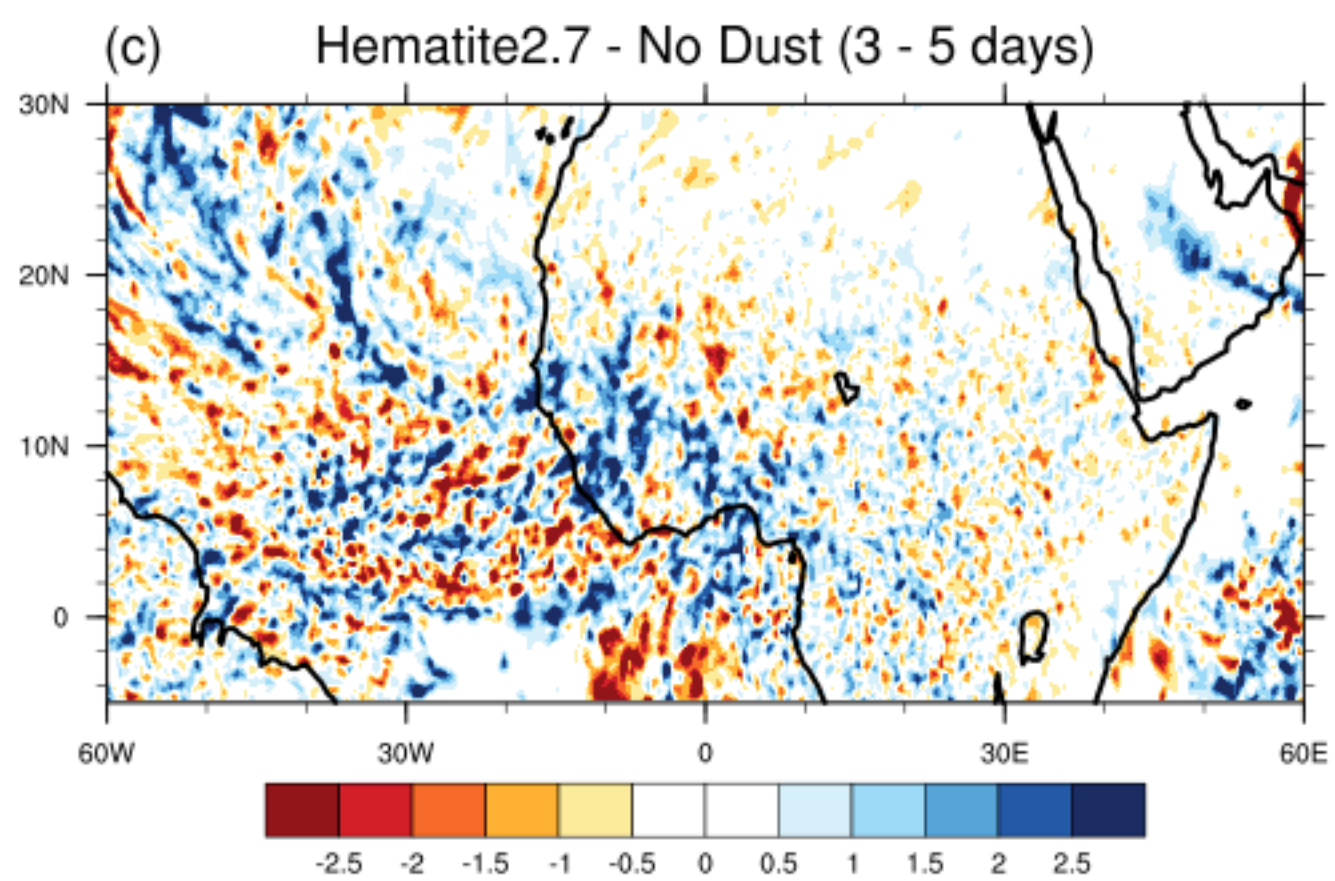
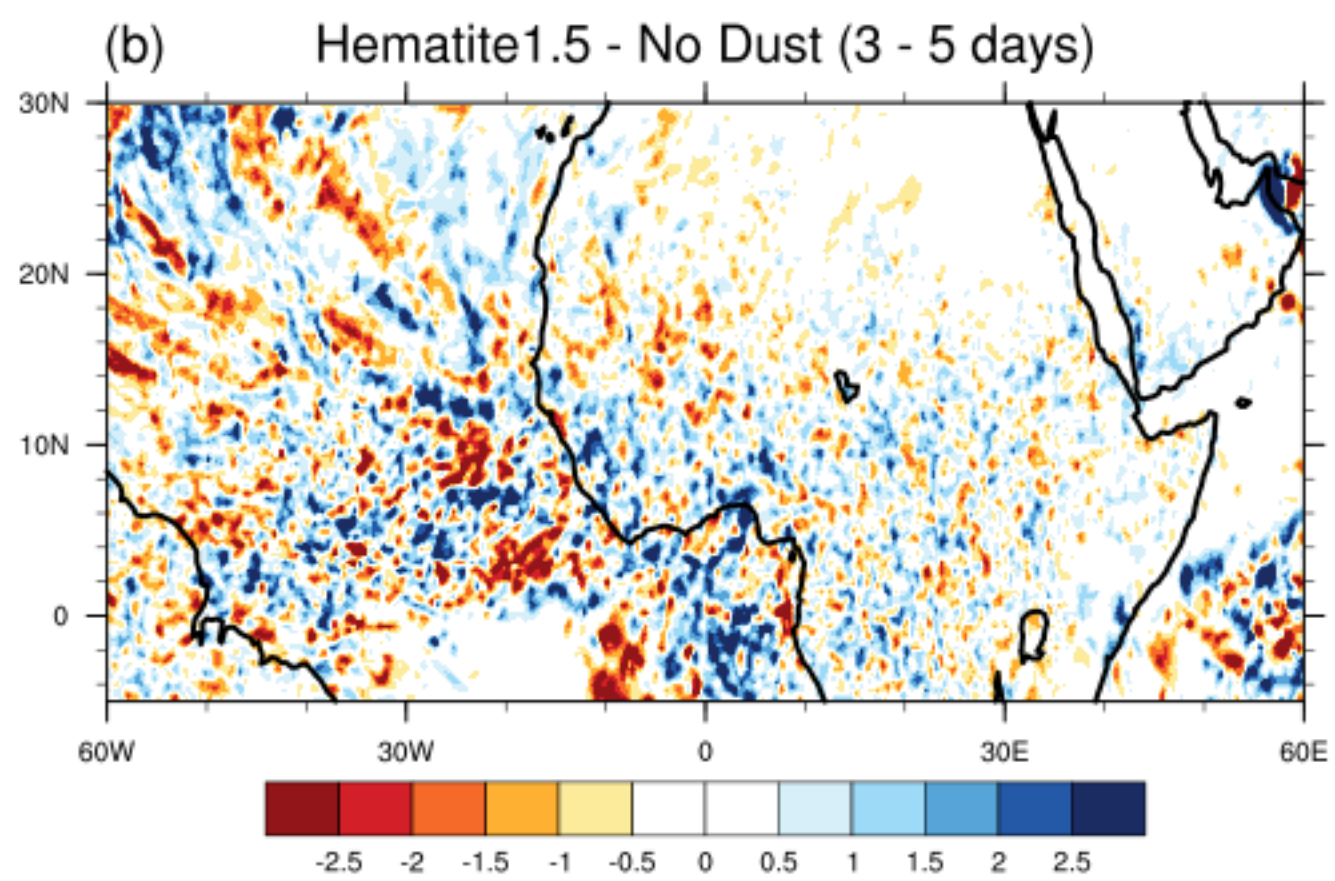
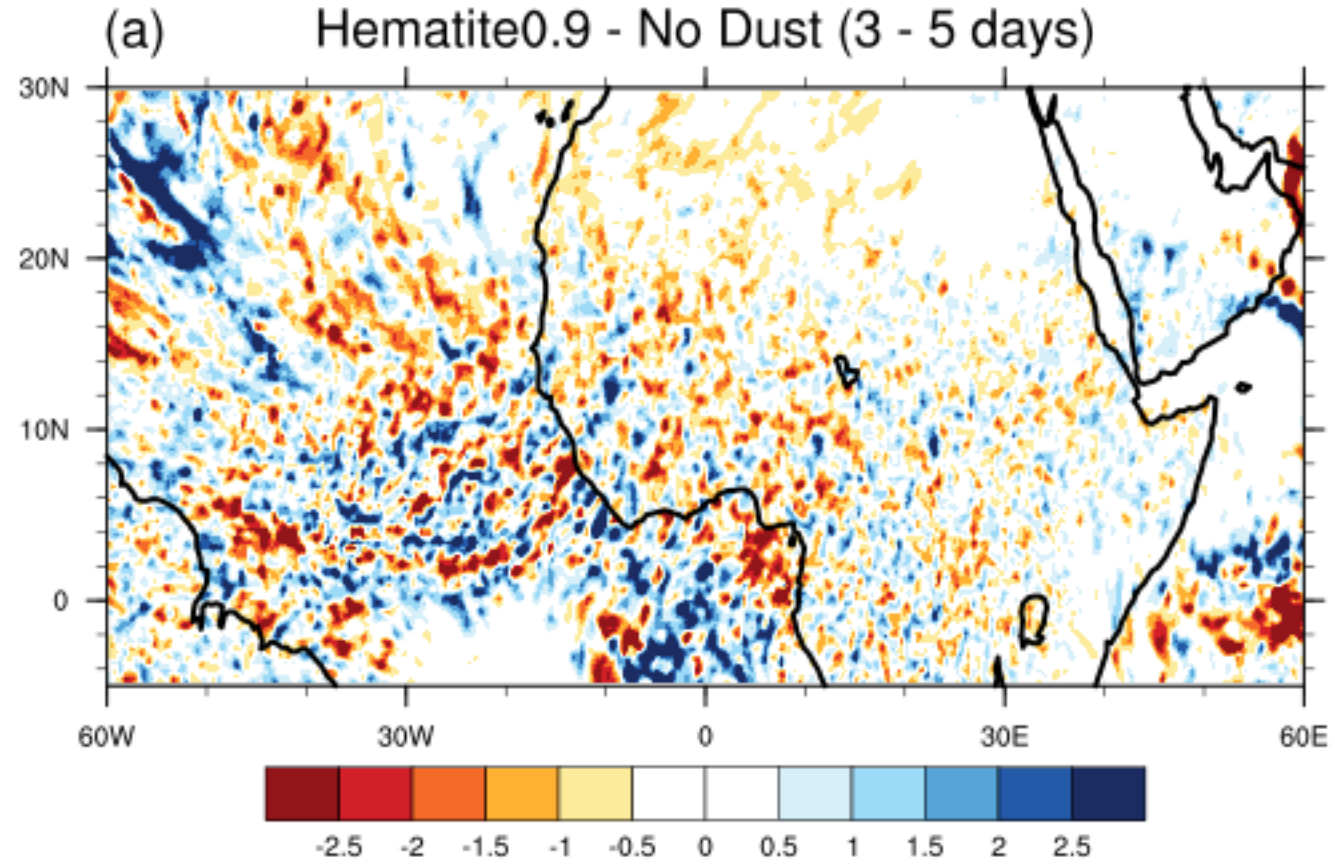


CONTOUR FROM 13 TO 21 BY 3

Net\_HeatingMeridionaMENA\_ocean\_JJA15.eps.

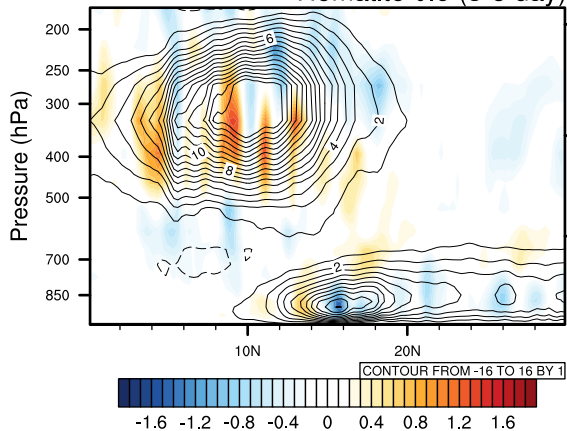


bpf\_35\_bias.png.

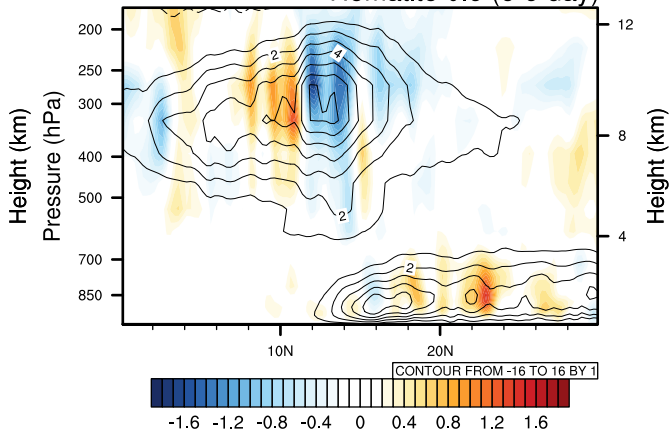


bc\_land.eps.

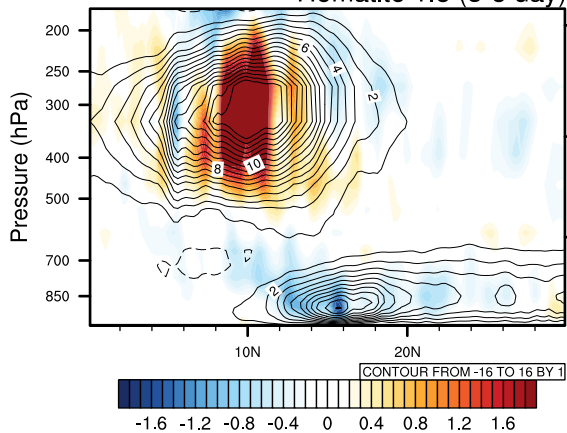
Hematite 0.9 (3-5 day)



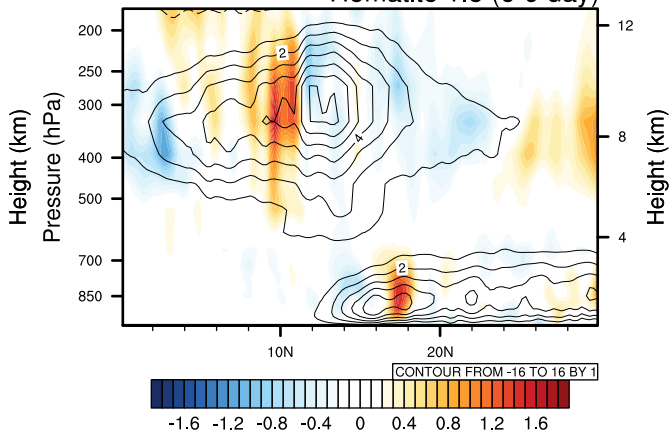
Hematite 0.9 (6-9 day)



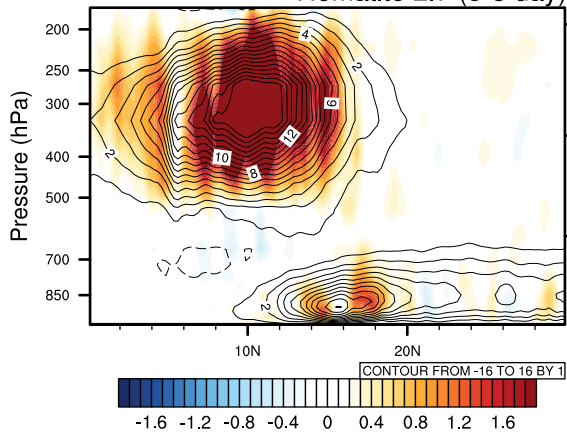
Hematite 1.5 (3-5 day)



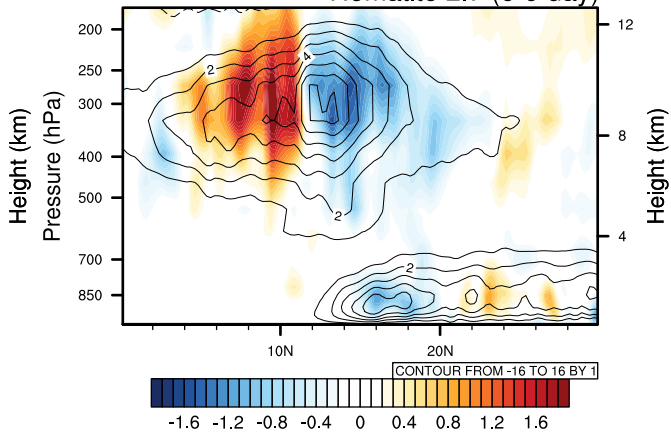
Hematite 1.5 (6-9 day)



Hematite 2.7 (3-5 day)

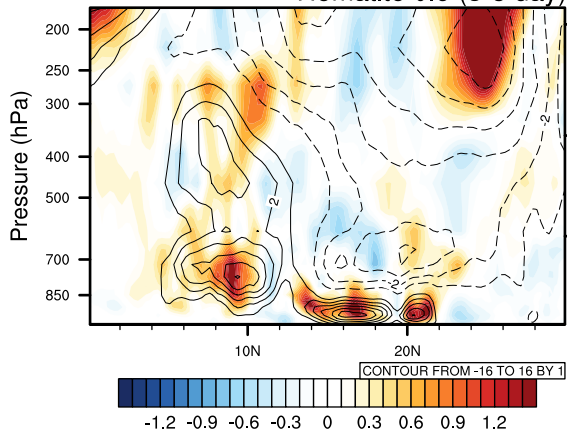


Hematite 2.7 (6-9 day)

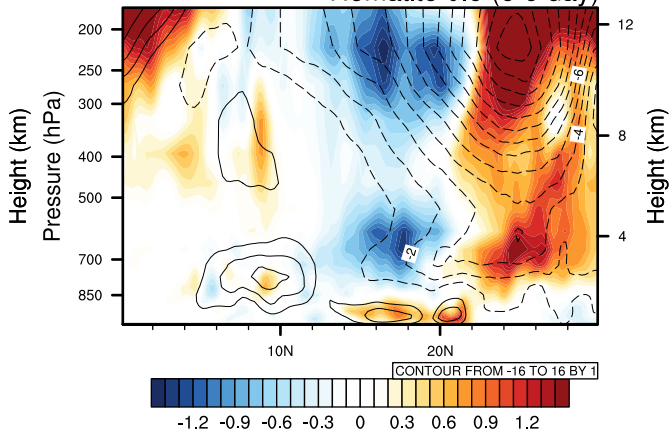


bt\_ocean.eps.

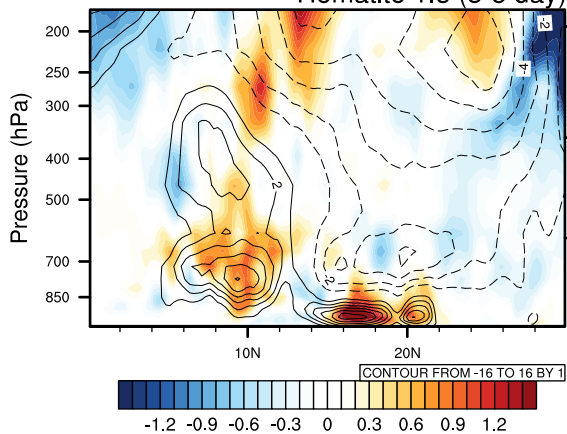
Hematite 0.9 (3-5 day)



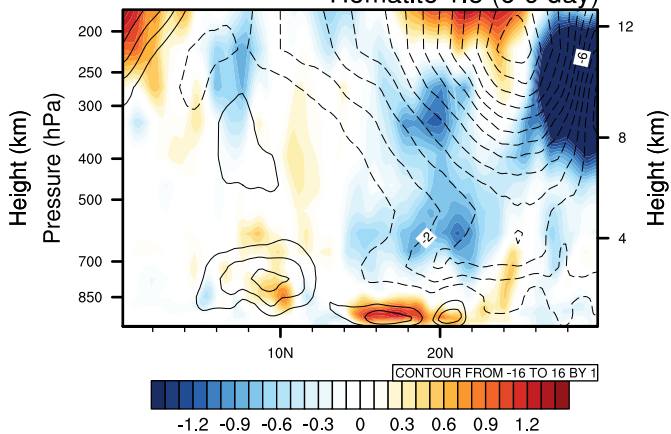
Hematite 0.9 (6-9 day)



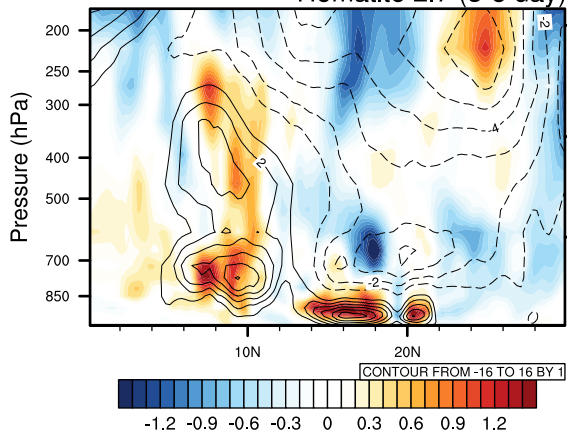
Hematite 1.5 (3-5 day)



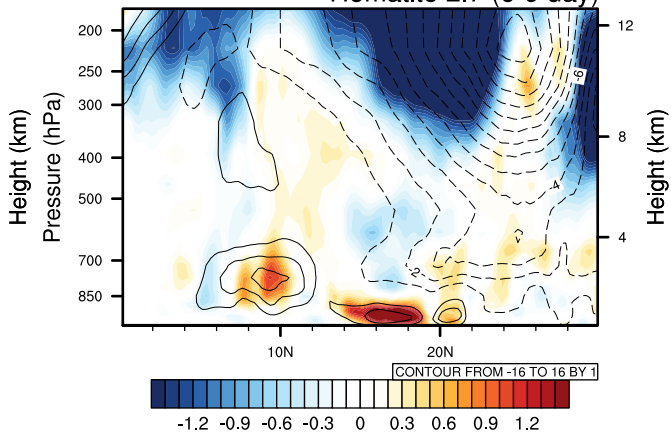
Hematite 1.5 (6-9 day)



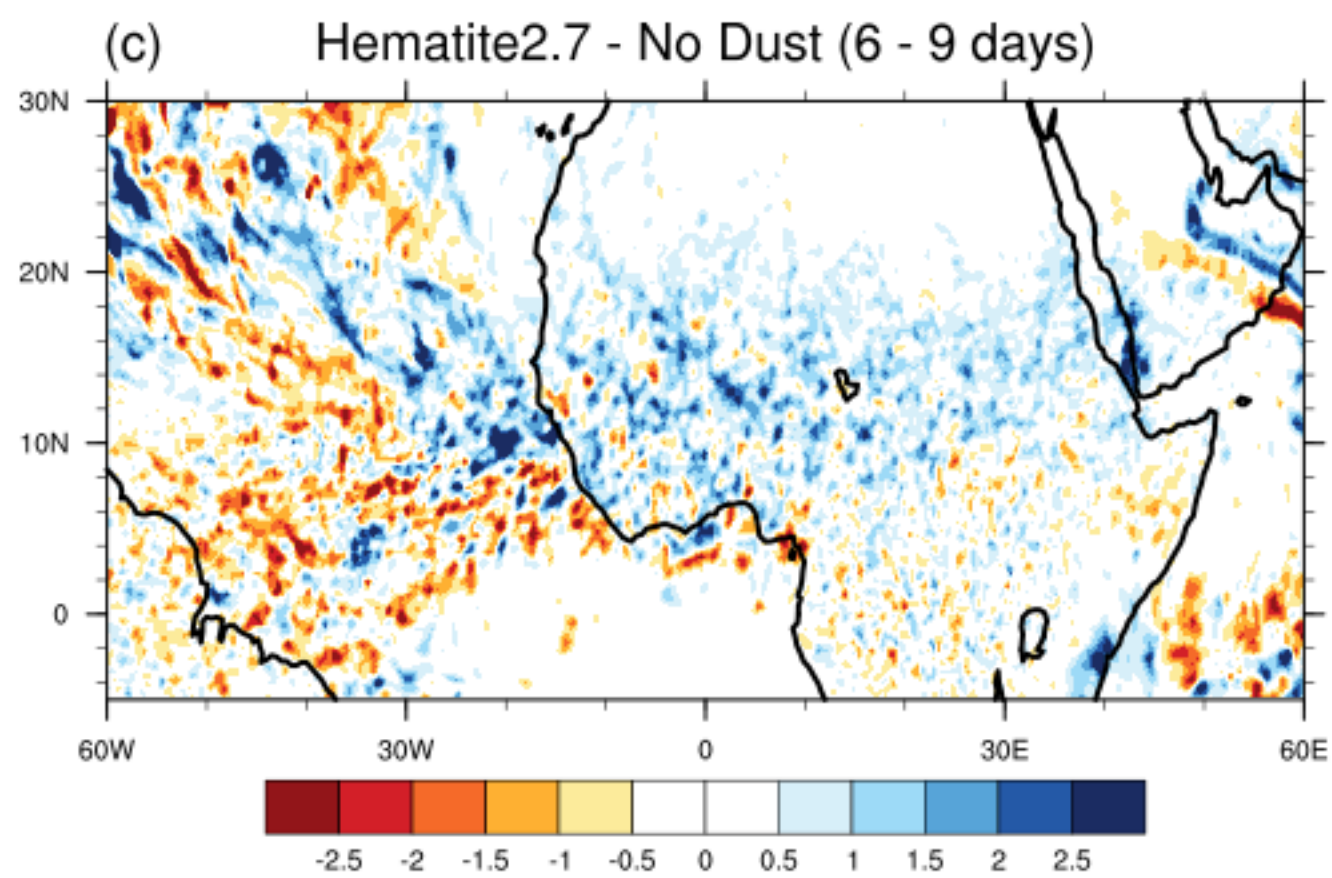
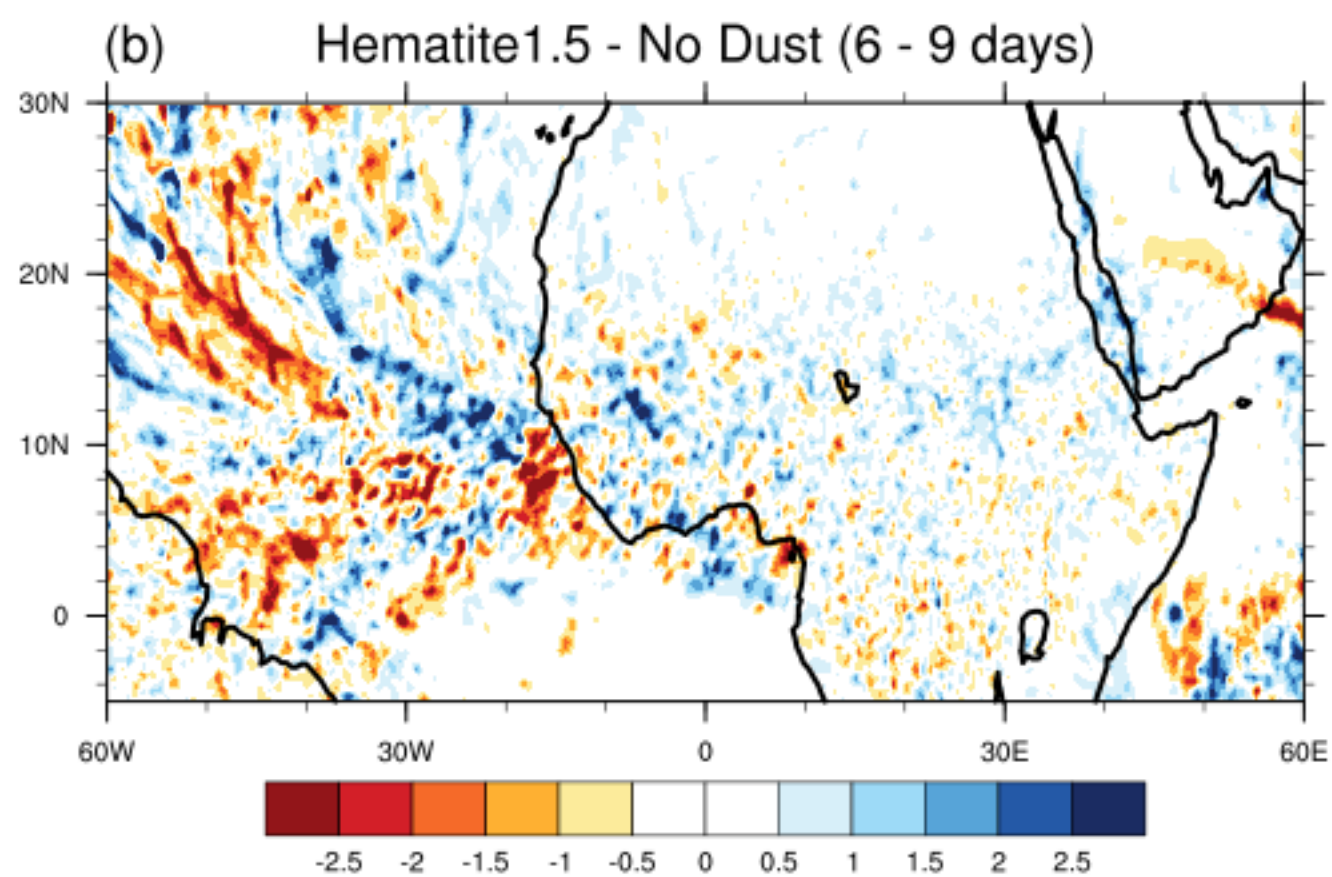
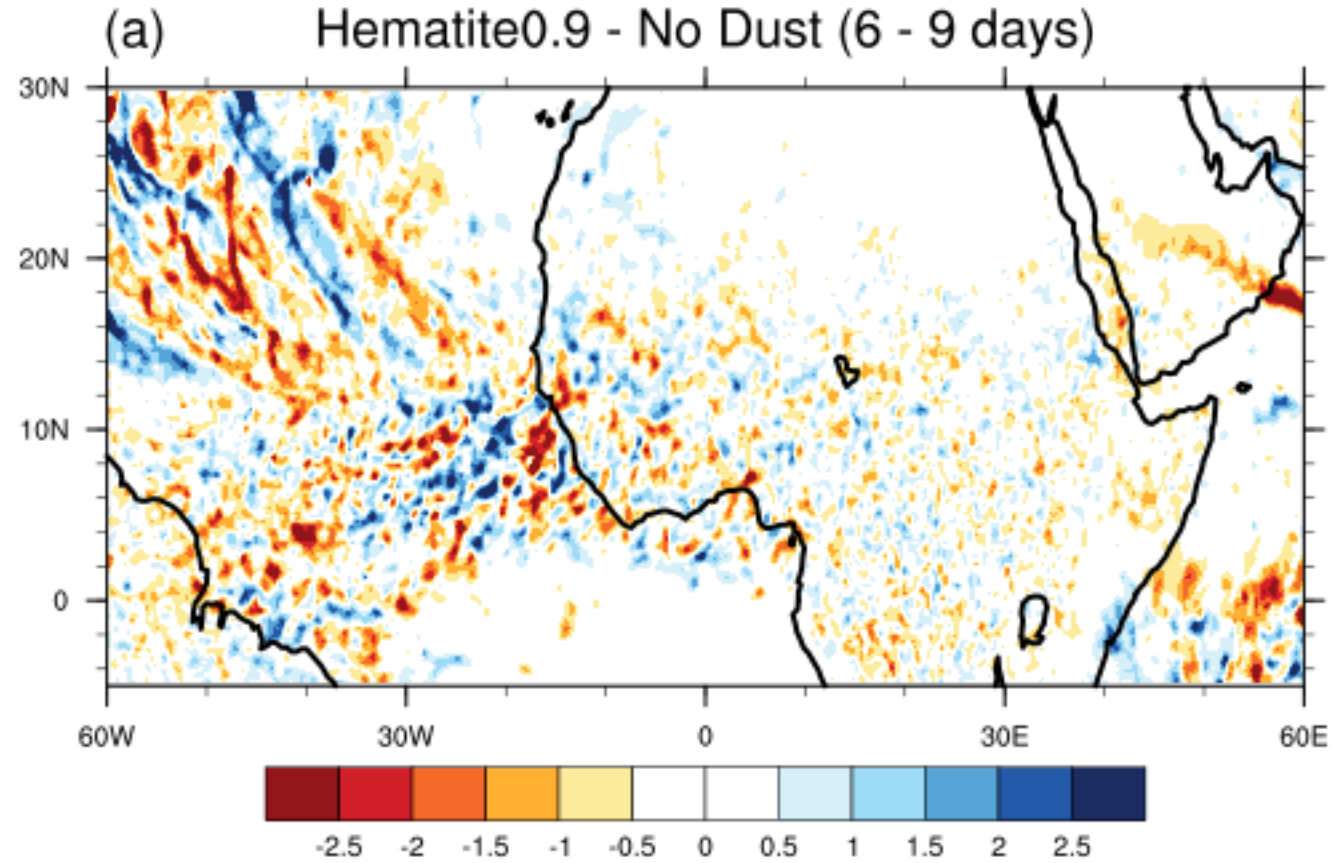
Hematite 2.7 (3-5 day)



Hematite 2.7 (6-9 day)

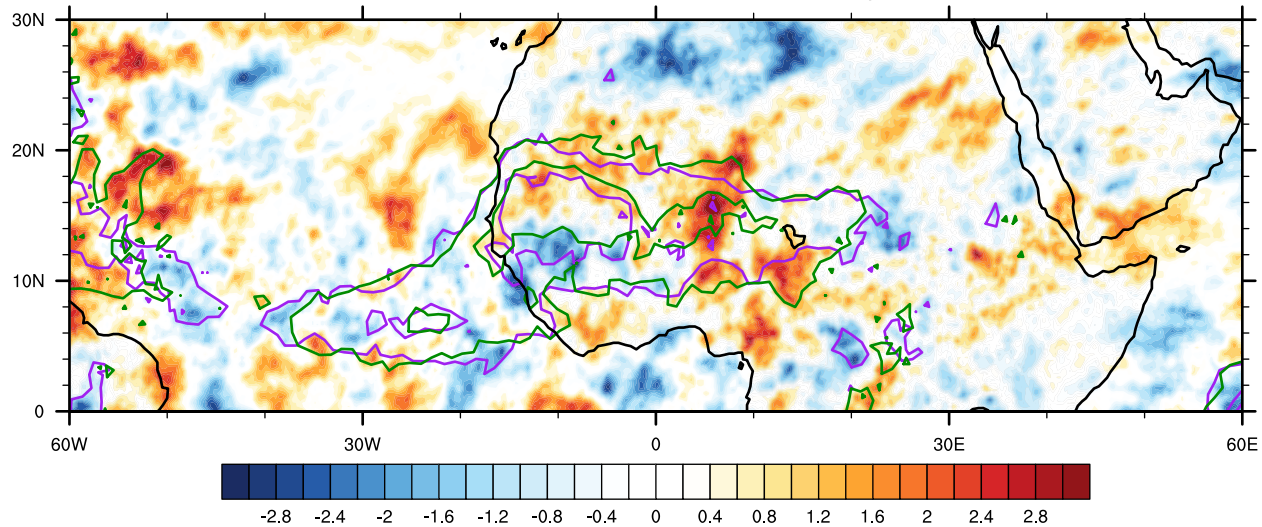


bpf\_69\_bias.png.



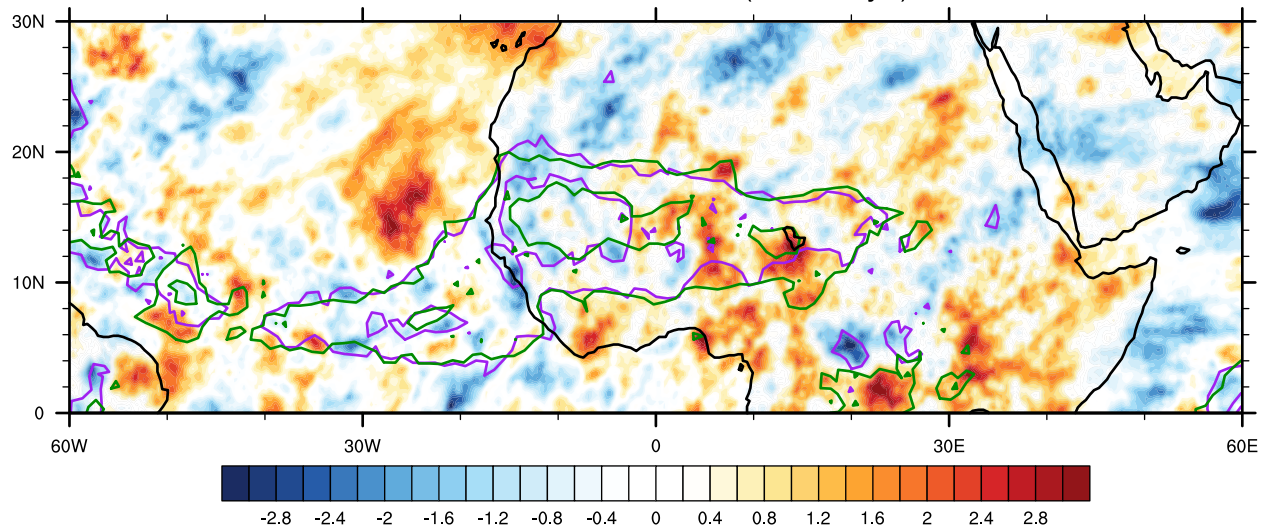
bpf\_69\_olr\_bias.eps.

Hematite0.9 - No Dust (6 - 9 days)



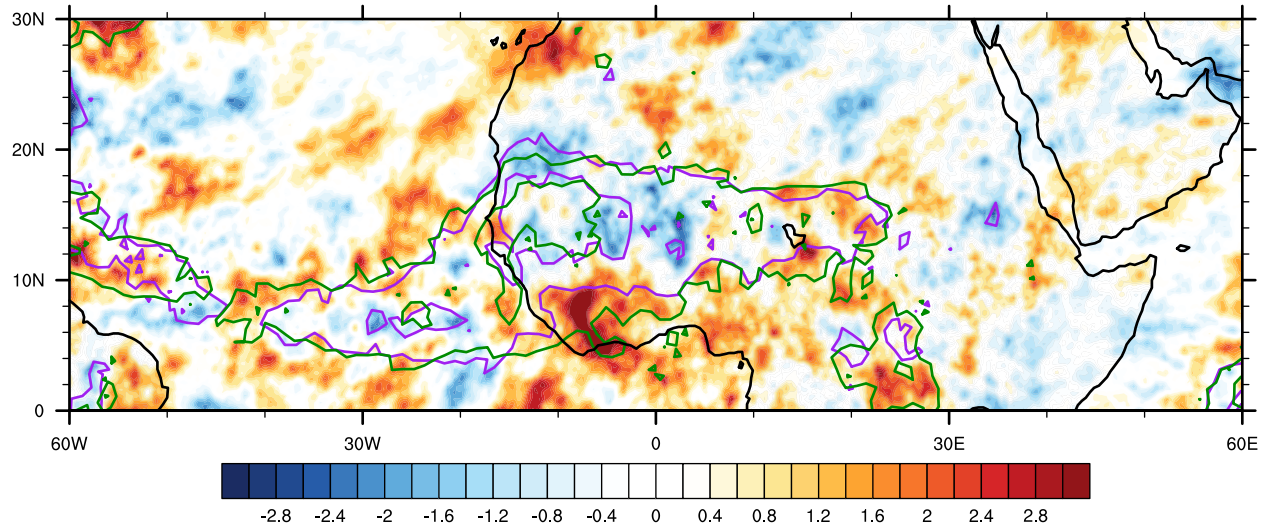
CONTOUR FROM 12 TO 18 BY 3

Hematite1.5 - No Dust (6 - 9 days)



CONTOUR FROM 12 TO 18 BY 3

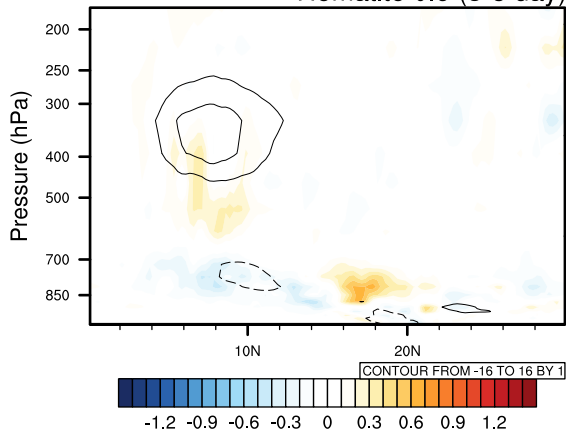
Hematite2.7 - No Dust (6 - 9 days)



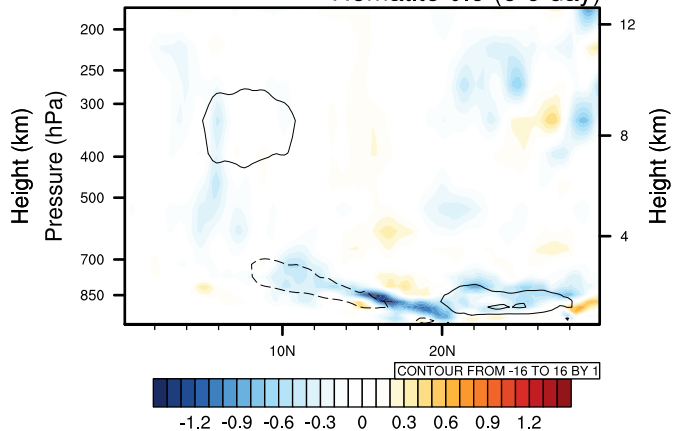
CONTOUR FROM 12 TO 18 BY 3

dh\_ocean.eps.

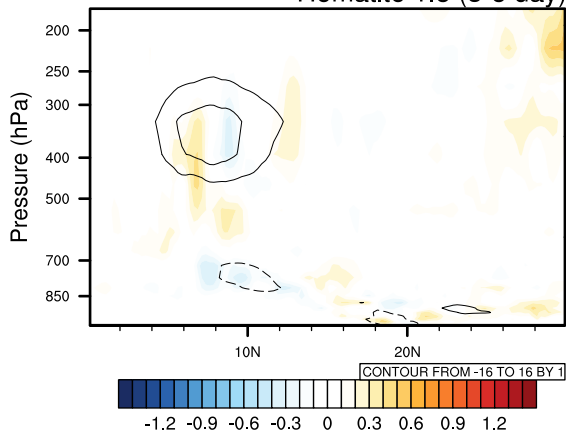
Hematite 0.9 (3-5 day)



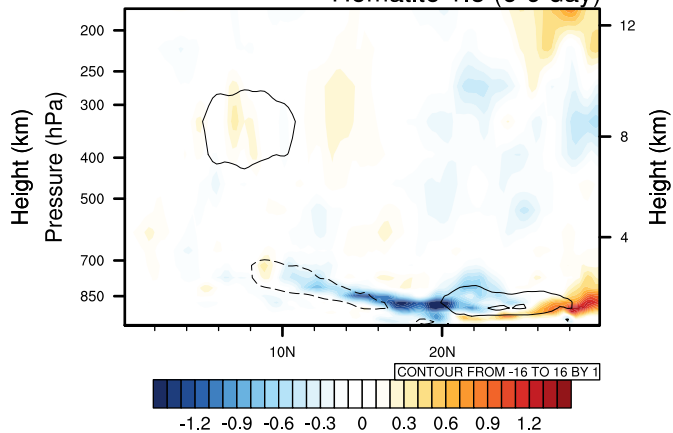
Hematite 0.9 (6-9 day)



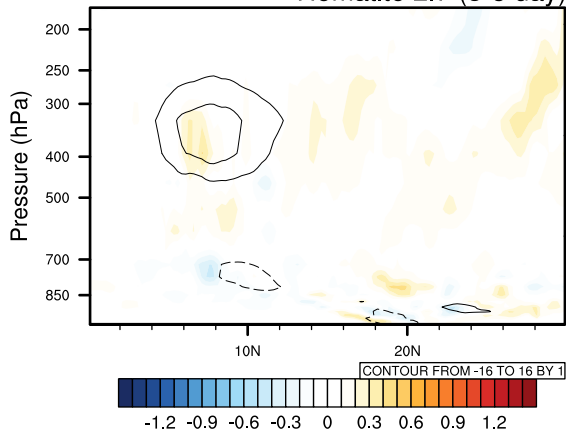
Hematite 1.5 (3-5 day)



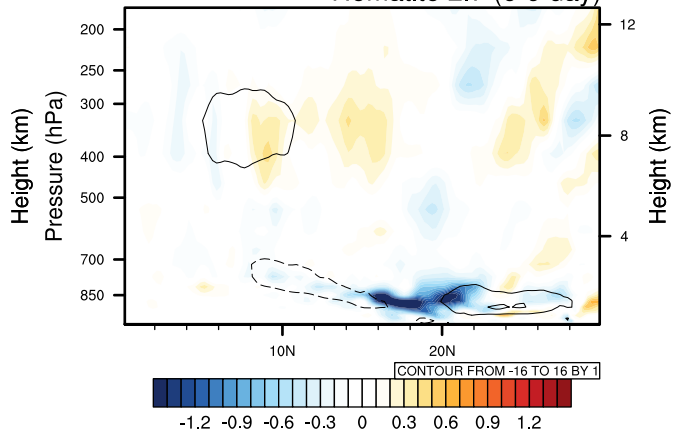
Hematite 1.5 (6-9 day)



Hematite 2.7 (3-5 day)

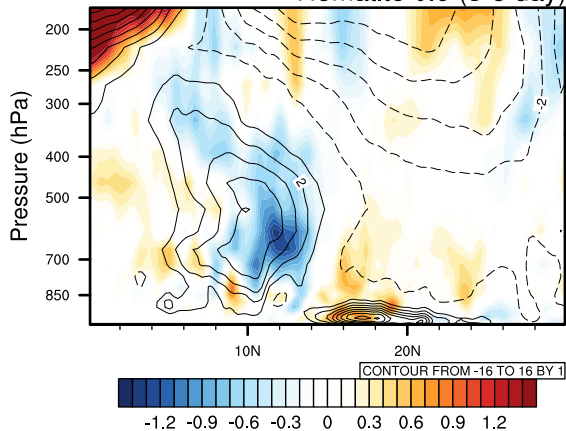


Hematite 2.7 (6-9 day)

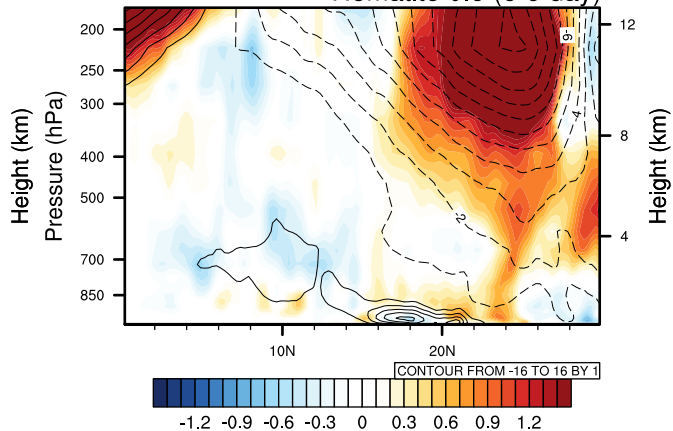


bt\_land.eps.

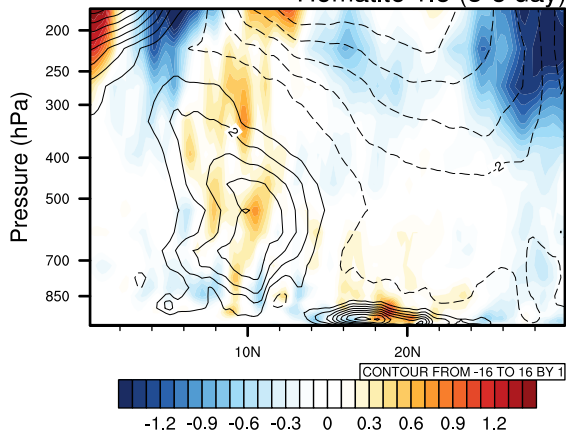
Hematite 0.9 (3-5 day)



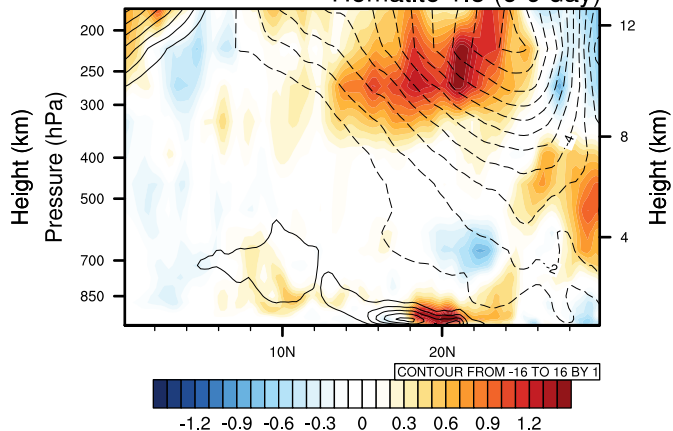
Hematite 0.9 (6-9 day)



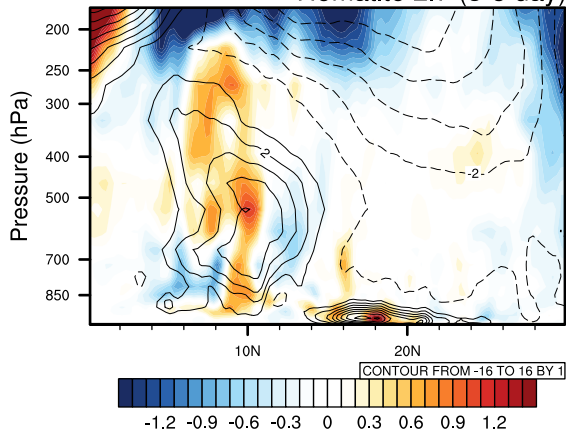
Hematite 1.5 (3-5 day)



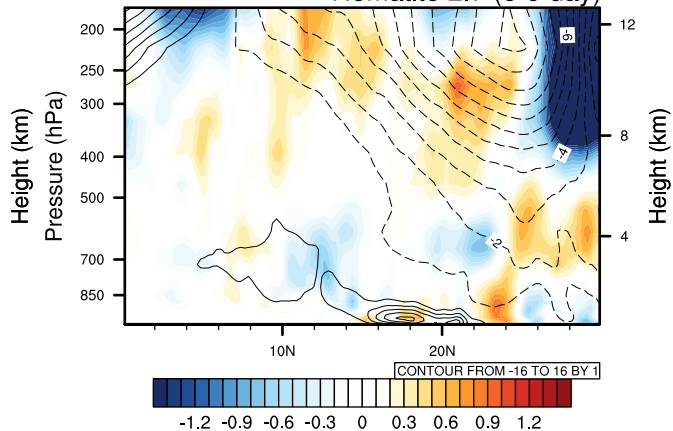
Hematite 1.5 (6-9 day)



Hematite 2.7 (3-5 day)

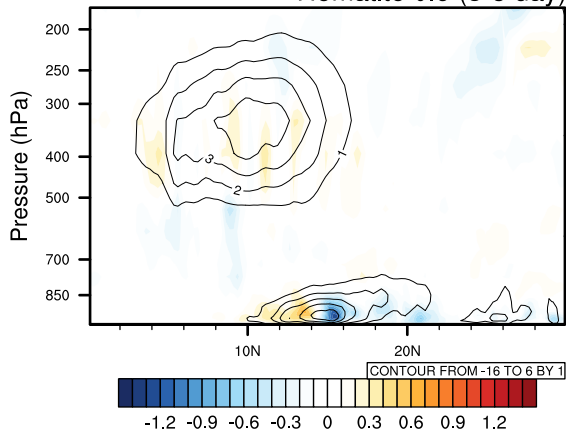


Hematite 2.7 (6-9 day)

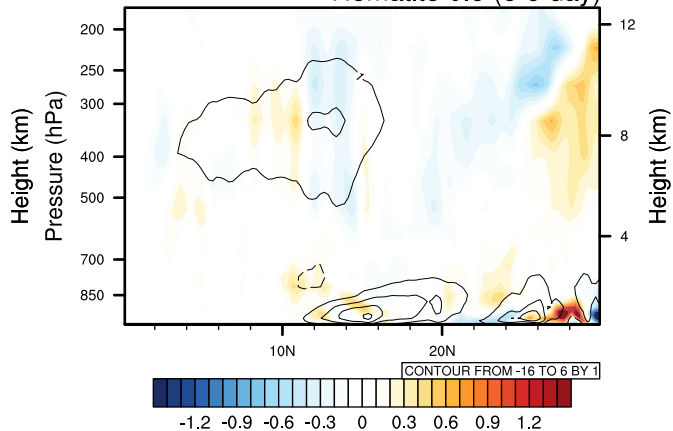


dh\_land.eps.

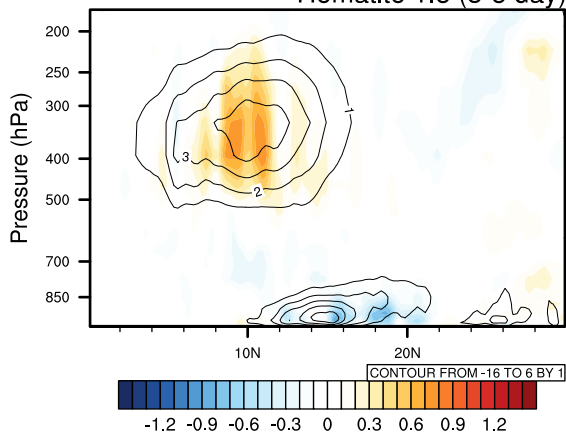
Hematite 0.9 (3-5 day)



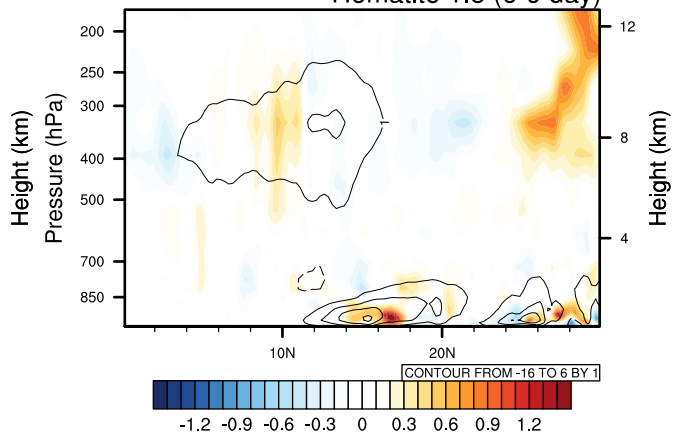
Hematite 0.9 (6-9 day)



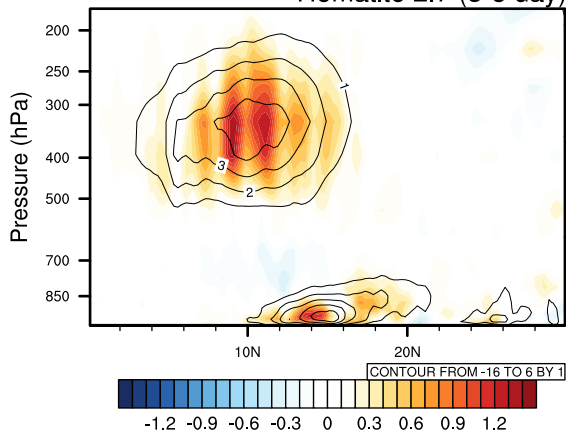
Hematite 1.5 (3-5 day)



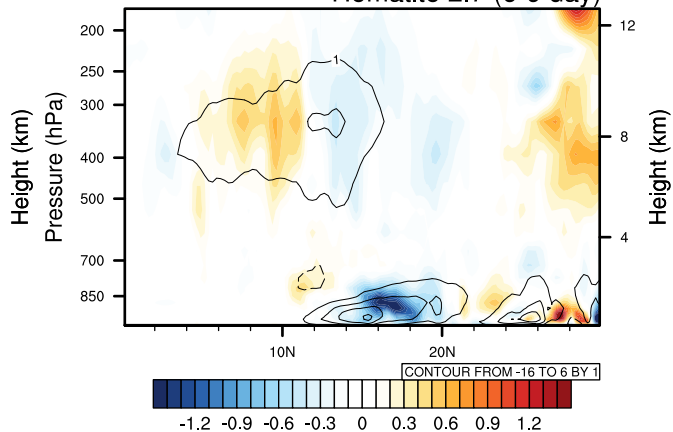
Hematite 1.5 (6-9 day)



Hematite 2.7 (3-5 day)

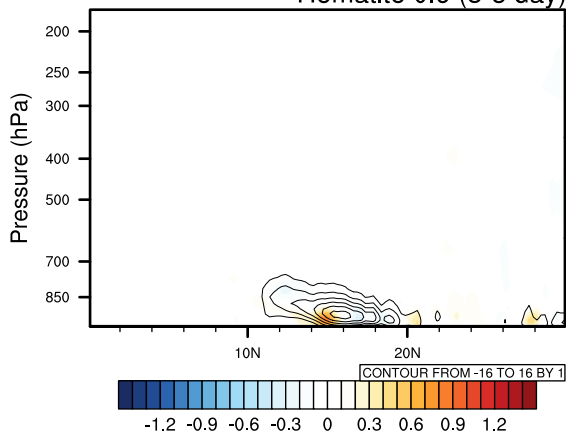


Hematite 2.7 (6-9 day)

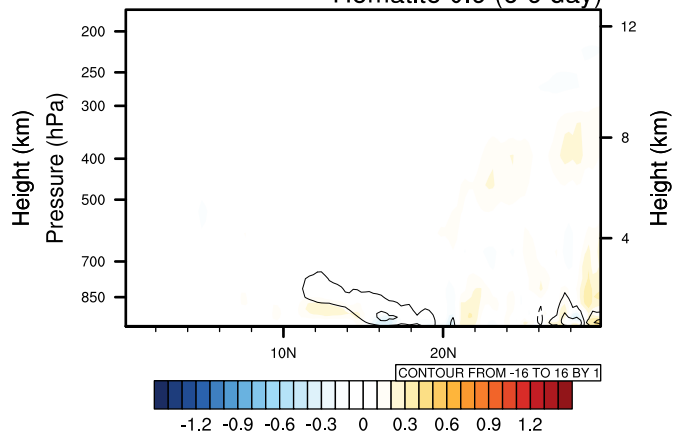


map\_e\_land.eps.

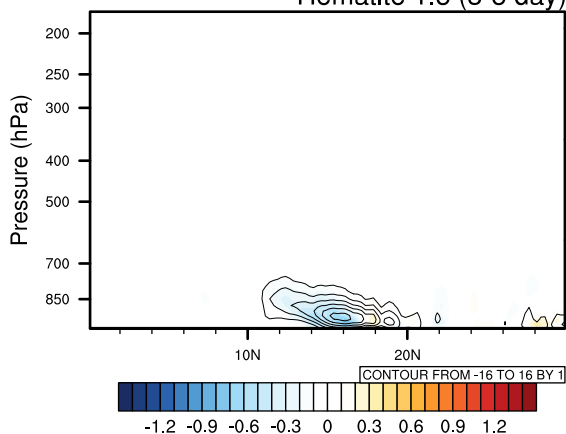
Hematite 0.9 (3-5 day)



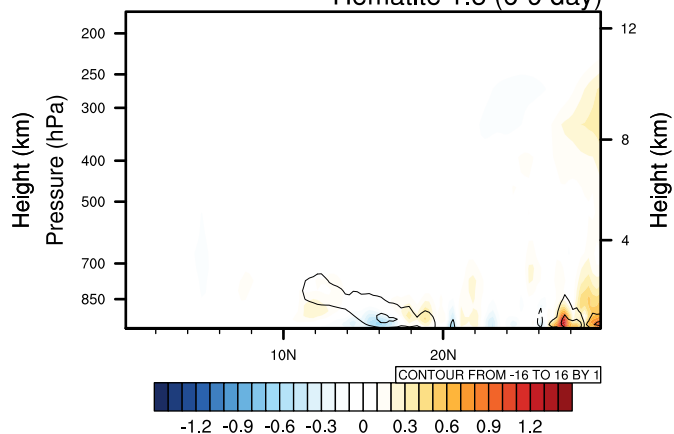
Hematite 0.9 (6-9 day)



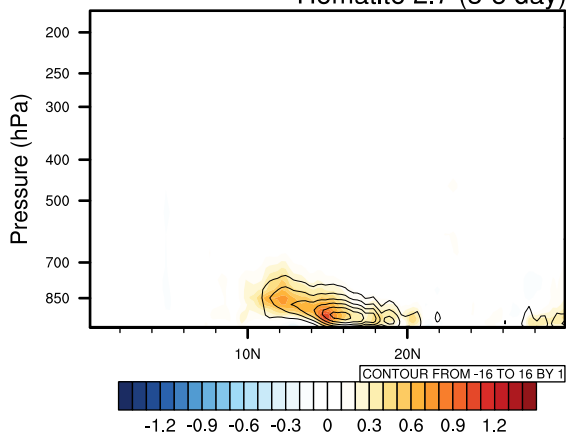
Hematite 1.5 (3-5 day)



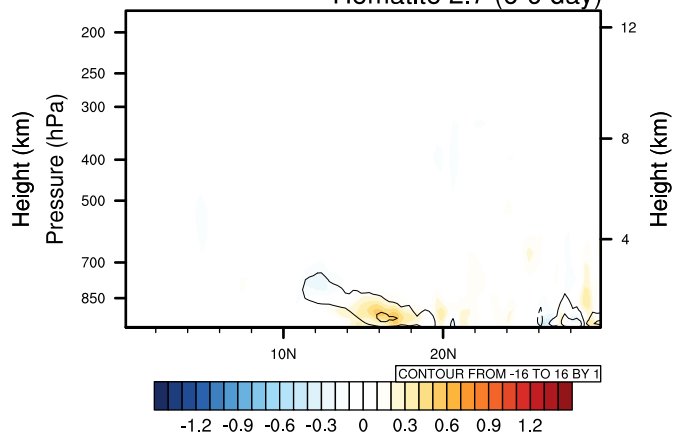
Hematite 1.5 (6-9 day)



Hematite 2.7 (3-5 day)

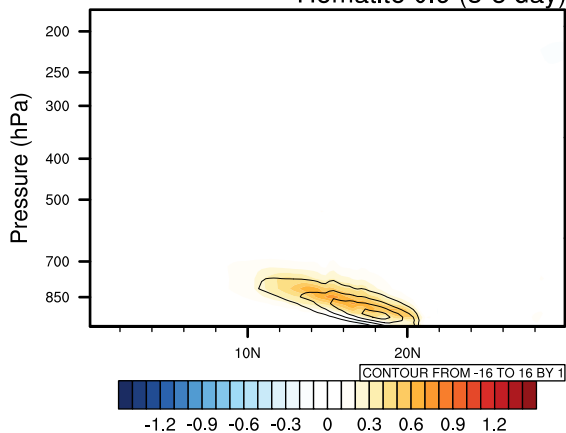


Hematite 2.7 (6-9 day)

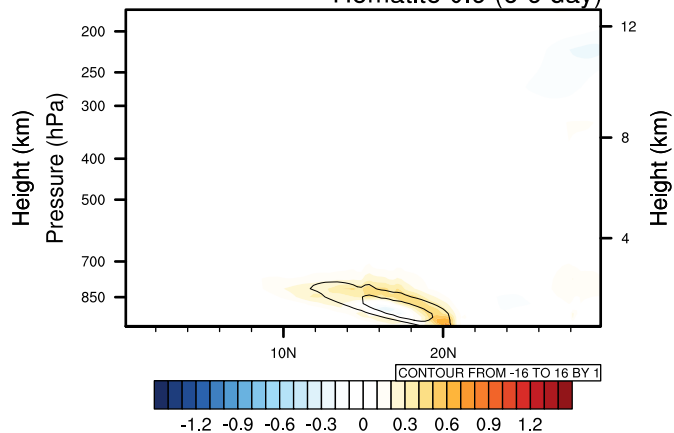


mapo\_ocean.eps.

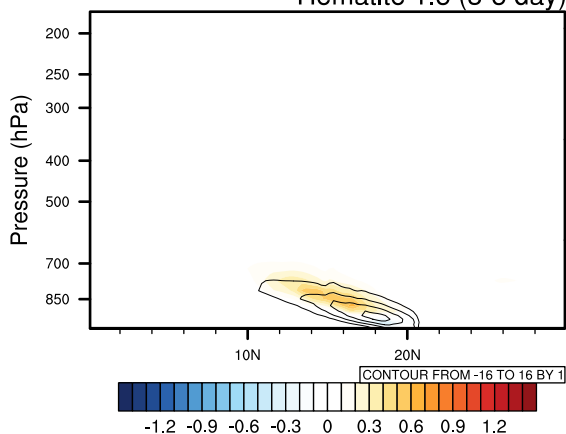
Hematite 0.9 (3-5 day)



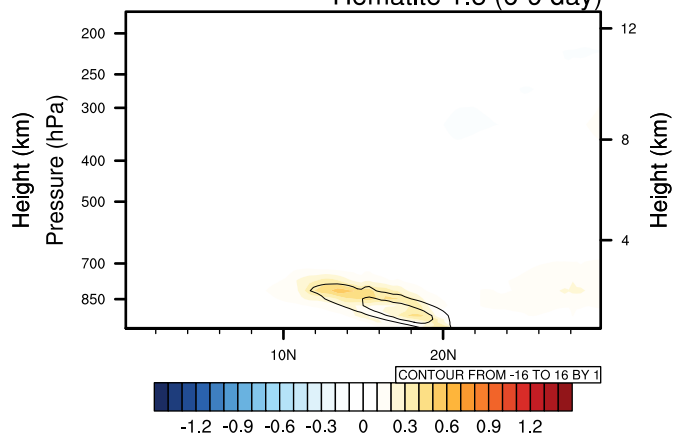
Hematite 0.9 (6-9 day)



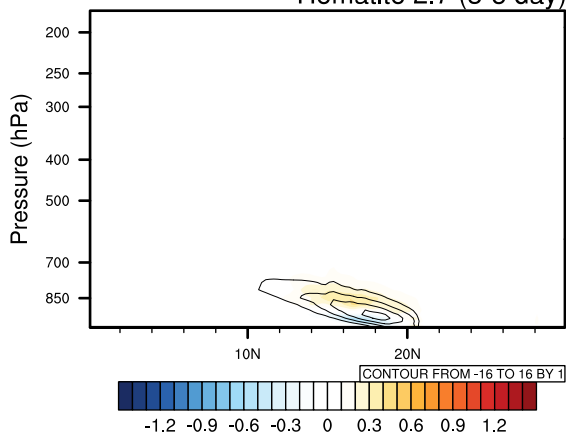
Hematite 1.5 (3-5 day)



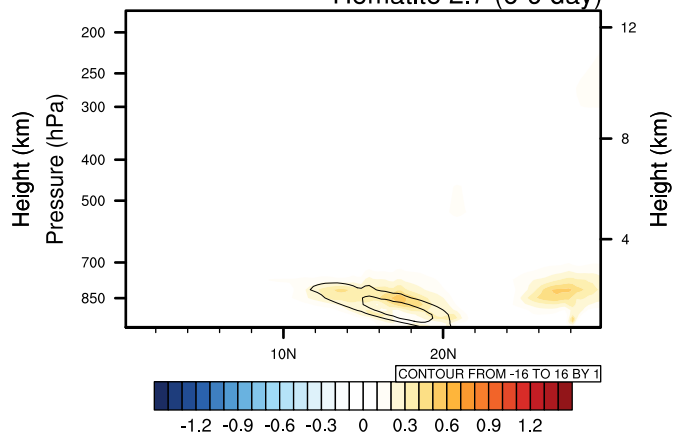
Hematite 1.5 (6-9 day)



Hematite 2.7 (3-5 day)

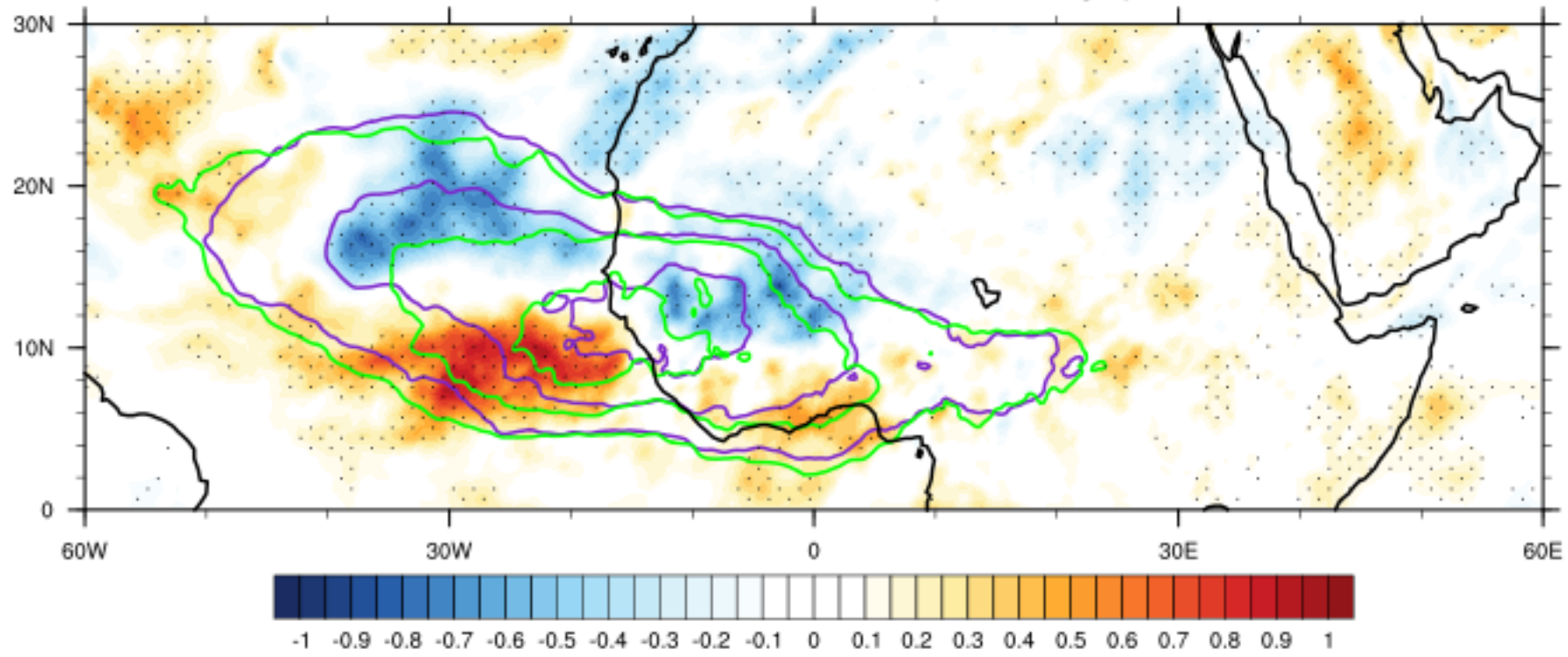


Hematite 2.7 (6-9 day)



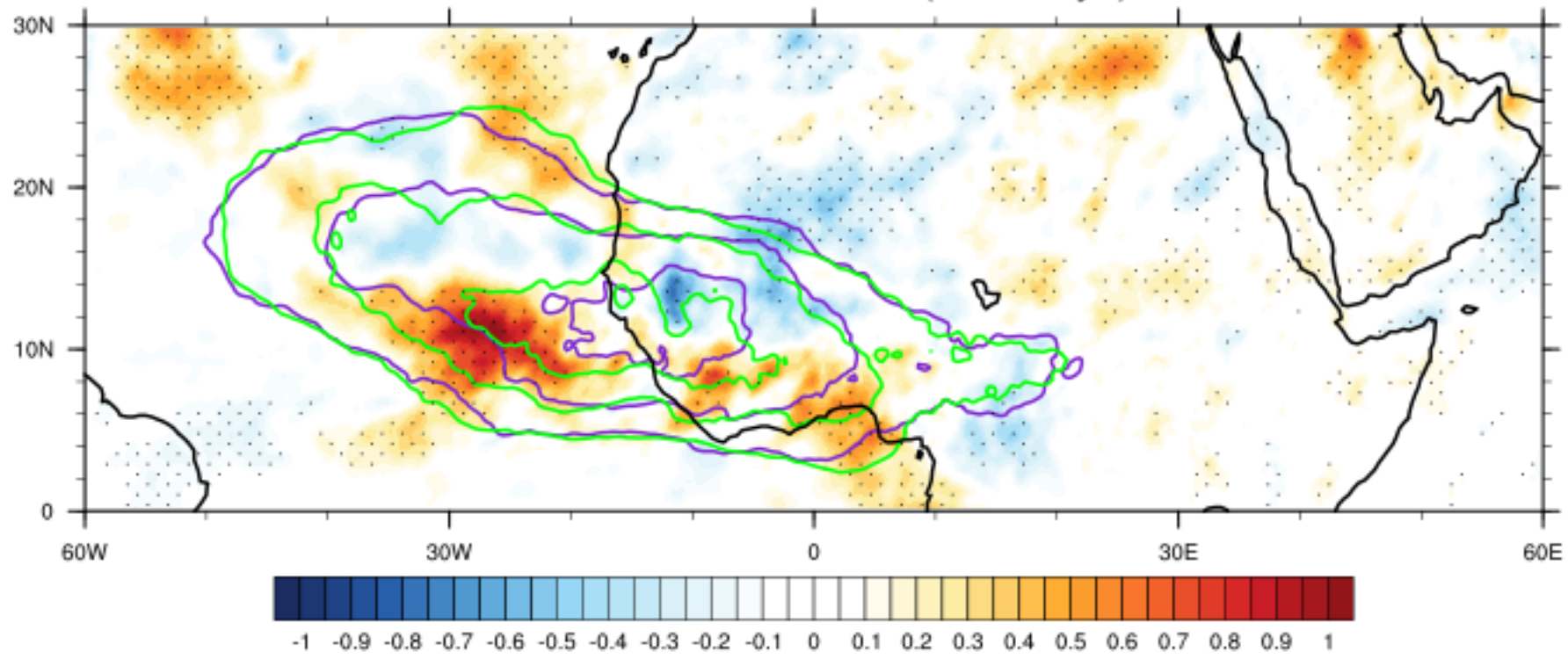
eke\_35\_bias\_700.png.

Hematite0.9 - NoDust (3 - 5 days)



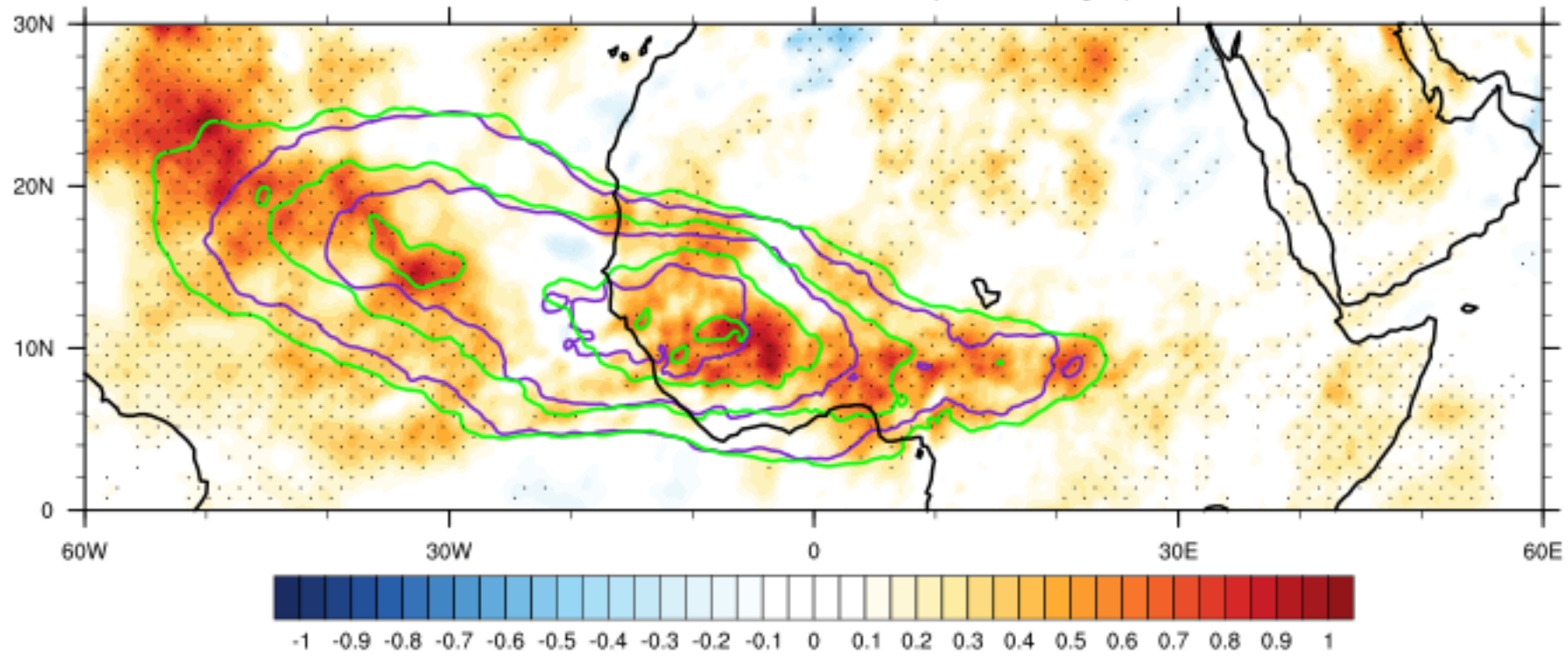
CONTOUR FROM 3 TO 7 BY 1

Hematite1.5 - NoDust (3 - 5 days)



CONTOUR FROM 3 TO 7 BY 1

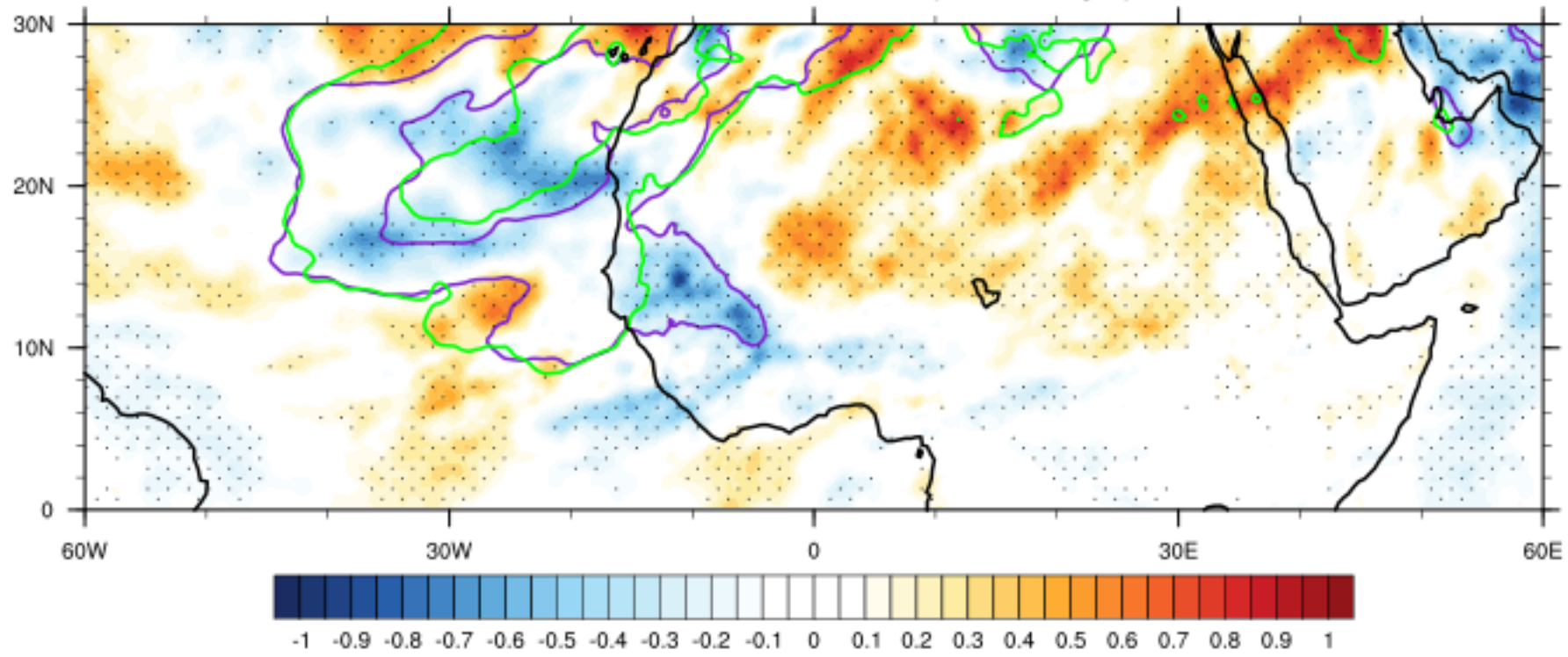
Hematite2.7 - No Dust (3 - 5 days)



CONTOUR FROM 3 TO 7 BY 1

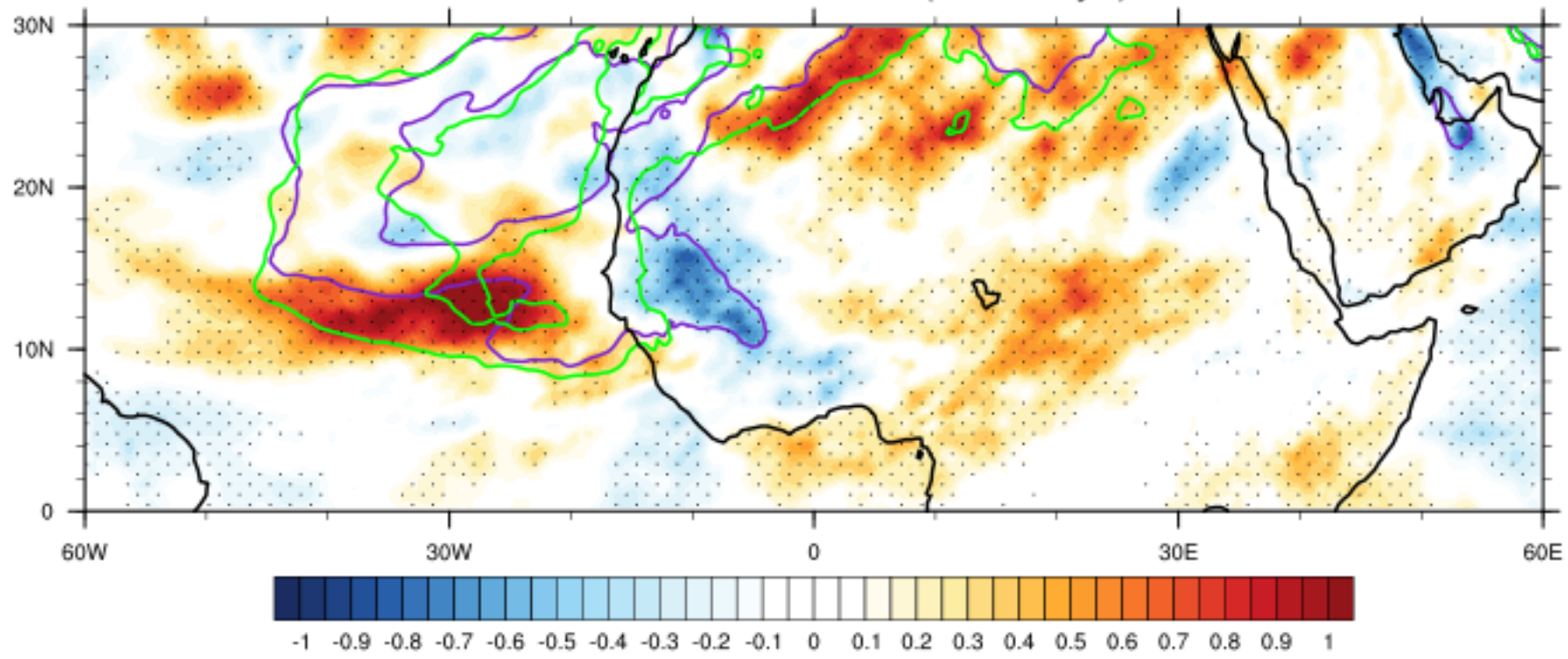
eke\_69\_bias\_700.png.

Hematite0.9 - NoDust (6 - 9 days)



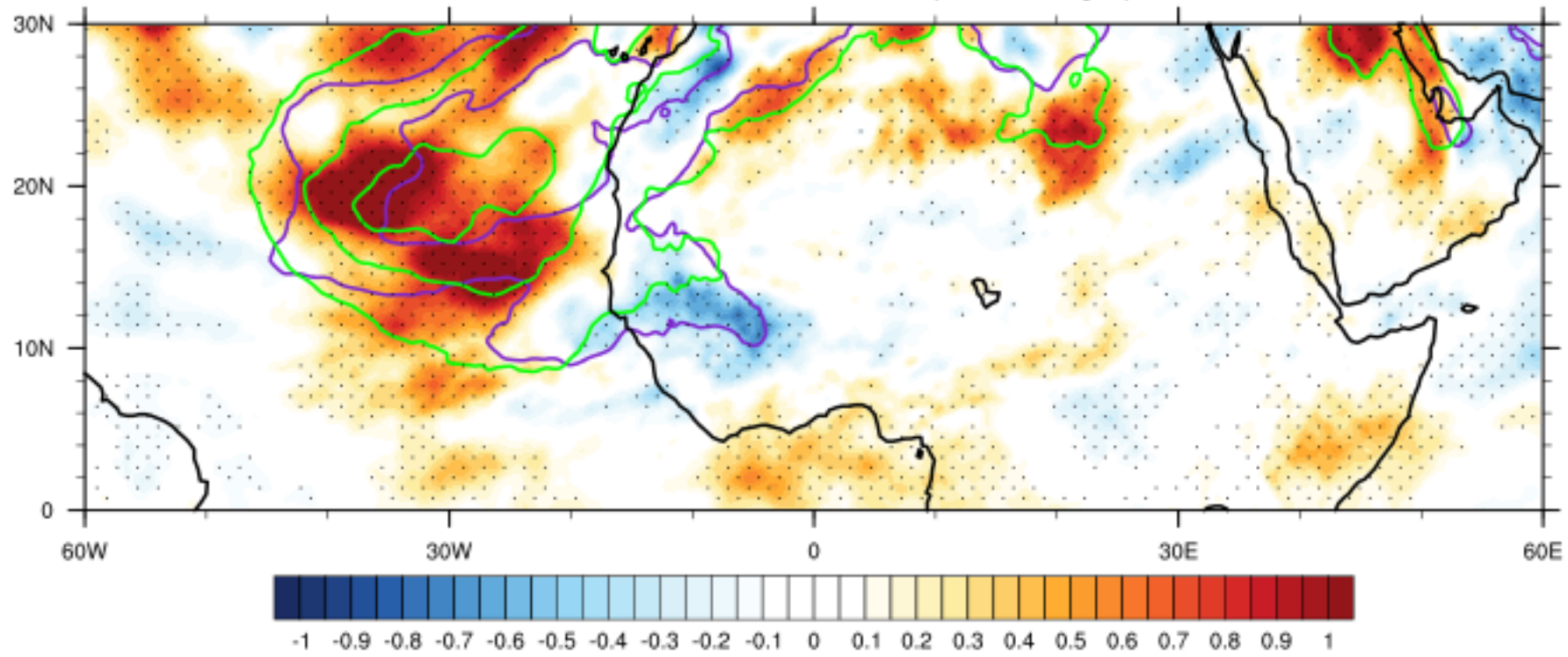
CONTOUR FROM 3 TO 7 BY 1

Hematite1.5 - NoDust (6 - 9 days)



CONTOUR FROM 3 TO 7 BY 1

Hematite2.7 - No Dust (6 - 9 days)



CONTOUR FROM 3 TO 7 BY 1